JETP Letters, Vol. 71, No. 6, 2000, pp. 217–221. Translated from Pis'ma v Zhurnal Éksperimental'noĭ i Teoreticheskoĭ Fiziki, Vol. 71, No. 6, 2000, pp. 315–321.

FIELDS, PARTICLES, NUCLEI

Gell-Mann–Low Function in the φ^4 Theory

I. M. Suslov

Kapitza Institute for Physical Problems, Russian Academy of Sciences, ul. Kosygina 2, Moscow, 117973 Russia
e-mail: suslov@kapitza.ras.ru

Received November 1, 1999; in final form, February 2, 2000

An algorithm is proposed for the determination of the asymptotics of a sum of a perturbation series from the given values of its coefficients in the strong-coupling limit. When applied to the φ^4 theory, the algorithm yields the $\beta(g) \propto g^\alpha$ behavior with $\alpha \approx 1$ at large g for the Gell-Mann–Low function. © *2000 MAIK "Nauka/Interperiodica".*

PACS numbers: 11.10.-z

Many problems in theoretical physics require advance in the strong-coupling region. The best known of them concern the dependence of the effective coupling constant g on the distance scale L; the problems of electrodynamics at ultrashort distances and confinement are among them. The dependence of g on L in the renormalizable theories is determined by the equation

$$-dg/d\ln L = \beta(g) \tag{1}$$

and generally requires information on the Gell-Mann–Low function $\beta(g)$ for arbitrary g [1]. Over many years, the problem of reconstruction of the β-function seemed to be absolutely hopeless because the information on this function was provided solely by perturbation theory, which allowed the calculation of the first several terms of the expansion

$$\begin{gathered}\beta(g) = \sum_{N=0}^{\infty} \beta_N (-g)^N \\ = \beta_2 g^2 - \beta_3 g^3 + \ldots + \beta_N (-g)^N + \ldots, \\ \beta_0 = \beta_1 = 0.\end{gathered} \tag{2}$$

Lipatov [2] proposed a method allowing the calculation of the β_N asymptotics at large N, which was found to be factorial for most problems:

$$\beta_N^{as} = c a^N \Gamma(N+b) \approx c a^N N^{b-1} N! \tag{3}$$

Matching the Lipatov asymptotics (3) with the first β_N coefficients provides information on all terms of the series and makes it possible to approximately reconstruct the β-function, but this requires a special procedure for the summation of divergent series [3]. Kazakov *et al.* [4] attempted to implement this procedure and arrived at the conclusion that the Gell-Mann–Low function in the φ^4 theory with the action functional

$$S\{\varphi\} = \int d^4x \left\{ \frac{1}{2}(\partial\varphi)^2 + \frac{16\pi^2}{4!} g\varphi^4 \right\} \tag{4}$$

behaves at large g as $0.9g^2$, which differs only in the coefficient from the one-loop result $1.5g^2$ valid at $g \longrightarrow 0$; similar behavior was obtained for $\beta(g)$ by Kubyshin [5]. If this result is valid,[1] then the φ^4 theory is self-contradictory. This conclusion seems to be strange from the viewpoint of solid-state applications: a reasonable model of a disordered system [7, 8], well-defined in the continuous limit, is mathematically reduced to the φ^4 model. Moreover, it was recently proved [9] that there are no renormalization singularities in the φ^4 theory; and this can be treated as evidence for the self-consistency of the theory.

This paper is aimed at revising the results obtained in [4, 5]. We start with the same premises as in [5], i.e., with the known first four coefficients of the β-function expansion [6, 10]

$$\beta(g) = \frac{3}{2}g^2 - \frac{17}{6}g^3 + \frac{154.14}{8}g^4 - \frac{2338}{16}g^5 + \ldots, \tag{5}$$

and the Lipatov asymptotics with the first-order correction term calculated in [11]:

$$\beta_N = \frac{1.096}{16\pi^2} N^{7/2} N! \left\{ 1 - \frac{4.7}{N} + \ldots \right\}. \tag{6}$$

The method is different from [4, 5] in that a direct relation between the $\beta(g)$ asymptotics and the expansion coefficients is used and the interpolation is carried out in an explicit form.

[1] The authors of [4] do not insist on their statement and emphasize that it has a tentative character (see also [6]).

1. Let us formulate the problem of reconstruction of the β-function asymptotics

$$\beta(g) = \beta_\infty g^\alpha, \quad g \longrightarrow \infty \tag{7}$$

from the coefficients β_N of series (2) that grow according to factorial law (3) and are assumed to be numerically specified. As in the case of the introduction of critical indices in phase-transition theory, the slow (logarithmic) corrections to law (7) are considered to be beyond accuracy.

Treating the sum of series (2) in the Borel sense, we use a modified definition of the Borel transform $\beta(g)$:

$$\beta(g) = \int_0^\infty dx e^{-x} x^{b_0-1} B(gx), \quad B(g) = \sum_{N=0}^\infty B_N (-g)^N, \tag{8}$$
$$B_N = \frac{\beta_N}{\Gamma(N+b_0)},$$

where b_0 is an arbitrary parameter that is conveniently used for optimizing the summation procedure [3]. As was assumed in [3] and proved recently in [9], the Borel transform is analytical in the complex g plane with a cut from $-1/a$ to $-\infty$. To analytically continue $B(g)$ from the convergence circle $|g| < 1/a$ to arbitrary complex g values, a conformal transformation $g = f(u)$ mapping the plane with the cut onto the unit circle is used; in this case, the reexpansion of $B(g)$ in u powers

$$B(g) = \sum_{N=0}^\infty B_N (-g)^N\Big|_{g=f(u)} \longrightarrow B(u) = \sum_{N=0}^\infty U_N u^N \tag{9}$$

gives a series convergent at arbitrary g values. We restrict ourselves to the analytic continuation of $B(g)$ to the positive semiaxis [which is sufficient for the integration in Eq. (8)] and use a modified conformal transformation $g = (u/a)/(1-u)$ mapping the plane with cut $(-1/a, -\infty)$ onto the plane with cut $(1, \infty)$. This removes the $g = -1/a$ singularity to infinity, while the $g = \infty$ singularity becomes the nearest to the origin and determines the following asymptotics for the U_N coefficients:

$$U_N = \frac{\beta_\infty}{a^\alpha \Gamma(\alpha)\Gamma(b_0+\alpha)} N^{\alpha-1}, \quad N \longrightarrow \infty. \tag{10}$$

This result can easily be obtained by representing the expansion coefficients as

$$U_N = \oint_C \frac{du}{2\pi i} \frac{B(u)}{u^{N+1}} \tag{11}$$

and deforming the contour C enveloping the point $u = 0$ in such a way that it passes around the cut with allowance made for the singularity $B(u) \sim (1-u)^{-\alpha}$ at the point $u = 1$. The reexpansion of series (9) gives the following relation between U_N and B_N:

$$U_0 = B_0, \quad U_N = \sum_{K=1}^N B_K \left(-\frac{1}{a}\right)^K C_{N-1}^{K-1} \ (N \geq 1). \tag{12}$$

As a result, we arrive at the following simple algorithm: the coefficients B_N are calculated from given β_N [cf. Eq. (8)] and recalculated to U_N according to Eq. (12); then the U_N coefficients at large N are fitted to the power law $U_N = U_\infty N^{\alpha-1}$, whose parameters determine β_∞ and α according to Eq. (10). The β_∞ value is convenient to calculate by treating U_∞ as a function of b_0 and determining the slope of linear dependence $U_\infty \propto (b_0 + \alpha)$ at small $b_0 + \alpha$; this provides an independent estimate for the α index from the root of the $U_\infty(b_0)$ function.

2. The authors of the majority of works formulated the algorithm in such a way as to avoid mention of the coefficients β_N for intermediate N values. Such an approach is conceptually inconsistent, because a finite number of coefficients and their asymptotics can ensure the construction of a function with any prescribed behavior at infinity.[2] The problem can be reasonably formulated if *all* β_N are approximately defined; in this case, the function $\beta(g)$ can be reconstructed within a certain accuracy. For this reason, the interpolation and estimation of its accuracy is the necessary step in solving the problem. Of course, this is possible only on the assumption that β_N is a smooth function of N.

The interpolation is convenient to carry out for the reduced coefficient function

$$F_N = \frac{\beta_N}{\beta_N^{as}} = 1 + \frac{A_1}{N} + \frac{A_2}{N^2} + \ldots + \frac{A_K}{N^K} + \ldots, \tag{13}$$

which varies within the finite limits and has a regular expansion in $1/N$. Retaining in the series a finite number of terms and adjusting the coefficients A_K to the known F_N values, one obtains the desired interpolation formula. Its accuracy is

$$\delta F_N \sim \frac{A_{m+m_0+1}(N-L_0)(N-L_0-1)\ldots(N-L)}{N^{m+m_0+1}\, L(L-1)\ldots L_0}, \tag{14}$$

if the interpolation is performed using m known values $F_{L_0}, F_{L_0+1}, \ldots, F_L$ $(m = L - L_0 + 1)$ for m_0 known coefficients $A_1, A_2, \ldots, A_{m_0}$. Estimate (14) is based on the fact that series (13) is asymptotic [12], so that the error of its approximation by trincation is of the order of the first omitted term, while the error of interpolating the

[2] A function of a factorial series has the same asymptotics for coefficients (3), but with different c value [8]; the statement formulated in the text can easily be proved by choosing an appropriate linear combination of several functions.

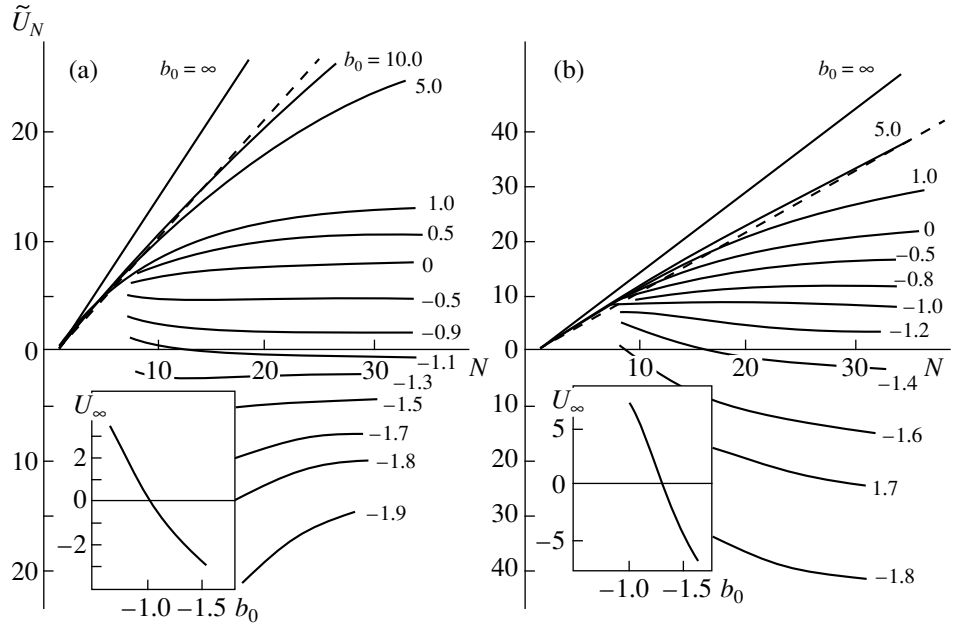

Fig. 1. Plots of $\tilde{U}_N = U_N\Gamma(b_0 + 2)$ vs. N at different b_0 values for the parametrization of the asymptotics in the form (a) $\beta_N^{as} = ca^N N^{b-1} N!$ and (b) $\beta_N^{as} = ca^N \Gamma(N + b)$. The inserts show U_∞ as a function of b_0.

$(m + m_0 + 1)$-order polynomial by the $(m + m_0)$-order polynomial can be calculated exactly. In the case under consideration, $L_0 = 2$, $L = 5$, and $m_0 = 1$, so that δF_N is determined by the coefficient A_6, which can be estimated by factorial-law extrapolation of the found $A_1, \ldots, A_5$ values [12].

The ambiguity of the interpolation procedure is manifested, in particular, in the possibility to differently parametrize the asymptotics [4, 13], e.g., as $ca^N\Gamma(N + b)$, $ca^N N^{b-1} N!$ etc. The asymptotics in the instanton calculations [2] has the form $\tilde{c}\tilde{a}^N N^{\tilde{b}} N^N$, which is very close to the Lipatov parametrization $ca^N N^{b-1} N!$ obtained from the former by applying the Stirling formula, whose accuracy is better than 10% even at $N = 1$. With this respect, the parametrization $ca^N N^{b-1} N!$ is "natural," whereas its representation in alternative functional forms requires additional assumptions [e.g., $N \gg b$ for $ca^N\Gamma(N + b)$].

Figure 1a shows the coefficients $\tilde{U}_N = U_N\Gamma(b_0 + 2)$ (normalized so that they have a finite limit at $b_0 \longrightarrow \infty$) for the natural parametrization $ca^N N^{b-1} N!$. At large N, these coefficients distinctly tend to the constant values (excepting the curves for $b_0 \gg 1$ and $b_0 \approx -2$, for which the large parameters retard the attainment of asymptotics), which corresponds to the value $\alpha = 1$. The U_∞ vs. b_0 curve goes through zero at $b_0 = -1.03$ (see insert in Fig. 1a), which gives another estimate $\alpha = 1.03$ demonstrating excellent consistency of the results. Determining β_∞ from the slope at $b_0 = -\alpha$, one obtains for the asymptotics of the β-function

$$\beta(g) \approx 8g \quad g \longrightarrow \infty. \tag{15}$$

A situation occurring at the alternative ways of interpolation is shown in Fig. 1b, where the parametrization $\beta_N^{as} = ca^N\Gamma(N + b)$ is used. There is also seen curve flattening, but it is not as distinct as in the preceding case. The processing of the curves under the assumption that $\alpha = 1$ yields the b_0 dependence of U_∞ (see insert in Fig. 1b) going through zero at $b_0 = -1.3$, which corresponds to $\alpha = 1.3$. Hence, the results show a substantial inconsistency. Curve processing with the power-law dependence yields an α value slightly exceeding unity (different for different b_0), but in this case U turns to zero at $b_0 = -0.8$ (at this value, the increase in the curves in Fig. 1b changes to a decrease), leading to the same inconsistency. Correspondingly, the result for the $\beta(g)$ asymptotics becomes less defined, $\beta(g) \approx 24g^\alpha$ and $\alpha = 0.8$–1.3.

Parametrizing the asymptotics as $\beta_N^{as} = ca^N N^{b-\tilde{b}-1}\Gamma(N + \tilde{b} + 1)$ and expanding F_N in inverse powers of $(N - N_0)$, one obtains a two-parameter ($\tilde{b}$ and N_0) set of the interpolation formulas. The table presents the results for several such interpolations, for which the distinctions in the interpolation curves approximately fit the error range estimated by Eq. (14) for the natural interpolation. With allowance made for the uncertain-

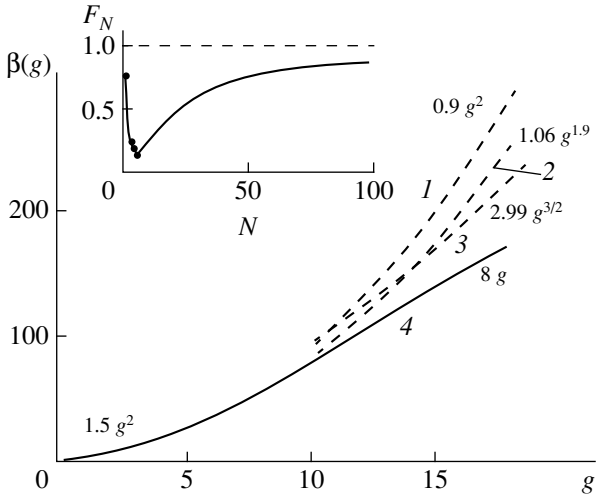

Fig. 2. Qualitative behavior of the Gell-Mann–Low function in the φ^4 theory. Curves *1*, *2*, *3*, and *4* are obtained in [4], [5], [14], and this work, respectively. The insert shows the coefficient function $F_N = \beta_N/\beta_N^{as}$ with the $\beta_N^{as} = ca^N\Gamma(N + b)$ parametrization convenient for an analysis of Eq. (12); the dependence on the interpolation procedure is immaterial on this scale.

ties, the α index is virtually independent of the particular interpolation; systematic deviations occur only for some "extreme" cases for which the interpolation curve is partially beyond the error range. The interpolation with $\tilde{b} = 0$ and $N_0 = 0$, which we treated as "natural" from computational considerations, stands out as the most self-consistent algorithm. Therefore, the corresponding result (15) should be considered as the most reliable. For a fixed interpolation, its error is less than 0.05 for the α index and 10% for β_∞, which is an optimistic estimate for the accuracy. The error caused by the interpolation ambiguity is seen from the table: it can be as great as several tenths for the α index, whereas the β_∞ value can differ from Eq. (15) by a factor of 2–3.

3. Let us consider the behavior of the β-function at finite g values. For $N < 10$, Fig. 1 demonstrates a linear portion $\tilde{U}_N \approx 1.1(N-1)$ (dashed line) corresponding to a $\beta(g) \approx 1.1g^2$ dependence close to the results obtained in [4, 5]. This portion is insensitive to changes in b_0 and to the interpolation procedure and can pretend to the role of the true asymptotics, provided that the results for $N > 10$ are treated as being due to the interpolation errors. But such is actually not the case, because the stability of this portion is caused by the presence of a characteristic dip in the reduced coefficient function F_N at $N \lesssim 10$ (see insert in Fig. 2). If one models this dip by setting $F_3 = F_4 = \ldots = F_{10} = 0$, then the result $\tilde{U}_N \approx 1.5(N-1)$ determined by the first nonvanishing coefficient F_2 (see curve for $b_0 = \infty$) is obtained at $N \leq 10$ for all b_0; this is close to the actual situation.[3] Such modeling of the dip demonstrates that the one-loop law $1.5g^2$ for the β-function extends up to $g \sim 10$. More precisely (see footnote 3), the result valid in the interval $1 \lesssim g \lesssim 10$ is given by the function derived in [4, 5] and yielding the value $\beta(g) \approx 90$ for $g = 10$ (see Fig. 2), in accordance with [14]. Asymptotics Eq. (15) matches well with the indicated value, providing indirect support to the optimistic estimation for the accuracy.

Although the available information allows only a rough estimation for the Gell-Mann–Low function, one can state with assurance that it is nonzero at finite g values and its behavior at $g \longrightarrow \infty$ is compatible with the assumption that the φ^4 theory is self-consistent. The substitution of Eq. (15) in Eq. (1) yields the $g(L) \propto L^{-\gamma}$ dependence with $\gamma \approx 8$ at small L, which is slightly modified if the α index is other than unity or if logarithmic branching is present.

The results obtained allow an understanding of why the numerical simulations on a lattice indicate that the φ^4 theory is "trivial" (see [15] and references therein): because of the absence of zeros of the β-function, the $g(L)$ interaction always decreases with distance; and, owing to the extended one-loop law, the behavior is indistinguishable from the trivial in a wide range of parameters [at $g \lesssim 300$, for the most popular charge definition when the term with interaction in Eq. (4) has the form $g\varphi^4/4$].

This work was supported by the INTAS (grant no. 96-0580) and the Russian Foundation for Basic Research (project no. 00-02-17129).

Table

Interpolation with $N_0 = 0$	β_∞	α	Interpolation with $\tilde{b} = 0$	β_∞	α
$\tilde{b} = 3.5$	24	0.8–1.3	$N_0 = 0.5$	5.4	1.1–1.6
$\tilde{b} = 1.5$	14	1.0–1.1	$N_0 = 0.3$	16	0.8–1.2
$\tilde{b} = 0$	8.1	1.0			
$\tilde{b} = -1.5$	10	1.0–1.1	$N_0 = -0.3$	4.3	0.9–1.0
$\tilde{b} = -2.5$	2.7	1.5–1.7	$N_0 = -0.5$	2.3	0.9–1.0

REFERENCES

1. N. N. Bogoliubov and D. V. Shirkov, *Introduction to the Theory of Quantized Fields*, 3rd ed. (Nauka, Moscow, 1984, 4th ed.; Wiley, New York, 1980, 3rd ed.).

[3] If one sets $F_3 = F_4 = \ldots = F_{10} = \epsilon$, then Eq. (12) yields a linear dependence with the slope $1.5(1 - \epsilon/F_2)$ for $b_0 = b - p$ with integer p in the interval $p + 2 \leq N \leq 10$. For $\epsilon = 0.2$ (see Fig. 2); the correct slope 1.1 and a weak dependence on b_0 occur in the interval $-1 < b_0 < 10$.

2. L. N. Lipatov, Zh. Éksp. Teor. Fiz. **72**, 411 (1977) [Sov. Phys. JETP **45**, 216 (1977)].
3. J. C. Le Guillou and J. Zinn-Justin, Phys. Rev. Lett. **39**, 95 (1977); Phys. Rev. B **21**, 3976 (1980).
4. D. I. Kazakov, O. V. Tarasov, and D. V. Shirkov, Teor. Mat. Fiz. **38**, 15 (1979).
5. Yu. A. Kubyshin, Teor. Mat. Fiz. **58**, 137 (1984).
6. A. A. Vladimirov and D. V. Shirkov, Usp. Fiz. Nauk **129**, 407 (1979) [Sov. Phys. Usp. **22**, 860 (1979)].
7. M. V. Sadovskiĭ, Usp. Fiz. Nauk **133**, 223 (1981) [Sov. Phys. Usp. **24**, 96 (1981)].
8. I. M. Suslov, Usp. Fiz. Nauk **168**, 503 (1998) [Phys. Usp. **41**, 441 (1998)].
9. I. M. Suslov, Zh. Éksp. Teor. Fiz. **116**, 369 (1999) [JETP **89**, 197 (1999)].
10. F. M. Dittes, Yu. A. Kubyshin, and O. V. Tarasov, Teor. Mat. Fiz. **37**, 66 (1978).
11. Yu. A. Kubyshin, Teor. Mat. Fiz. **57**, 363 (1983).
12. I. M. Suslov, Zh. Éksp. Teor. Fiz. **117** (2000) (in press).
13. V. S. Popov, V. L. Eletskiĭ, and A. V. Turbiner, Zh. Éksp. Teor. Fiz. **74**, 445 (1978) [Sov. Phys. JETP **47**, 232 (1978)].
14. A. N. Sissakian, I. L. Solovtsov, and O. P. Solovtsova, Phys. Lett. B **321**, 381 (1994).
15. A. Agodi, G. Andronico, P. Cea, *et al.*, Mod. Phys. Lett. A **12**, 1011 (1997); hep-ph/9702407.

Translated by R. Tyapaev

JETP Letters, Vol. 71, No. 6, 2000, pp. 222–226. From Pis'ma v Zhurnal Éksperimental'noĭ i Teoreticheskoĭ Fiziki, Vol. 71, No. 6, 2000, pp. 322–327.

FIELDS, PARTICLES, NUCLEI

Nonforward Color Octet BFKL Kernel[1]

V. S. Fadin and D. A. Gorbachev

Budker Institute of Nuclear Physics, Siberian Division, Russian Academy of Sciences, pr. Akademika Lavrent'eva 11, Novosibirsk, 630090 Russia

Novosibirsk State University, ul. Pirogova 2, Novosibirsk, 630090 Russia

Received February 11, 2000

The kernel of the nonforward BFKL equation is obtained in the case of the antisymmetric color octet state of the two Reggeized gluons in the t-channel. The explicit form of the kernel is presented. © *2000 MAIK "Nauka/Interperiodica".*

PACS numbers: 12.38.Bx

The most common basis for the description of the processes at small $x = Q^2/s$ values (Q^2 is a typical virtuality and $\sqrt{s}$ is the cms energy) in the framework of the perturbative QCD is the BFKL equation [1]. The equation was originally derived in the leading logarithmic approximation (LLA), which means the resummation of all terms of the type $[\alpha_s \ln s]^n$. Recently, the kernel of this equation was obtained in the next-to-leading approximation (NLA) [2] for the case of forward scattering, i.e., for the momentum transfer $t = 0$ and the vacuum quantum numbers in the t-channel. The next step should be the calculation of a nonforward kernel. In this paper, we present the nonforward kernel for the case of a gluon channel (antisymmetric color octet state of two Reggeized gluons). This channel is extremely important, because the derivation of the BFKL equation is based on one of the remarkable properties of QCD, viz., gluon Reggeization. The color octet kernel enters the "bootstrap" equations [3], appearing as the requirement for the compatibility of gluon Reggeization with s-channel unitarity.

We will consider pure gluodynamics, since the quark part of the kernel was calculated in [4]. We use the Sudakov decomposition for the particle momenta, assuming, without loss of generality, that the masses of the colliding particles with momenta p_A and p_B are equal to zero: $p_A^2 = p_B^2 = 0$, $(p_A + p_B)^2 = 2(p_A p_B) = s$. The BFKL equation is the equation for the Mellin transform of the Green's function of two Reggeized gluons. If the initial momenta of these gluons in the s-channel are $q_1 \simeq \beta p_A + q_{1\perp}$ and $-q_2 \simeq \alpha p_B - q_{2\perp}$ and the momentum transfer is $q \simeq q_\perp$, then the equation has the form [3]

$$\omega G_\omega^{(\mathcal{R})}(\mathbf{q}_1, \mathbf{q}_2, \mathbf{q}) = \mathbf{q}_1^2 \mathbf{q}_1'^2 \delta^{(D-2)}(\mathbf{q}_1 - \mathbf{q}_2) + \int \frac{d^{D-2} r}{\mathbf{r}^2 \mathbf{r}'^2} \mathcal{H}^{(\mathcal{R})}(\mathbf{q}_1, \mathbf{r}; \mathbf{q}) G_\omega^{(\mathcal{R})}(r, \mathbf{q}_2; \mathbf{q}), \quad (1)$$

where $\mathcal{R}$ denotes the representation of the color group in the t-channel. The transverse momenta are spacelike, and we use the vector sign for them. Here and below we use for brevity $v' \equiv v - q$ for any v. The space–time dimension $D = 4 + 2\epsilon$ is taken different from 4 to regularize the infrared divergences. We use the normalization adopted in [3].

The nonforward kernel, as well as the forward one, is given by the sum of a "virtual" part defined by the gluon trajectory $j(t) = 1 + \omega(t)$ and a "real" part $\mathcal{H}_r^{(\mathcal{R})}$ related to the real particle production in the Reggeon–Reggeon collisions:

$$\mathcal{H}^{(\mathcal{R})}(\mathbf{q}_1, \mathbf{q}_2; \mathbf{q}) = [\omega(-\mathbf{q}_1^2) + \omega(-\mathbf{q}_1'^2)] \times \mathbf{q}_1^2 \mathbf{q}_1'^2 \delta^{(D-2)}(\mathbf{q}_1 - \mathbf{q}_2) + \mathcal{H}_r^{(\mathcal{R})}(\mathbf{q}_1, \mathbf{q}_2; \mathbf{q}). \quad (2)$$

As is seen from Eq. (2), the gluon trajectory enters into the equation in the universal (independent of $\mathcal{R}$) way. It was calculated [5] in the NLA and we do not discuss it here. The real part for the gluon channel in the LLA is [1, 6]

$$\mathcal{H}_r^{(8)B}(\mathbf{q}_1, \mathbf{q}_2; \mathbf{q}) = \frac{g^2 N}{2(2\pi)^{D-1}} \left(\frac{\mathbf{q}_1^2 \mathbf{q}_2'^2 + \mathbf{q}_2^2 \mathbf{q}_1'^2}{(\mathbf{q}_1 - \mathbf{q}_2)^2} - \mathbf{q}^2 \right), \quad (3)$$

where the superscript B means the LLA (Born) approximation. It should be emphasized that in this paper we systematically use the perturbative expansion in terms

[1] This article was submitted by the authors in English.

of the bare coupling g. In the NLA, the real part of the kernel can be represented as [3]

$$\begin{aligned}\mathcal{H}_r^{(8)}(\mathbf{q}_1,\mathbf{q}_2;\mathbf{q}) &= \frac{f_{c_1c_1'c}f_{c_2c_2'c}}{2N(N^2-1)}\int_0^\infty \frac{ds_{RR}}{(2\pi)^D}\theta(s_\Lambda - s_{RR})\\ &\times\sum_{\{f\}}\int\gamma_{c_1c_2}^{\{f\}}(q_1,q_2)\left(\gamma_{c_1'c_2'}^{\{f\}}(q_1',q_2')\right)^* d\rho_f\\ &-\frac{1}{2}\int\frac{d^{D-2}r}{\mathbf{r}^2\mathbf{r}'^2}\mathcal{H}_r^{(8)B}(\mathbf{q}_1,\mathbf{r};\mathbf{q})\mathcal{H}_r^{(8)B}(\mathbf{r},\mathbf{q}_2;\mathbf{q})\\ &\times\ln\left(\frac{s_\Lambda^2}{(\mathbf{r}-\mathbf{q}_1)^2(\mathbf{r}-\mathbf{q}_2)^2}\right).\end{aligned} \tag{4}$$

Here, f_{abc} are the group structure constants; N is the number of colors ($N = 3$ in QCD); $s_{RR} = (q_1 - q_2)^2 = s\alpha\beta - (\mathbf{q}_1 - \mathbf{q}_2)^2$ is the squared invariant mass of the Reggeons; the sum $\{f\}$ goes over all states f produced in the Reggeon–Reggeon collisions and over all discrete quantum numbers of these states; $\gamma_{c_1c_2}^{\{f\}}(q_1, q_2)$ is the effective vertex for the production of the state f; and $d\rho_f$ is the phase-space element for this state,

$$\begin{aligned}d\rho_f &= \frac{1}{n!}(2\pi)^D\delta^{(D)}\left(q_1-q_2-\sum_{i\in f}k_i\right)\\ &\times\prod_{i\in f}\frac{d^{D-1}k_i}{(2\pi)^{(D-1)}2\epsilon_i},\end{aligned} \tag{5}$$

where n is the number of identical particles in the state f. The second term on the rhs of Eq. (4) serves as the subtraction of the contribution from the region of large s_{RR} to the first term, in order to avoid double counting of this region in the BFKL equation. The intermediate s_Λ parameter in Eq. (4) must be taken tending to infinity. At large s_{RR}, only the contribution of the two-gluon production survives in the first integral, so that the dependence on s_Λ disappears in Eq. (4) due to the factorization property of the two-gluon production vertex [3]. In the LLA, only the one-gluon production contributes, and Eq. (4) gives for the kernel its LLA value (3); in the NLA, the contributing states also include the two-gluon and the quark–antiquark states. The normalization of the corresponding vertices is defined in [3].

The gluon contribution to the Reggeon–Reggeon–gluon vertex in the limit $\epsilon \longrightarrow 0$ was calculated in [7]. Substituting the results of [7] in Eq. (4), we obtain for the contribution to the kernel from the one-gluon production in the Reggeon–Reggeon collisions

$$\begin{aligned}\mathcal{H}_{RRG}^{(8)}(\mathbf{q}_1,\mathbf{q}_2;\mathbf{q}) &= \frac{g^2N}{2(2\pi)^{D-1}}\\ &\times\left\{\left(\frac{\mathbf{q}_1^2\mathbf{q}_2'^2+\mathbf{q}_1'^2\mathbf{q}_2^2}{\mathbf{k}^2}-\mathbf{q}^2\right)\left(\frac{1}{2}+\frac{g^2N\Gamma(1-\epsilon)}{2(4\pi)^{2+\epsilon}}\right.\right.\\ &\left.\times\left[-(\mathbf{k}^2)^\epsilon\left(\frac{2}{\epsilon^2}-\pi^2+4\epsilon\zeta(3)\right)-\ln^2\left(\frac{\mathbf{q}_1^2}{\mathbf{q}_2^2}\right)\right]\right)\\ &+\frac{g^2N\Gamma(1-\epsilon)}{6(4\pi)^{2+\epsilon}}\left(\left[\frac{\mathbf{q}_1'^2-\mathbf{q}_2'^2}{\mathbf{q}_1^2-\mathbf{q}_2^2}\right.\right.\\ &\left.-\frac{\mathbf{k}^2}{(\mathbf{q}_1^2-\mathbf{q}_2^2)^2}(\mathbf{q}_1^2+\mathbf{q}_2^2+4\mathbf{q}_1'\mathbf{q}_2'-2\mathbf{q}^2)\right]\\ &\times\left[\frac{2\mathbf{q}_1^2\mathbf{q}_2^2}{\mathbf{q}_1^2-\mathbf{q}_2^2}\ln\left(\frac{\mathbf{q}_1^2}{\mathbf{q}_2^2}\right)-\mathbf{q}_1^2-\mathbf{q}_2^2\right]\\ &+11\left[\frac{2\mathbf{q}_1^2\mathbf{q}_2^2}{\mathbf{q}_1^2-\mathbf{q}_2^2}+\frac{\mathbf{q}_1^2\mathbf{q}_2'^2-\mathbf{q}_1'^2\mathbf{q}_2^2}{\mathbf{k}^2}-\frac{\mathbf{q}_1^2+\mathbf{q}_2^2}{\mathbf{q}_1^2-\mathbf{q}_2^2}\mathbf{q}^2\right]\\ &\left.\left.\times\ln\left(\frac{\mathbf{q}_1^2}{\mathbf{q}_2^2}\right)-2\mathbf{q}_1'\mathbf{q}_2'\right)\right\}+\frac{g^2N}{2(2\pi)^{D-1}}\left\{\mathbf{q}_i\longleftrightarrow\mathbf{q}_i'\right\},\end{aligned} \tag{6}$$

where $\mathbf{k} = \mathbf{q}_1 - \mathbf{q}_2$, $\Gamma(x)$ is the Euler gamma function, and $\zeta(\eta)$ is the Riemann zeta function. The effective vertex for the two-gluon production in the Reggeon–Reggeon collisions was calculated in [8]. The contribution to the kernel from the two-gluon production can be obtained by substituting the results of [8] in Eq. (4), taking the sum over the color and spin states of the produced gluons, and performing integration. Unfortunately, the integral (4) cannot be expressed in terms of elementary functions (and dilogarithms) at arbitrary ϵ. For this reason, we present the result (see details of the calculation in [9]) in a "combined" form, leaving untouched the terms which cannot be integrated in elementary functions:

$$\begin{aligned}\mathcal{H}_{RRGG}^{(8)}(\mathbf{q}_1,\mathbf{q}_2;\mathbf{q}) &= \frac{4g^4N^2\Gamma(1-\epsilon)}{(4\pi)^D\pi^{1+\epsilon}}\frac{\Gamma^2(1+\epsilon)}{\Gamma(1+2\epsilon)}\\ &\times\left\{\frac{(\mathbf{k}^2)^{\epsilon-1}}{4\epsilon}\left[(\mathbf{q}_1'^2\mathbf{q}_2^2+\mathbf{q}_2'^2\mathbf{q}_1^2)\left(\frac{1}{\epsilon}+\psi(1)+\psi(1+\epsilon)\right.\right.\right.\end{aligned}$$

$$-2\psi(1+2\epsilon)-\frac{11+7\epsilon}{2(1+2\epsilon)(3+2\epsilon)}\Big)-\frac{\mathbf{q}^2\mathbf{k}^2}{\epsilon}\Big]$$

$$+\frac{(\mathbf{q}^2)^{\epsilon+1}}{4\epsilon}\Big(-\frac{1}{\epsilon}+\psi(1)-\psi(1-\epsilon)+2\psi(1+\epsilon)$$

$$-2\psi(1+2\epsilon)-\frac{11+7\epsilon}{2(1+2\epsilon)(3+2\epsilon)}\Big)$$

$$-\frac{11+7\epsilon}{4\epsilon(1+2\epsilon)(3+2\epsilon)}\mathbf{q}_1^2\mathbf{q}_2^2$$

$$\times\frac{(\mathbf{q}_1^2)^\epsilon-(\mathbf{q}_2^2)^\epsilon}{\mathbf{q}_1^2-\mathbf{q}_2^2}+\frac{\mathbf{q}^2}{\epsilon(1+2\epsilon)}\frac{(\mathbf{q}_1^2)^{\epsilon+1}-(\mathbf{q}_2^2)^{\epsilon+1}}{\mathbf{q}_1^2-\mathbf{q}_2^2} \quad (7)$$

$$+\frac{\mathbf{q}^2}{4\epsilon}\Big(\frac{1}{2\epsilon}-\psi(1+\epsilon)+\psi(1+2\epsilon)\Big)((\mathbf{q}_1^2)^\epsilon+(\mathbf{q}_2^2)^\epsilon)$$

$$+\frac{1}{8\epsilon(1+2\epsilon)(3+2\epsilon)}\Big[(2(1+\epsilon)\mathbf{q}_1^2\mathbf{q}_2^2((\mathbf{q}_1^2)^\epsilon-(\mathbf{q}_2^2)^\epsilon)$$

$$-\epsilon(\mathbf{q}_1^2+\mathbf{q}_2^2)((\mathbf{q}_1^2)^{\epsilon+1}-(\mathbf{q}_2^2)^{\epsilon+1}))\Big(\frac{\mathbf{k}^2}{(\mathbf{q}_1^2-\mathbf{q}_2^2)^3}(\mathbf{q}_1^2+\mathbf{q}_2^2$$

$$+2\mathbf{q}_1'^2+2\mathbf{q}_2'^2-2\mathbf{k}^2-2\mathbf{q}^2)-\frac{\mathbf{q}_1'^2-\mathbf{q}_2'^2}{(\mathbf{q}_1^2-\mathbf{q}_2^2)^2}\Big)$$

$$+\frac{(\mathbf{q}_1^2)^{\epsilon+1}-(\mathbf{q}_2^2)^{\epsilon+1}}{\mathbf{q}_1^2-\mathbf{q}_2^2}(\epsilon(\mathbf{q}_1'^2+\mathbf{q}_2'^2-\mathbf{k}^2)-2(1+\epsilon)\mathbf{q}^2)\Big]$$

$$+\frac{\Gamma(1+2\epsilon)}{4\Gamma^2(1+\epsilon)}I(\mathbf{q}_1,\mathbf{q}_2;\mathbf{q})\Big\}+\frac{4g^4N^2}{(4\pi)^D\pi^{1+\epsilon}}\Gamma(1-\epsilon)$$

$$\times\frac{\Gamma^2(1+\epsilon)}{\Gamma(1+2\epsilon)}\{q_1\longleftrightarrow q_1',\ q_2\longleftrightarrow q_2'\},$$

where $\psi(x)=\Gamma'(x)/\Gamma(x)$ and

$$I(\mathbf{q}_1,\mathbf{q}_2;\mathbf{q})=4\hat{\mathcal{S}}\int_0^1\frac{dx}{x(1-x)_+}\int\frac{d^{2+2\epsilon}k_1}{\pi^{1+\epsilon}\Gamma(1-\epsilon)}\Big(\frac{x\mathbf{q}_2^2}{2\mathbf{\Lambda}^2\tilde{t}_1}$$

$$\times\Big[\frac{x(\mathbf{q}_1^2(\mathbf{k}_1\mathbf{q}_1')-\mathbf{q}_1'^2(\mathbf{k}_1\mathbf{q}_1))}{\mathbf{k}_1^2}-(\mathbf{q}\mathbf{q}_1')\Big]-\frac{x^2(1-x)}{4\mathbf{\Lambda}^2\tilde{t}_1}$$

$$\times\Big[\frac{\mathbf{q}_1'^2\mathbf{q}_2^4}{\Sigma}+\frac{\mathbf{q}_1^4\mathbf{q}_2'^2-\mathbf{q}_1^2\mathbf{q}^2\mathbf{k}^2}{\mathbf{k}_1^2}\Big]\Big)-\frac{\Gamma^2(\epsilon)}{\Gamma(2\epsilon)}\frac{(\mathbf{k}^2)^{\epsilon-1}}{2\epsilon} \quad (8)$$

$$\times(\mathbf{q}_1^2\mathbf{q}_2'^2+\mathbf{q}_2^2\mathbf{q}_1'^2-\mathbf{q}^2\mathbf{k}^2)-\frac{(\mathbf{q}^2)^2}{4}\frac{1}{\pi^{1+\epsilon}\Gamma(\Gamma-\epsilon)}$$

$$\times\int\frac{d^{2+2\epsilon}l}{(\mathbf{q}_1-\mathbf{l})^2(\mathbf{q}_1'-\mathbf{l})^2}\ln\Big(\frac{\mathbf{l}^2(\mathbf{l}-\mathbf{k})^2}{\mathbf{q}^4}\Big).$$

Here, $\hat{\mathcal{S}}$ denotes the operator of symmetrization with respect to the substitution $\mathbf{q}_1\longleftrightarrow-\mathbf{q}_2$, $\mathbf{q}_1'\longleftrightarrow-\mathbf{q}_2'$; $(1-x)_+$ means the subtraction

$$\int_0^1\frac{dx}{(1-x)_+}f(x)\equiv\int_0^1\frac{dx}{(1-x)}[f(x)-f(1)]; \quad (9)$$

$$\Sigma=(1-x)\mathbf{k}_1^2+x(\mathbf{k}-\mathbf{k}_1)^2;$$
$$\tilde{t}_1=-\frac{1}{x}((1-x)\mathbf{k}_1^2+x(\mathbf{k}_1-\mathbf{q}_1)^2); \quad (10)$$

and $\mathbf{\Lambda}=\mathbf{k}_1-x\mathbf{k}$. In the limit $\epsilon\longrightarrow 0$, we have

$$\mathcal{H}^{(8)}_{RRGG}(\mathbf{q}_1,\mathbf{q}_2;\mathbf{q})=\frac{g^4N^2\Gamma(1-\epsilon)}{(4\pi)^D\pi^{1+\epsilon}}$$

$$\times\Big\{(\mathbf{k}^2)^{\epsilon-1}(\mathbf{q}_1'^2\mathbf{q}_2^2+\mathbf{q}_2'^2\mathbf{q}_1^2-\mathbf{q}^2\mathbf{k}^2)\Big(\frac{1}{\epsilon^2}-\frac{11}{6\epsilon}+\frac{67}{18}$$

$$-4\zeta(2)+\epsilon\Big(-\frac{202}{27}+9\zeta(3)+\frac{11}{6}\zeta(2)\Big)\Big)$$

$$+\mathbf{q}^2\Big[\frac{1}{2}\Big(\frac{1}{\epsilon}+\ln\mathbf{q}^2\Big)\ln\Big(\frac{\mathbf{q}_1^2\mathbf{q}_2^2}{\mathbf{q}^4}\Big)-2\zeta(2)$$

$$+\frac{11}{6}\Big(\ln\Big(\frac{\mathbf{q}_1^2\mathbf{q}_2^2}{\mathbf{k}^2\mathbf{q}^2}\Big)+\frac{\mathbf{q}_1^2+\mathbf{q}_2^2}{\mathbf{q}_1^2-\mathbf{q}_2^2}\ln\Big(\frac{\mathbf{q}_1^2}{\mathbf{q}_2^2}\Big)\Big) \quad (11)$$

$$+\frac{1}{4}\ln^2\Big(\frac{\mathbf{q}_1^2}{\mathbf{q}^2}\Big)+\frac{1}{4}\ln^2\Big(\frac{\mathbf{q}_2^2}{\mathbf{q}^2}\Big)\Big]+\frac{\mathbf{q}_1\mathbf{q}_2}{3}-\frac{11}{6}(\mathbf{q}_1^2+\mathbf{q}_2^2)$$

$$-\frac{1}{6}\Big(11-\frac{\mathbf{k}^2}{(\mathbf{q}_1^2-\mathbf{q}_2^2)^2}(\mathbf{q}_1^2+\mathbf{q}_2^2+4(\mathbf{q}_1'\mathbf{q}_2')-2\mathbf{q}^2)$$

$$+\frac{\mathbf{q}_1'^2-\mathbf{q}_2'^2}{\mathbf{q}_1^2-\mathbf{q}_2^2}\Big)\Big(\frac{2\mathbf{q}_1^2\mathbf{q}_2^2}{\mathbf{q}_1^2-\mathbf{q}_2^2}\ln\Big(\frac{\mathbf{q}_1^2}{\mathbf{q}_2^2}\Big)-\mathbf{q}_1^2-\mathbf{q}_2^2\Big)$$

$$+I(\mathbf{q}_1,\mathbf{q}_2;\mathbf{q})\Big\}+\frac{g^4N^2\Gamma(1-\epsilon)}{(4\pi)^D\pi^{1+\epsilon}}\{\mathbf{q}_i\longleftrightarrow\mathbf{q}_i'\}.$$

In this limit, the function $I(\mathbf{q}_1, \mathbf{q}_2; \mathbf{q})$ takes the form

$$I(\mathbf{q}_1, \mathbf{q}_2; \mathbf{q}) = \frac{1}{2}\int_0^1 \frac{dx}{(\mathbf{q}_1(1-x)+\mathbf{q}_2 x)^2}$$
$$\times \ln\left(\frac{\mathbf{q}_1^2(1-x)+\mathbf{q}_2^2 x}{\mathbf{k}^2 x(1-x)}\right)\Bigg[\mathbf{q}^2(\mathbf{k}^2-\mathbf{q}_1^2-\mathbf{q}_2^2)+2\mathbf{q}_1^2\mathbf{q}_2^2$$
$$-\mathbf{q}_1^2\mathbf{q}_2'^2-\mathbf{q}_2^2\mathbf{q}_1'^2+\frac{\mathbf{q}_1^2\mathbf{q}_2'^2-\mathbf{q}_2^2\mathbf{q}_1'^2}{\mathbf{k}^2}(\mathbf{q}_1^2-\mathbf{q}_2^2)\Bigg] \quad (12)$$
$$+\frac{\mathbf{q}^2}{2}\left(4\zeta(2)-\frac{1}{2}\ln^2\left(\frac{\mathbf{q}_1^2}{\mathbf{q}_2^2}\right)\right)-\frac{\mathbf{q}_1^2\mathbf{q}_2'^2-\mathbf{q}_2^2\mathbf{q}_1'^2}{4\mathbf{k}^2}\ln\left(\frac{\mathbf{q}_1^2}{\mathbf{q}_2^2}\right)$$
$$\times\ln\left(\frac{\mathbf{q}_1^2\mathbf{q}_2^2}{\mathbf{k}^4}\right)-\frac{\mathbf{q}^2}{2}\Bigg[\left(\frac{1}{\epsilon}+\ln\mathbf{q}^2\right)\ln\left(\frac{\mathbf{q}_1^2\mathbf{q}_2^2\mathbf{q}_1'^2\mathbf{q}_2'^2}{\mathbf{q}^8}\right)$$
$$+\frac{1}{2}\ln^2\left(\frac{\mathbf{q}_1^2}{\mathbf{q}_1'^2}\right)+\frac{1}{2}\ln^2\left(\frac{\mathbf{q}_2^2}{\mathbf{q}_2'^2}\right)\Bigg].$$

The integral in Eq. (12) can be recast as

$$\int_0^1 \frac{dx}{(\mathbf{q}_1(1-x)+\mathbf{q}_2 x)^2}\ln\left(\frac{\mathbf{q}_1^2(1-x)+\mathbf{q}_2^2 x}{\mathbf{k}^2 x(1-x)}\right)$$
$$=\int_0^\infty \frac{dz}{z+\mathbf{k}^2}\frac{1}{\sqrt{(\mathbf{q}_1^2+\mathbf{q}_2^2+z)^2-4\mathbf{q}_1^2\mathbf{q}_2^2}} \quad (13)$$
$$\times\ln\left(\frac{\mathbf{q}_1^2+\mathbf{q}_2^2+z+\sqrt{(\mathbf{q}_1^2+\mathbf{q}_2^2+z)^2-4\mathbf{q}_1^2\mathbf{q}_2^2}}{\mathbf{q}_1^2+\mathbf{q}_2^2+z-\sqrt{(\mathbf{q}_1^2+\mathbf{q}_2^2+z)^2-4\mathbf{q}_1^2\mathbf{q}_2^2}}\right).$$

It is also possible to express the integral in Eq. (12) in terms of dilogarithms, but this expression is not very convenient:

$$\int_0^1 \frac{dx}{(\mathbf{q}_1(1-x)+\mathbf{q}_2 x)^2}\ln\left(\frac{\mathbf{q}_1^2(1-x)+\mathbf{q}_2^2 x}{\mathbf{k}^2 x(1-x)}\right)$$
$$=-\frac{2}{|\mathbf{q}_1||\mathbf{q}_2|\sin\phi} \quad (14)$$
$$\times\left[\ln\rho\arctan\frac{\rho\sin\phi}{1-\rho\cos\phi}+\mathrm{Im}(L(\rho\exp i\phi))\right],$$

where ϕ is the angle between $\mathbf{q}_1$ and $\mathbf{q}_2$ and

$$\rho = \min\left(\frac{|\mathbf{q}_1|}{|\mathbf{q}_2|}, \frac{|\mathbf{q}_2|}{|\mathbf{q}_1|}\right), \quad L(z) = \int_0^z \frac{dt}{t}\ln(1-t). \quad (15)$$

The real part of the kernel, related to real particle production in the Reggeon–Reggeon collisions, is given in the NLA by the one- and two-gluon contributions. Since the radiative corrections to the effective vertex of the one-gluon production are known only in the limit $\epsilon \longrightarrow 0$, the total real part of the kernel can be obtained only in this limit. It is given by the sum of Eqs. (6) and (11). After powerful cancellations (in particular, of the terms with singularities $1/\epsilon^2$ and all terms with $\mathbf{q}_1^2 - \mathbf{q}_2^2$ in the denominators), we obtain

$$\mathcal{H}_r^{(8)}(\mathbf{q}_1, \mathbf{q}_2; \mathbf{q}) = \frac{g^2 N}{2(2\pi)^{D-1}}\Bigg\{\left(\frac{\mathbf{q}_1^2\mathbf{q}_2'^2+\mathbf{q}_1'^2\mathbf{q}_2^2}{\mathbf{k}^2}-\mathbf{q}^2\right)$$
$$\times\left(\frac{1}{2}+\frac{g^2 N\Gamma(1-\epsilon)(\mathbf{k}^2)^\epsilon}{(4\pi)^{2+\epsilon}}\left(-\frac{11}{6\epsilon}+\frac{67}{18}-\zeta(2)\right.\right.$$
$$\left.\left.+\epsilon\left(-\frac{202}{27}+7\zeta(3)+\frac{11}{6}\zeta(2)\right)\right)\right)+\frac{g^2 N\Gamma(1-\epsilon)}{(4\pi)^{2+\epsilon}}$$
$$\times\Bigg[\mathbf{q}^2\left(\frac{11}{6}\ln\left(\frac{\mathbf{q}_1^2\mathbf{q}_2^2}{\mathbf{q}^2\mathbf{k}^2}\right)+\frac{1}{4}\ln\left(\frac{\mathbf{q}_1^2}{\mathbf{q}^2}\right)\ln\left(\frac{\mathbf{q}_1'^2}{\mathbf{q}^2}\right)+\frac{1}{4}\ln\left(\frac{\mathbf{q}_2^2}{\mathbf{q}^2}\right)\right.$$
$$\left.\times\ln\left(\frac{\mathbf{q}_2'^2}{\mathbf{q}^2}\right)+\frac{1}{4}\ln^2\left(\frac{\mathbf{q}_1^2}{\mathbf{q}_2^2}\right)\right)-\frac{\mathbf{q}_1^2\mathbf{q}_2'^2+\mathbf{q}_2^2\mathbf{q}_1'^2}{2\mathbf{k}^2}\ln\left(\frac{\mathbf{q}_1^2}{\mathbf{q}_2^2}\right) \quad (16)$$
$$+\frac{\mathbf{q}_1^2\mathbf{q}_2'^2-\mathbf{q}_2^2\mathbf{q}_1'^2}{\mathbf{k}^2}\ln\left(\frac{\mathbf{q}_1^2}{\mathbf{q}_2^2}\right)\left(\frac{11}{6}-\frac{1}{4}\ln\left(\frac{\mathbf{q}_1^2\mathbf{q}_2^2}{\mathbf{k}^4}\right)\right)$$
$$+\frac{1}{2}\Bigg[\mathbf{q}^2(\mathbf{k}^2-\mathbf{q}_1^2-\mathbf{q}_2^2)+2\mathbf{q}_1^2\mathbf{q}_2^2-\mathbf{q}_1^2\mathbf{q}_2'^2-\mathbf{q}_2^2\mathbf{q}_1'^2$$
$$+\frac{\mathbf{q}_1^2\mathbf{q}_2'^2-\mathbf{q}_2^2\mathbf{q}_1'^2}{\mathbf{k}^2}(\mathbf{q}_1^2-\mathbf{q}_2^2)\Bigg]\int_0^1\frac{dx}{(\mathbf{q}_1(1-x)+\mathbf{q}_2 x)^2}$$
$$\times\ln\left(\frac{\mathbf{q}_1^2(1-x)+\mathbf{q}_2^2 x}{\mathbf{k}^2 x(1-x)}\right)\Bigg]\Bigg\}+\frac{g^2 N}{2(2\pi)^{D-1}}\{\mathbf{q}_i \longleftrightarrow \mathbf{q}_i'\}.$$

After the cancellation of the terms $\sim 1/\epsilon^2$, the leading singularity in the kernel is $1/\epsilon$. It again turns into $\sim 1/\epsilon^2$ after subsequent integrations of the kernel because of the singular behavior of the kernel at $\mathbf{k}^2 = 0$. The additional singularity arises from the region of small $\mathbf{k}^2$, where $\epsilon|\ln\mathbf{k}^2| \sim 1$. Therefore, we do not expand the term $(\mathbf{k}^2)^\epsilon$ in ϵ. The terms $\sim\epsilon$ are taken into account in the coefficient of the expression divergent at $\mathbf{k}^2 = 0$ in order to retain, after the integrations, all contributions not vanishing in the limit $\epsilon \longrightarrow 0$.

In conclusion, note that in [10] the octet kernel was obtained using the bootstrap relation and the specific ansatz as a basis for its solution. Our results disagree with the results obtained in [10]. To make sure of the disagreement it would suffice to realize that the kernel obtained in [10] is expressed in terms of elementary functions. We conclude that the ansatz used in [10] is not correct.

REFERENCES

1. V. S. Fadin, E. A. Kuraev, and L. N. Lipatov, Phys. Lett. B **60**, 50 (1975); E. A. Kuraev, L. N. Lipatov, and V. S. Fadin, Zh. Éksp. Teor. Fiz. **71**, 840 (1976) [Sov. Phys. JETP **44**, 443 (1976)]; Zh. Éksp. Teor. Fiz. **72**, 377 (1977) [Sov. Phys. JETP **45**, 199 (1977)]; Ya. Ya. Balitskiĭ and L. N. Lipatov, Yad. Fiz. **28**, 1597 (1978) [Sov. J. Nucl. Phys. **28**, 822 (1978)].
2. V. S. Fadin and L. N. Lipatov, Phys. Lett. B **429**, 127 (1998); M. Ciafaloni and G. Camici, Phys. Lett. B **430**, 349 (1998).
3. V. S. Fadin and R. Fiore, Phys. Lett. B **440**, 359 (1998).
4. V. S. Fadin, R. Fiore, and A. Papa, Phys. Rev. D **60**, 074025 (1999).
5. V. S. Fadin, Pis'ma Zh. Éksp. Teor. Fiz. **61**, 342 (1995) [JETP Lett. **62**, 346 (1995)]; V. S. Fadin, R. Fiore, and A. Quartarolo, Phys. Rev. D **53**, 2729 (1996); M. I. Kotsky and V. S. Fadin, Yad. Fiz. **59**, 1080 (1996) [Phys. At. Nucl. **59**, 1035 (1996)]; V. S. Fadin, R. Fiore, and M. I. Kotsky, Phys. Lett. B **359**, 181 (1995); Phys. Lett. B **387**, 593 (1996).
6. V. S. Fadin, Preprint No. 98-55, IYaF RAN (Budker Institute of Nuclear Physics, Siberian Division, Russian Academy of Sciences, Novosibirsk, 1998); hep-ph/9807528; talk given at the International Conference "LISHEP98," Rio de Janeiro, 1998.
7. L. N. Lipatov and V. S. Fadin, Pis'ma Zh. Éksp. Teor. Fiz. **49**, 311 (1989) [JETP Lett. **49**, 352 (1989)]; Yad. Fiz. **50**, 1141 (1989) [Sov. J. Nucl. Phys. **50**, 712 (1989)]; V. S. Fadin and L. N. Lipatov, Nucl. Phys. B **406**, 259 (1993); V. S. Fadin, R. Fiore, and M. I. Kotsky, Phys. Lett. B **389**, 737 (1996).
8. V. S. Fadin and L. N. Lipatov, Nucl. Phys. B **477**, 767 (1996); V. S. Fadin, M. A. Kotsky, and L. N. Lipatov, Phys. Lett. B **415**, 97 (1997); Yad. Fiz. **61**, 716 (1998) [Phys. At. Nucl. **61**, 641 (1998)].
9. V. S. Fadin and D. A. Gorbachev, Preprint No. 99-115, IYaF RAN (Budker Institute of Nuclear Physics, Siberian Division, Russian Academy of Sciences, Novosibirsk, 1999).
10. M. Braun and G. P. Vacca, Phys. Lett. B **454**, 319 (1999).

JETP Letters, Vol. 71, No. 6, 2000, pp. 227–230. From Pis'ma v Zhurnal Éksperimental'noĭ i Teoreticheskoĭ Fiziki, Vol. 71, No. 6, 2000, pp. 328–332.

FIELDS, PARTICLES, NUCLEI

Compton Tensor with Heavy Photon for Longitudinally Polarized Electron with Next-to-Leading Accuracy[1]

G. I. Gakh, M. I. Konchatnij, and N. P. Merenkov

Kharkov Institute of Physics and Technology, Ukrainian Scientific Center, Akademicheskaya ul. 1, Kharkiv, 310108 Ukraine

Received February 15, 2000

Compton tensor for scattering of a longitudinally polarized electron by a heavy photon is considered. The result obtained can be used for the analysis of electromagnetic corrections to the spin–spin correlation in quasi-elastic and deep inelastic scattering with next-to-leading accuracy. © *2000 MAIK "Nauka/Interperiodica".*

PACS numbers: 12.20.Ds

1. Recent polarized experiments on deep inelastic scattering [1, 2] cover the kinematic region of the Bjorken variable $y \simeq 0.9$, where the electromagnetic corrections to the cross section are extremely large. Within the framework of the one-photon-exchange approximation, the squared matrix element for the DIS process can be written as a contraction of leptonic $L_{\mu\nu}$ and hadronic $H_{\mu\nu}$ tensors

$$|M|^2 = \frac{1}{q^4} L_{\mu\nu} H_{\mu\nu}, \tag{1}$$

where q is the transferred momentum. The model-independent radiative correction implies the corresponding correction to the leptonic tensor on the right-hand side of Eq. (1). The first-order QED correction to $L_{\mu\nu}$ includes contributions from the real and virtual single photon emission. It was computed in [3] and was found to be of the order of unity at large values of the y variable. Therefore, the calculation of the second-order QED correction to $L_{\mu\nu}$ becomes very important for the interpretation of the polarized experiments in terms of hadronic structure functions.

The second-order correction to the leptonic tensor includes the contributions from the e^+e^--pair production [4], double hard-photon emission [5], one-loop-corrected single-photon emission [6], and two-loop vertex function [7]. In the case of a longitudinally polarized electron beam, all these contributions are known with next-to-leading accuracy, except for the one due to the one-loop-corrected single-photon emission (Compton tensor). The calculation performed in [6] corresponded to the case when a hard photon is radiated at large angle to the 3-momentum of both the initial and scattered electron. Therefore, some contributions that can be essential at small angles were omitted in [6]. The goal of our letter is to calculate these contributions.

[1] This article was submitted by the authors in English.

2. We define the Compton tensor for the process

$$e^-(p_1) + \gamma^*(q) \longrightarrow \gamma(k_1) + e^-(p_2) \tag{2}$$

in the following way:

$$L_{\mu\nu} = -\frac{1}{4}\mathrm{Sp}(\hat{p}_2 + m)[Q^{(0)}_{\mu\rho} + Q^{(1)}_{\mu\rho}](\hat{p}_1 + m) \times \left[1 + \eta\gamma_5\left(1 + \frac{m\hat{g}}{p_1 g}\right)\right][Q^{(0)}_{\nu\rho} + Q^{(1)}_{\nu\rho}]^+, \tag{3}$$

where $m(\eta)$ is the electron mass (doubled helicity of the initial electron) and 4-vector g has components ε, $-\mathbf{p}$, provided that 4-vector $p_1 = (\varepsilon, \mathbf{p})$. The $Q^{(0)}_{\mu\rho}$ tensor describes the Born approximation for the amplitude of the process {for the corresponding Born and one-loop-corrected Feynman diagrams of process (2), see [6, 8]} and has the form

$$Q^{(0)}_{\mu\rho} = \gamma_\mu \frac{(\hat{p}_2 - \hat{q} + m)}{t}\gamma_\rho + \gamma_\rho \frac{(\hat{p}_1 + \hat{q} + m)}{s}\gamma_\mu, \tag{4}$$

where $t = -2p_1k_1$, $s = 2p_2k_1$.

The $Q^{(1)}_{\mu\rho}$ tensor corresponds to the one-loop-corrected amplitude of process (2). After some algebra, it can be written in the gauge-invariant form

$$Q^{(1)}_{\nu\rho} = \frac{\alpha}{4\pi}(1 + \hat{T}\hat{S})\left[\frac{2a}{m}Q_\mu\gamma_\rho + \left(\frac{2}{(0)(q)t} - \frac{2b}{m^2}\right)P_{2\mu}\gamma_\rho \right.$$
$$+ \frac{\gamma_\lambda(\hat{p}_2 - \hat{k} + m)(P_{2\mu} - 2\tilde{k}_\mu)\gamma_\lambda(\hat{p}_2 - \hat{q} + m)}{(0)(2)(q)t}\gamma_\rho$$
$$+ \frac{\gamma_\lambda(\hat{p}_2 - \hat{k} + m)(P_{2\mu} - 2\tilde{k}_\mu)\gamma_\rho(\hat{p}_1 - \hat{k} + m)\gamma_\lambda}{(0)(1)(2)(q)} \tag{5}$$
$$\left. + \frac{\gamma_\lambda(\hat{p}_2 - \hat{q} - \hat{k} + m)\gamma_\rho(\hat{p}_1 - \hat{k} + m)\gamma_\lambda P_{2\mu}}{(0)(1)(q)t}\right.$$

0021-3640/00/7106-0227$20.00

$$-\frac{\gamma_\lambda Q_\mu \gamma_\rho (\hat{p}_1 - \hat{k} + m)\gamma_\lambda}{(0)(1)(q)}\Bigg],$$

where k is the 4-momentum of a virtual photon and the following notations are used:

$$(0) = k^2 - \lambda^2,\ (1) = (p_1 - k)^2 - m^2,$$
$$(2) = (p_2 - k)^2 - m^2,\ (q) = (p_2 - k - q)^2 - m^2,$$
$$Q_\mu = \gamma_\mu - \frac{q_\mu \hat{q}}{q^2},\ P_{2\mu} = 2\tilde{p}_{2\mu} + q_\mu - \gamma_\mu \hat{q},$$
$$\bar{k}_{/mu} = k_\mu - \frac{kq}{q^2}q_\mu,\ \tilde{p}_{2\mu} = p_{2\mu} - \frac{p_2 q}{q^2}q_\mu,$$
$$a = \frac{m^2}{2(t+m^2)}\left(1 - \frac{2m^2 + 3t}{t+m^2}l_t\right), \quad (6)$$
$$b = -\frac{m^2}{2t}\Bigg[\frac{2m^2 + t}{t+m^2}$$
$$+ \frac{t^2 - 4m^2 t - 4m^4}{(t+m^2)^2}l_t + 2\left(1 + \ln\frac{\lambda^2}{m^2}\right)\Bigg],$$
$$l_t = \ln\frac{-t}{m^2},$$

where λ is the photon "mass."

The substitution operator $\hat{S}$ on the right-hand side of Eq. (5) acts as

$$\hat{S}F(p_2, q) = F(p_1 - q), \quad (7)$$

and the operator $\hat{T}$ changes the order of γ's matrices:

$$\hat{T}\{\gamma_\alpha \gamma_\beta \ldots \gamma_\sigma \gamma_\rho\} = \{\gamma_\rho \gamma_\sigma \ldots \gamma_\beta \gamma_\alpha\}. \quad (8)$$

For those terms on the right-hand side of Eq. (5) which depend on the 4-momentum k of the virtual photon, 4-dimension loop integration is implied, e.g.,

$$\frac{1}{(0)q} \longrightarrow \int \frac{d^4k}{i\pi^2}\frac{1}{(0)(q)} \quad (9)$$

and so on.

One can easily see that under the action of substitution $\hat{S}$ the large logarithm l_t becomes complex:

$$\hat{S}l_t \longrightarrow l_s = \ln\frac{-s}{m^2} = \ln\frac{s}{m^2} - i\pi. \quad (10)$$

In what follows, we will neglect the imaginary part appearing on the right-hand side of Eq. (5) under the action of the $\hat{S}$ operator, in accordance with Eq. (10). This approximation is operative when our result is applied to an analysis of the spin–spin correlations in the quasi-elastic and deep inelastic scattering processes, because the imaginary part in Eq. (5) can contribute only to the one-spin correlation. Moreover, to observe such correlations, in principle, it is necessary to detect the components perpendicular to the initial electron 3-momentum for both hard photon and scattered electron [9]. As will be seen below, the term to be calculated makes no contribution in this case. This justifies the chosen approximation.

In this approximation, the spin-dependent part of the Compton tensor can be expressed in terms of two gauge-invariant structures $\epsilon_{\mu\nu\alpha\beta}q_\alpha p_{1\beta}$ and $\epsilon_{\mu\nu\alpha\beta}q_\alpha p_{2\beta}$ that appear at the Born approximation level {in the general case, if the imaginary part on the right-hand side of Eq. (5) is retained, the structure of the leptonic tensor becomes more complicated, as is shown in [6]}. Neglecting terms of the order of α^2 on the right-hand side of (3), one gets

$$L_{\mu\nu} = S_{\mu\nu} + i\eta P_{\mu\nu},\ P_{\mu\nu} = P^{(0)}_{\mu\nu} + \frac{\alpha}{2\pi}P^{(1)}_{\mu\nu}, \quad (11)$$

where $P^{(0)}_{\mu\nu}$ is the well-known Born contribution [3, 6],

$$P^{(0)}_{\mu\nu} = 2\Bigg\{(\mu\nu q p_1)\Bigg[\frac{u+t}{st} - 2m^2\left(\frac{1}{s^2} + \frac{1}{t^2}\right)\Bigg]$$
$$+ (m\nu q p_2)\left(\frac{u+s}{st} - \frac{2m^2 s}{t^2 u}\right)\Bigg\}, \quad (12)$$

and we use the notations $u = (p_1 - p_2)^2$ and $(\mu\nu q p_{1,2}) = \epsilon_{\mu\nu\alpha\beta}q_\alpha p_{1,2\beta}$.

As for the $P^{(1)}_{\mu\nu}$ tensor, it can be written in the form

$$P^{(1)}_{\mu\nu} = \rho P^{(0)}_{\mu\nu} + R_{\mu\nu},\ R_{\mu\nu} = R^{(0)}_{\mu\nu} + 2m^2 R^{(m)}_{\mu\nu}. \quad (13)$$

With the loop correction, only the Born-like structure depends on the photon mass λ on the right-hand side of Eq. (13). To eliminate it the corrections due to the soft photon emission (with energy smaller than $\Delta\varepsilon$) should be added. The corresponding procedure was described in [6, 8], and the overall effect can be described by quantity ρ. We follow [8] and use

$$\rho = 2(l_u - 1)\ln\frac{\Delta^2}{Y} + 3l_q$$
$$- \ln^2 Y - \frac{\pi^2}{3} - \frac{9}{2} + 2L_{i2}(\cos\theta), \quad (14)$$

where

$$Y = \varepsilon_2/\varepsilon,\ l_u = \ln(-u/m^2),\ l_q = \ln(-q^2/m^2),$$

and ε_2 is the energy of the scattered electron. This form of ρ slightly differs from that used in [6].

The $R^{(0)}_{\mu\nu}$ tensor includes singular and finite terms in the $m \longrightarrow 0$ limit and has the form

$$R^{(0)}_{\mu\nu} = \left\{\frac{2s(s+u)+u(u+t)}{s^2t}G + \frac{u(t-u)}{st^2}\tilde{G}\right.$$
$$+\frac{s+u-t}{st} - \frac{u+t}{t(s+u)} - \frac{4u}{s(s+t)} - \frac{2u(s-t)}{st(s+u)}(l_t - l_u)$$
$$+\frac{3}{t+u}(l_q - l_u) + \frac{t+u}{(s+u)^2}(l_q - l_t) - \frac{2u}{st}(l_s - l_t) \quad (15)$$
$$\left.+2\left[\frac{u+t}{t(s+u)} + \frac{u}{s(s+t)} - \frac{uq^2(s-t)}{st(s+t)^2}\right](l_q - l_u)\right\}$$
$$\times(\mu\nu q p_2) + (t \longleftrightarrow s,\ p_2 \longrightarrow p_1).$$

The functions G and $\tilde{G}$ are given in [6, 8]. In fact, both ρ and $R^{(0)}_{\mu\nu}$ can be reconstructed from the results in [6] if one eliminates the imaginary part of l_s.

3. The $R^{(m)}_{\mu\nu}$ tensor is the main result of our calculations. It can be written in the following form:

$$R^{(m)}_{\mu\nu} = A_1(\mu\nu q p_1) + A_2(\mu\nu q p_2), \quad (16)$$

$$A_1 = -\frac{4s^2}{u^2t^2}G - \frac{4}{s^2}\tilde{G} + \frac{\pi^2}{3}\left(-\frac{1}{s^2} - \frac{2}{t^2} - \frac{m^2s(2s+u)}{u^2t^3}\right)$$
$$+\frac{9u^2-8s^2}{u^2t^2} + \frac{9}{s^2} - \frac{m^2}{s^2(s+m^2)} + \frac{2(s^2+t^2)}{s^2t^2}(l_q^2 - l_u^2)$$
$$+\frac{-ut^2(2s+3u) - m^2t(2u^2-4s^2-us) + 2m^4s(2s+u)}{t^2u^2(t+m^2)^2}l_t \quad (17)$$
$$+\frac{2}{s^2}L_{i2}\left(1+\frac{s}{m^2}\right) + \frac{2s^2}{u^2t^2}\left(2+\frac{m^2}{t}\right)L_{i2}\left(1+\frac{t}{m^2}\right),$$

$$A_2 = -\frac{4}{t^2}G + \frac{\pi^2}{3}\left(\frac{u-2s}{ut^2} - \frac{m^2t}{us^3}\right) + \frac{7(s-u)}{ut^2} - \frac{9t+7u}{us^2}$$
$$-\frac{m^2}{t^2(t+m^2)} + \frac{2s}{ut^2}(l_q^2 - l_u^2)$$
$$+\frac{-s^2(2t+3u) + m^2s(t-2u) + 2m^4t}{us^2(s+m^2)^2}l_s \quad (18)$$
$$+\frac{2m^2t}{us^3}L_{i2}\left(1+\frac{s}{m^2}\right) + \frac{2(ut+m^2s)}{ut^3}L_{i2}\left(1+\frac{t}{m^2}\right).$$

One can see from Eqs. (17) and (18) that the $R^{(m)}_{\mu\nu}$ tensor, in contrast to $R^{(0)}_{\mu\nu}$, is not symmetric about the substitution ($t \longleftrightarrow s$, $p_2 \longleftrightarrow p_1$). In addition, the 4-vector g disappears from the final result, much as it happened to pair production [4] and double-photon emission [5]. It is also obvious that this tensor is of importance only in the collinear regions ($\mathbf{k}_1 \parallel \mathbf{p}_1$) [or ($\mathbf{k}_1 \parallel \mathbf{p}_2$)] where the t (or s) invariant can be of the order of m^2. [In fact, the g vector enters via a combination of the type $m^2(k_1g)/(t^2(p_1g))$, and we can use approximation $k_1 = xp_1$, $x = -s/u$ to eliminate it.] In the collinear regions, we can perform model-independent angular integration for a hard photon with 4-momentum k_1. In the ($\mathbf{k}_1 \parallel \mathbf{p}_1$) region, we have

$$\frac{\alpha}{4\pi^2}\int\frac{d^3k_1}{\omega_1}P_{\mu\nu}(\mathbf{k}_1 \parallel \mathbf{p}_1) = i\eta\frac{\alpha}{2\pi}\left\{\left[\frac{1+(1-x)^2}{x}\ln z_0\right.\right.$$
$$\left.-\frac{2(1-x+x^2)}{x}\right]\left(1+\frac{\alpha}{2\pi}\rho\right) + \frac{\alpha}{2\pi}\left[\frac{1+(1-x)^2}{x}\right.$$
$$\times((\ln z_0 - 2l_u)\ln(1-x) - 2F(1-x)) + \frac{2-x^2}{2x}\Big]\ln z_0$$
$$+\frac{\alpha}{2\pi}\left[\frac{2(1-x+x^2)}{x}(2\ln(1-x)l_u + 4F(1-x)\right. \quad (19)$$
$$-4\ln(1-x) - \ln^2(1-x)) - \frac{1+x^2}{x} - 2x\ln x$$
$$+\frac{\pi^2}{6x}(3+6x^3) + (2-2x+3x^2)\ln^2 x$$
$$\left.\left.+\frac{-3+8x-8x^2+6x^3}{x}L_{i2}(1-x)\right]\right\}(\mu\nu p_1 p_2),$$

where $x = \omega_1/\varepsilon$ is the fractional energy of a hard photon, $z_0 = \varepsilon^2\theta_0^2/m^2$, and θ_0 is the limiting angle defining collinear region ($\mathbf{k}_1 \parallel \mathbf{p}_1$): $\mathbf{k}_1\hat{\mathbf{p}}_1 < \theta_0$. Function F on the right-hand side of Eq. (19) is defined as

$$F(z) = \int_1^{1/z}\frac{dx}{x}\ln(1-x).$$

The corresponding contribution to the one-loop-corrected leptonic tensor from the ($\mathbf{k}_1 \parallel \mathbf{p}_2$) region is

$$\frac{\alpha}{4\pi^3}\int\frac{d^3k_1}{\omega_1}P_{\mu\nu}(\mathbf{k}_1 \parallel \mathbf{p}_2) = i\eta\frac{\alpha}{2\pi}\left\{\left[\frac{1+(1+y)^2}{y}\ln\bar{z}_0\right.\right.$$
$$\left.-\frac{2(1+y)}{y}\right]\left(1+\frac{\alpha}{2\pi}\rho\right) + \frac{\alpha}{2\pi}\left[\frac{1+(1+y)^2}{y}\right.$$
$$\left.\times(\ln(\bar{z}_0 - 2l_u)\ln(1+y) - 2F(1+y)) + \frac{2-y^2}{2y}\right]\ln\bar{z}_0$$

$$+\frac{\alpha}{2\pi}\left[\frac{2(1+y)}{y}(2\ln(1+y)l_u+4F(1+y)\right.$$
$$-4\ln(1+y)-\ln^2(1+y)-y\ln^2 y)-\frac{1}{y}$$
$$+\frac{\pi^2}{6y}(3+10y+8y^2)$$
$$\left.-\frac{3+6y+4y^2}{y}L_{i2}(1+y)\right]\Bigg\}(\mu\nu p_1 p_2), \quad (20)$$
$$\bar{z}_0 = z_0 Y^2,\ y = \frac{\omega_1}{\varepsilon_2}.$$

The last two lines on the right-hand sides of both Eqs. (19) and (20) appear due to the contribution from tensor $R_{\mu\nu}^{(m)}$. Therefore, we see that in the collinear kinematics the term proportional to the squared electron mass in Eq. (13) contributes with next-to-leading (via terms containing l_u) and next–next-to-leading accuracy. It cannot be reconstructed from the result in [6], but can be important for the description of events in experimental conditions when the angle of the hard photon in process (2) is not observed.

We thank I.V. Akushevich for discussions. This work was supported in part (N.P.M) by the INTAS (grant no. 93-1867 ext) and by the Ukranian DFFD (grant no. 24/379).

REFERENCES

1. D. Adams *et al.*, Phys. Rev. D **56**, 5330 (1997).
2. K. Acherstaff *et al.*, Phys. Lett. B **404**, 383 (1997).
3. T. V. Kukhto and N. M. Shumeiko, Nucl. Phys. B **219**, 412 (1983); I. V. Akushevich and N. M. Shumeiko, J. Phys. G **20**, 513 (1994).
4. M. Konchatnij, N. P. Merenkov, and O. N. Shekhovzova, hep-ph/9903384.
5. M. Konchatnij and N. P. Merenkov, JETP Lett. **69**, 893 (1999).
6. I. V. Akushevich, A. B. Arbuzov, and E. A. Kuraev, Phys. Lett. B **432**, 222 (1998).
7. R. Barbieri, J. A. Mignaco, and E. Remiddi, Nuovo Cimento A **11**, 824 (1972).
8. E. A. Kuraev, N. P. Merenkov, and V. S. Fadin, Yad. Fiz. **45**, 782 (1987) [Sov. J. Nucl. Phys. **45**, 486 (1987)].
9. A. B. Arbuzov *et al.*, Yad. Fiz. **59**, 878 (1996) [Phys. At. Nucl. **59**, 841 (1996)].

JETP Letters, Vol. 71, No. 6, 2000, pp. 231–234. From Pis'ma v Zhurnal Éksperimental'noĭ i Teoreticheskoĭ Fiziki, Vol. 71, No. 6, 2000, pp. 333–337.

FIELDS, PARTICLES, NUCLEI

P-Vortices, Nexuses, and Effects of Gauge Copies[1]

V. G. Bornyakov*, D. A. Komarov, M. I. Polikarpov**, and A. I. Veselov****

** Institute of High-Energy Physics, Protvino, Moscow region, 142284 Russia*

*** Institute of Theoretical and Experimental Physics, Bol'shaya Cheremushkinskaya ul. 25, Moscow, 117259 Russia*

Received February 17, 2000

We perform a careful study of the gauge copies problem for the direct center projection in $SU(2)$ lattice gauge theory. Our results indicate that this gauge is not appropriate for the investigation of the center vortices. We also show that the pointlike objects, nexuses, are important for confinement dynamics. © *2000 MAIK "Nauka/Interperiodica".*

PACS numbers: 11.15.Ha; 12.38.Gc

1. The old idea about the role of center vortices in confinement phenomena [1] has been revived recently with the use of lattice regularization. Both gauge-invariant [2] and gauge-dependent [3] approaches were developed. The gauge-dependent studies were done in a particular gauge, named the center gauge. Such a gauge leaves intact center group local gauge-invariance. It is believed that gauge-dependent P-vortices defined on the lattice plaquettes are able to locate thick gauge-invariant center vortices and thus provide the essential evidence for the center vortex picture of confinement. So far, three different center gauges have been used in practical computations: the indirect center gauge [3], the direct center gauge [4], and the Laplacian center gauge [5]. It is known that the first two of these gauges suffer from the gauge copies problem. Many results supporting the above-mentioned role of P-vortices were obtained in the direct center gauge. Recently, the following feature of this gauge has been discovered [6]: there are gauge copies that correspond to higher maxima of the gauge-fixing functional F (see below for a definition) than usually obtained; and, at the same time, these new gauge copies produce P-vortices, evidently with no center vortex finding ability, since the projected Wilson loops have no area law. It was argued in [7] that one can still use the direct center gauge to locate center vortices, if one uses a gauge-fixing algorithm avoiding "bad" copies of [6]. Below, we subject this statement to a careful check. Another goal of this paper is to investigate properties of recently introduced new objects called nexuses [8, 9] or center monopoles [10]. One can define a nexus in $SU(N)$ gauge theory as a 3D object formed by N center vortices meeting at the center, or nexus, with zero (mod N) net flux. We use P-vortices in the center projection to define nexuses in $SU(2)$ lattice gauge theory.

2. Direct center gauge is defined by the maximization of the following functional of the lattice gauge field $U_{n,\mu}$ [4]:

$$F(U) = \frac{1}{4V}\sum_{n,\mu}\left(\frac{1}{2}\mathrm{Tr}U_{n,\mu}\right)^2 = \frac{1}{4V}\sum_{n,\mu}\frac{1}{4}(\mathrm{Tr}_{adj}U_{n,\mu}+1) \quad (1)$$

with respect to local gauge transformations, and can be considered as the Landau gauge for adjoint representation; V is the lattice volume. Condition (1) fixes the gauge up to the $Z(2)$ gauge transformation. Fixed configuration can be decomposed into the $Z(2)$ and coset parts: $U_{n,\mu} = Z_{n,\mu}V_{n,\mu}$, where $Z_{n,\mu} = \mathrm{sgn}\mathrm{Tr}U_{n,\mu}$. Plaquettes constructed from the $Z_{n,\mu}$ field have values ± 1. Those taking -1 values compose the so-called P-vortices. P-vortices form closed surfaces in 4D space. Some evidence has been collected that P-vortices in the direct center gauge can serve to locate gauge-invariant center vortices. It has been reported [4] that the projected Wilson loops computed via linking the number of static quark trajectories and P-vortices have an area law with the string tension $\sigma_{Z(2)}$ very close to the string tension of the nonabelian theory $\sigma_{SU(2)}$. This fact was called center dominance. Another important observation was that the density of P-vortices scales as a physical quantity [4, 11]. We inspect these statements using a careful gauge-fixing procedure.

The most common method of fixing the gauge of type (1) is the relaxation algorithm which makes maximization iteratively site by site. The relaxation is made more effective with the help of overrelaxation. It is known that another algorithm—simulated annealing—is more effective and very useful when the gauge copies problem becomes severe [12]. Here, we do not employ simulated annealing but apply the gauge-fixing procedure explained in detail in [4]. We call it the RO (relaxation–overrelaxation) procedure.

[1] This article was submitted by the authors in English.

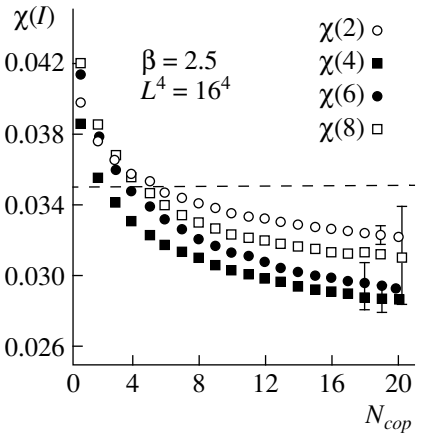

Fig. 1. Dependence of the Creutz ratios $\chi(I)$ on the number of gauge copies N_{cop} for $\beta = 2.5$, $L^4 = 16^4$. The error bars are shown for one value of N_{cop} only, and they are characteristic of the other data points. The dashed line corresponds to the nonabelian string tension, $\sigma_{SU(2)}$.

The main problem of direct center gauge fixing is that the functional $F(U)$ (1) has many local maxima. We call configurations corresponding to these local maxima gauge copies. They are lattice Gribov copies in fact. It is well known that for some gauge conditions which are formulated as the maximization of a nonlocal functional (e.g., Landau, Coulomb, and Maximal Abelain gauges), the gauge-dependent quantities depend strongly on the local maxima picked up, whereas it is impossible to find out the global maximum. Thus, it is necessary to approach the global maximum as closely as possible. We use the following procedure proposed and checked in [12]: for a given configuration we generate N_{cop} gauge-equivalent copies applying random gauge transformations and fix the gauge for each gauge copy using the RO procedure. After that, we compute the gauge-dependent quantity X on the gauge copy corresponding to the highest maximum of (1), $F_{\max}(N_{cop})$. Averaging over statistically independent gauge field configurations and varying N_{cop}, we obtain the function $X(N_{cop})$ and extrapolate it to the $N_{cop} \longrightarrow \infty$ limit. This should provide a good estimation for X computed on the global maximum unless the algorithm in use does not permit us to reach the global maximum or its vicinity (the situation we also met with in the present study). The main difference of the present study from the calculations performed earlier is that we use a higher value of the gauge copies ($1 \le N_{cop} \le 20$) than was used in [3, 4, 7,11] and make a careful analysis of N_{cop} dependence. Due to that, our results differ drastically from those reported previously [3, 4, 7, 11].

We compute observables separately using the modified (LRO) gauge-fixing procedure [6]: every configuration was first fixed to the Landau gauge, and then the RO algorithm for the direct center gauge was applied. In this case, the effect of a large number of gauge copies N_{cop} is not very important, and we confirm the results of [6].

Note that there exists another proposal [13] for the general gauge-fixing procedure, which is free of the gauge copies problem. In some particular limit, this procedure corresponds to the search for the global maximum [12]. There is also a class of gauge conditions [5], [14] which do not suffer from the gauge copies problem.

3. Our computations were performed on lattice $L^4 = 12^4$ for $\beta = 2.3$; 2.4 and $L^4 = 16^4$ for $\beta = 2.5$. For $\beta = 2.3$, 2.4 ($\beta = 2.5$) we study 100 (50) statistically independent gauge field configurations. Using the gauge-fixing procedure described above, we calculate various observables as functions of the number of randomly generated gauge copies N_{cop} ($1 \le N_{cop} \le 20$).

(i) We confirm the conclusion of [6] that gauge copies generated via the LRO procedure have higher maxima of $F(U)$ and thus are closer to the global maximum of $F(U)$. We found that $F^{LRO}_{\max}(N_{cop}) > F^{RO}_{\max}(N_{cop})$ for any value of N_{cop} at any considered value of β.

(ii) We find that the LRO procedure gives copies with significantly lower density ρ of P-vortices than the RO procedure. We use the standard definition

$$\rho = \frac{1}{12V} \sum_{n;\mu>\nu} (1 - Z_{n,\mu\nu}).$$

Thus, gauge copies generated by the RO and LRO procedures are indeed different, even in the limit $N_{cop} \longrightarrow \infty$.

(iii) The difference between the LRO and RO results can be qualitatively explained as follows. Fixing the Landau gauge, we get a configuration almost without P-vortices; the subsequent RO procedure substantially increases the number of P-vortices, but a percolating cluster does not appear. The original gauge field configuration contains a lot of P-vortices, and the local RO procedure is not able to remove all large (and even

Comparison of $\sigma_{Z(2)}$, $\sigma_{SU(2)}$ and ρ for RO gauge fixing center projection

N_{cop}	$\sigma_{Z(2)}/\sigma_{SU(2)}$			$2\rho/\sigma_{SU(2)}a^2$		
	$\beta = 2.3$	$\beta = 2.4$	$\beta = 2.5$	$\beta = 2.3$	$\beta = 2.4$	$\beta = 2.5$
3	0.94(2)	0.93(2)	0.98(2)	1.30(1)	1.51(1)	1.74(1)
20	0.87(2)	0.80(2)	0.83(3)	1.27(1)	1.42(1)	1.61(2)
∞	0.82(3)	0.71(3)	0.71(3)	1.24(1)	1.33(2)	1.49(2)

wrapping) clusters of P-vortices. The field configuration after application of the LRO procedure contains many small P-vortex clusters; the field configuration after application of the RO procedure contains one large percolating cluster. It seems that this cluster is responsible for the area-law behavior of the projected Wilson loops (see below).

(iv) The most important observable is the $Z(2)$-projected Creutz ratio $\chi(I)$, which we calculate using the procedure suggested in [3, 4]. $\chi(I)$ is defined through the projected Wilson loops $W_{Z(2)}(C) = \exp\{i\pi\mathcal{L}(\Sigma_P, C)\}$. Here, $\mathcal{L}(\Sigma_P, C)$ is the 4D linking number of the closed surface, Σ_P, formed by the P-vortex and closed loop C.

In Fig. 1, we show the dependence of $\chi(I)$ on N_{cop} for $\beta = 2.5$. It happens that this dependence is nicely fitted by the function $C_1 + C_2/\sqrt{N_{cop}}$. The reason for such dependence is still to be understood. In the table we give the ratio[2] $\sigma_{Z(2)}/\sigma_{SU(2)}$. $\sigma_{Z(2)}$ is computed from $\chi(I)$ for $3 \le I \le 4$ data at 12^4 lattice and for $3 \le I \le 6$ data at 16^4 lattice. For $N_{cop} = 3$ (number of gauge copies used in [4]) $\sigma_{Z(2)}$ is close to $\sigma_{SU(2)}$. But it becomes significantly lower for $N_{cop} \longrightarrow \infty$. Thus, the results of the RO procedure strongly depend on N_{cop}. It is important that $\sigma_{Z(2)}$ is 20–30% lower than $\sigma_{SU(2)}$ for $N_{cop} \longrightarrow \infty$. This implies that even if one restricts oneself to the RO procedure, as is suggested in [7], one cannot conclude that P-vortices indeed well locate *all* center vortices.

(v) For gauge copies generated by the LRO procedure we confirm the result of [6] that $\chi(I)$ is zero within statistical errors for any value of N_{cop}.

(vi) In the table we also show the ratio $2\rho/\sigma_{SU(2)}a^2$ (ρ is the density of P-vortices). As is claimed in [11], in the case of uncorrelated plaquettes carrying P-vortices, 2ρ coincides with the dimensionless string tension $\sigma_{SU(2)}a^2$. The results presented in the table show that the density of P-vortices does not scale correctly, and therefore ρ is not proportional to $\sigma_{SU(2)}a^2$.

(vii) We also investigate the properties of the pointlike objects called nexuses. On the 4D lattice we have the conserved currents of nexuses defined after the center projection. We calculate the phase s_l of the $Z(2)$ link variable $Z_l = \exp(i\pi s_l)$, $s_l = 0, 1$. Then we define the plaquette variable $\sigma_P = ds \bmod 2$, ($\sigma_P = 0, 1$). The nexus current (or center monopole current [10]) is then defined as $^*j = \frac{1}{2}\delta{}^*\sigma_P$. These currents reside on the surface of the P-vortex (on the dual 4D lattice), and the P-vortex flux goes through the positive and negative nexuses in alternate order. The important characteristic of the cluster of currents is the condensate C defined [16] as the percolation probability. As is shown in [10], the condensate C of the nexus currents is the order parameter for the confinement–deconfinement phase transition. We found that C is nonzero for the gauge copies obtained via the RO procedure (when the projected Wilson loops have the area law). C is zero (in the thermodynamic limit $L \longrightarrow \infty$) for gauge copies obtained using the LRO procedure (when the projected Wilson loops have no area law). It is interesting that for the RO procedure C seems to scale as a physical quantity with the dimension $(mass)^4$. This is illustrated in Fig. 2, where we plot the β dependence of the ratio $C/(\sigma_{SU(2)}a^2)^2$. Thus, these new objects might be important degrees of freedom for the description of nonperturbative effects.

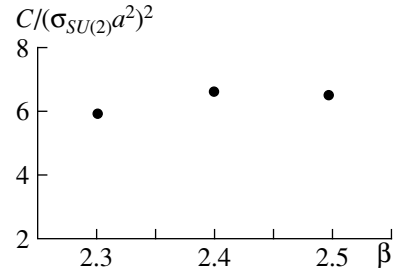

Fig. 2. The β dependence of the ratio of the nexus condensate C to the $SU(2)$ string tension in lattice units [15].

(viii) It is important to perform the same calculations for the indirect center gauge [3] and for the Laplacian center gauge [5].

This study was supported in part by the Russian Foundation for Basic Research (project nos. 96-15-96740 and 99-01230a), the INTAS (grant no. 96-370), and the Monbushu grant.

REFERENCES

1. G.'t Hooft, Nucl. Phys. B **138**, 1 (1978); J. M. Cornwall, Nucl. Phys. B **157**, 392 (1979); G. Mack, in *Recent Developments in Gauge Theories*, Ed. by G.'t Hooft *et al.* (Plenum, New York, 1980); H. B. Nielsen and P. Olesen, Nucl. Phys. B **160**, 380 (1979); J. Ambjorn and P. Olesen, Nucl. Phys. B **170**, 60, 265 (1980).
2. T. G. Kovacs and E. T. Tomboulis, J. Math. Phys. **40**, 4677 (1999).
3. L. Del Debbio, M. Faber, J. Greensite, and S. Olejnik, Phys. Rev. D **55**, 2298 (1997).
4. L. Del Debbio, M. Faber, J. Giedt, *et al.*, Phys. Rev. D **58**, 094501 (1998).
5. Ph. de Forcrand and M. D'Elia, Phys. Rev. Lett. **82**, 4582 (1999).
6. T. G. Kovacs and E. T. Tomboulis, Phys. Lett. B **463**, 104 (1999).
7. M. Faber, J. Greensite, S. Olejnik, and D. Yamada, J. High Energy Phys. **9912**, 12 (1999).
8. J. M. Cornwall, Phys. Rev. D **58**, 105028 (1998); Phys. Rev. D **59**, 125015 (1999); Preprint UCLA-99-TEP-35 (1999); hep-th/9911125.

[2] The data for $\sigma_{SU(2)}$ are taken from [15].

9. G. E. Volovik, cond-mat/9911486; Pis'ma Zh. Éksp. Teor. Fiz. **70**, 776 (1999) [JETP Lett. **70**, 792 (1999)]; cond-mat/9911374.

10. M. N. Chernodub, M. I. Polikarpov, A. I. Veselov, and M. A. Zubkov, Nucl. Phys. Proc. Suppl. **73**, 575 (1999).

11. K. Langfeld, O. Tennert, M. Engelhardt, and H. Reinhardt, Phys. Lett. B **452**, 301 (1999).

12. G. S. Bali, V. Bornyakov, M. Muller-Preussker, and K. Schilling, Phys. Rev. D **54**, 2863 (1996).

13. S. Fachin and C. Parrinello, Nucl. Phys. B Proc. Suppl. **26**, 429 (1992).

14. J. C. Vink and U.-J. Wiese, Phys. Lett. B **289**, 122 (1992); A. J. van der Sijs, Prog. Theor. Phys. Suppl. **131**, 149 (1998).

15. G. S. Bali, K. Schilling, and C. Schlichter, Phys. Rev. D **51**, 5165 (1995).

16. T. L. Ivanenko, A. V. Pochinsky, and M. I. Polikarpov, Phys. Lett. B **302**, 458 (1993); A. V. Pochinsky, M. I. Polikarpov, and B. N. Yurchenko, Phys. Lett. A **154**, 194 (1991).

JETP Letters, Vol. 71, No. 6, 2000, pp. 235–238. From Pis'ma v Zhurnal Éksperimental'noĭ i Teoreticheskoĭ Fiziki, Vol. 71, No. 6, 2000, pp. 338–343.

FIELDS, PARTICLES, NUCLEI

Eigenfunctions of $GL(N, \mathbb{R})$ Toda Chain: Mellin–Barnes Representation[1]

S. Kharchev and D. Lebedev

Institute of Theoretical and Experimental Physics, Bol'shaya Cheremushkinskaya ul. 25, Moscow, 117259 Russia

e-mail: kharchev@vitep5.itep.ru

e-mail: dlebedev@vitep5.itep.ru

Received February 17, 2000

The recurrent relations between the eigenfunctions of the $GL(N, \mathbb{R})$ and $GL(N-1, \mathbb{R})$ quantum Toda chains are derived. As a corollary, the Mellin–Barnes integral representation for the eigenfunctions of a quantum open Toda chain is constructed for the N-particle case. © *2000 MAIK "Nauka/Interperiodica".*

PACS numbers: 05.50.+q; 03.65.Fd; 02.20.Hj

Recently, a new method of construction of the eigenfunctions for the periodic Toda chain has been developed [1]. It relies on the generalized Fourier transform expansion in terms of eigenfunctions of an open Toda chain, which coincide with the Whittaker functions of the $GL(N-1, \mathbb{R})$ group [2–4].

In the original papers [2–4], the Whittaker functions were constructed by purely algebraic methods through the Iwasawa decomposition for the corresponding group. But it turns out that there is an alternative way to construct these functions directly on the level of R-matrix formalism essentially using the integrable properties of the model.

This paper was inspired by the remark of E. Sklyanin that the integral formula for the eigenfunction of a periodic Toda chain [1] can be used to obtain some recurrent relations between the N- and $(N-1)$-particle eigenfunctions of an open Toda chain. Sklyanin's motivation was based on the possibility to introduce a formal parameter into the Baxter equation [5], whereupon putting it equal to zero, transform the second-order difference equation to the first-order equation. In this paper, we find rigorous proof of this observation, which is free of the limiting procedure, and find the universal way to construct "auxiliary" eigenfunctions staying completely within the framework of the R-matrix formalism without any reference to the algebraic scheme developed in [2–4]. Compared to the well-known results on the eigenfunctions of an open Toda chain [6, 7], our approach not only presents a new integral representation of the eigenfunctions but, together with the generalized Fourier transform, provides a self-consistent method for the solution of the spectral problem for the periodic Toda chain. We believe that this method can be applied to some other classes of integrable systems.

[1] This article was submitted by the authors in English.

The model. We start with the R-matrix formalism for the quantum periodic Toda chain [5]. Let

$$L_n(\lambda) = \begin{pmatrix} \lambda - p_n & e^{-x_n} \\ -e^{x_n} & 0 \end{pmatrix} \tag{1}$$

be the corresponding Lax operator, where $[x_n, p_m] = i\hbar\delta_{nm}$. The N-particle monodromy matrix

$$T_N(\lambda) \stackrel{\text{def}}{=} L_N(\lambda)\ldots L_1(\lambda) \equiv \begin{pmatrix} A_n(\lambda) & B_N(\lambda) \\ C_N(\lambda) & D_N(\lambda) \end{pmatrix} \tag{2}$$

satisfies the standard RTT relations with the rational R-matrix. In particular,

$$\begin{aligned}(\lambda - \mu + i\hbar)A_n(\mu)C_N(\lambda) \\ = (\lambda - \mu)C_N(\lambda)A_N(\mu) + i\hbar A_N(\lambda)C_N(\mu).\end{aligned} \tag{3}$$

The eigenfunctions for the periodic spectral problem were constructed in [1] with the help of the Weyl-invariant function $\psi_{\gamma_1, \ldots, \gamma_{N-1}}(x_1, \ldots, x_{N-1}) \equiv \psi_{\boldsymbol{\gamma}}(\mathbf{x})$, which rapidly decreases in the regions $x_k \gg x_{k+1}$, ($k = 1, \ldots, N-1$) and satisfies equations

$$C_N(\lambda)\psi_{\boldsymbol{\gamma}} = -e^{x_N}\prod_{m=1}^{N-1}(\lambda - \gamma_m)\psi_{\boldsymbol{\gamma}}, \tag{4}$$

$$A_N(\gamma_j)\psi_{\boldsymbol{\gamma}} = i^{-N}e^{-x_N}\psi_{\boldsymbol{\gamma} - i\hbar\mathbf{e}_j} \quad (j = 1, \ldots, N-1), \tag{5}$$

where $\mathbf{e}_j$ is the jth basis vector in $\mathbb{R}^{N-1}$. One can easily see that Eq. (5) is compatible with Eq. (4) owing to commutation relation (3).

In fact, the function $\psi_{\boldsymbol{\gamma}}(\mathbf{x})$ is suited to the solution for the $(N-1)$-particle open Toda chain. Indeed, the operator $A_{N-1}(\lambda)$[arising in the $(N-1)$-particle prob-

lem] is the generating function for the Hamiltonians of the $GL(N-1, \mathbb{R})$ Toda chain. Using obvious relations between the elements of the monodromy matrices $T_N(\lambda)$ and $T_{N-1}(\lambda)$,

$$\begin{aligned} A_N(\lambda) &= (\lambda - p_N)A_{N-1}(\lambda) + e^{-x_N}C_{N-1}(\lambda), \\ C_N(\lambda) &= -e^{x_N}A_{N-1}(\lambda), \end{aligned} \tag{6}$$

one can write Eqs. (4) and (5) in the equivalent form

$$A_{N-1}(\lambda)\psi_{\boldsymbol{\gamma}} = \prod_{m=1}^{N-1}(\lambda - \gamma_m)\psi_{\boldsymbol{\gamma}}, \tag{7}$$

$$C_{N-1}(\gamma_j)\psi_{\boldsymbol{\gamma}} = i^{-N}\psi_{\boldsymbol{\gamma} - i\hbar\mathbf{e}_j} \quad (j = 1, \ldots, N-1). \tag{8}$$

These equations define (to an $i\hbar$-periodic common factor) the Weyl-invariant Whittaker function for the $GL(N-1, \mathbb{R})$ group. In [1], we chose the factor in such a way that $\psi_{\boldsymbol{\gamma}}$ is an entire function of γ and the following asymptotics holds:

$$\psi_{\gamma} \sim |\gamma_j|^{(2-N)/2}\exp\left\{-\frac{\pi}{2\hbar}(N-2)|\gamma_j|\right\} \tag{9}$$

as $|\mathrm{Re}\gamma_j| \longrightarrow \infty$ in a finite strip of the complex plane.

The function $C_{N-1}(\lambda)\psi_{\boldsymbol{\gamma}}$ is a polynomial in λ of order $N-2$. Therefore, this polynomial can be restored from its $N-1$ values at given points $\gamma_1, \ldots, \gamma_{N-1}$. One then obtains the interpolation formula

$$C_{N-1}(\lambda)\psi_{\boldsymbol{\gamma}} = i^{-N}\sum_{j=1}^{N-1}\psi_{\boldsymbol{\gamma} - i\hbar\mathbf{e}_j}\prod_{m\neq j}\frac{\lambda - \gamma_m}{\gamma_j - \gamma_m}. \tag{10}$$

Let us introduce the key object, viz., the *auxiliary* function

$$\Psi_{\boldsymbol{\gamma},\epsilon}(x_1, \ldots, x_N) \stackrel{\text{def}}{=} \exp\left\{\frac{i}{\hbar}\left(\epsilon - \sum_{m=1}^{N-1}\gamma_m\right)x_N\right\}\psi_{\boldsymbol{\gamma}}(\mathbf{x}), \tag{11}$$

where ϵ is an arbitrary parameter. One can readily see from Eqs. (7), (10), and (6) that this function satisfies equations

$$\begin{aligned} A_N(\lambda)_{\boldsymbol{\gamma},\epsilon} &= \left(\lambda - \epsilon + \sum_{m=1}^{N-1}\gamma_m\right)\prod_{j=1}^{N-1}(\lambda - \gamma_j)\Psi_{\boldsymbol{\gamma},\epsilon} \\ &\quad + i^{-N}\sum_{j=1}^{N-1}\Psi_{\boldsymbol{\gamma} - i\hbar\mathbf{e}_j,\epsilon}\prod_{m\neq j}\frac{\lambda - \gamma_m}{\gamma_j - \gamma_m}, \end{aligned} \tag{12}$$

$$C_N(\lambda)\Psi_{\boldsymbol{\gamma},\epsilon} = -e^{x_N}\prod_{j=1}^{N-1}(\lambda - \gamma_j)\Psi_{\boldsymbol{\gamma},\epsilon}. \tag{13}$$

The problem. Let there be given a Weyl-invariant Whittaker function $\psi_{\gamma_1, \ldots, \gamma_{N-1}}(x_1, \ldots, x_{N-1})$ for the $GL(N-1, \mathbb{R})$ Toda chain. The problem is to find the corresponding solution for the $GL(N, \mathbb{R})$ Toda chain using the above information, i.e., to construct in terms of the function $\psi_{\lambda_1, \ldots, \lambda_N}(x_1, \ldots, x_N)$ the Weyl-invariant Whittaker function $\psi_{\lambda_1, \ldots, \lambda_N}(x_1, \ldots, x_N)$ satisfying equations

$$A_N(\lambda)\psi_{\lambda_1, \ldots, \lambda_N} = \prod_{k=1}^{N}(\lambda - \lambda_k)\psi_{\lambda_1, \ldots, \lambda_N}, \tag{14a}$$

$$\begin{aligned} C_N(\lambda_n)\psi_{\lambda_1, \ldots, \lambda_N} &= i^{-N-1}\psi_{\lambda_1, \ldots, \lambda_n - i\hbar, \ldots, \lambda_N} \\ (n &= 1, \ldots, N) \end{aligned} \tag{14b}$$

and having asymptotics

$$\psi_{\lambda_1, \ldots, \lambda_N} \sim |\lambda_n|^{\frac{1-N}{2}}\exp\left\{-\frac{\pi}{2\hbar}(N-1)|\lambda_n|\right\} \tag{15}$$

as $|\lambda_n| \longrightarrow \infty$. It is clear that the action of the operators $A_N(\lambda)$ and $C_N(\lambda)$ on the auxiliary functions $\psi_{\boldsymbol{\gamma},\epsilon}(x_1, \ldots, x_N)$ is well defined. Therefore, it is reasonable to assume that the solution for the $GL(N, \mathbb{R})$ Toda chain is described by an appropriate (generalized) Fourier transform of the function $\Psi_{\boldsymbol{\gamma},\epsilon}(x_1, \ldots, x_N)$. This is in full analogy with the corresponding construction for the periodic case [1].

Main statements. *Theorem 1. Let $\Psi_{\boldsymbol{\gamma},\epsilon}(\mathbf{x}, x_N)$ be the auxiliary function for the N-periodic Toda chain, i.e., defined in terms of the Weyl-invariant Whittaker function for the GL(N – 1, ℝ) Toda chain according to Eq. (11). Let $\boldsymbol{\lambda} = (\lambda_1, \ldots, \lambda_n) \in \mathbb{C}^N$ be the set of unknowns. Let*

$$\mu(\gamma) = (2\pi\hbar)^{N-1}(N-1)!\prod_{j<k}\left|\Gamma\left(\frac{\gamma_j - \gamma_k}{i\hbar}\right)\right|^2, \tag{16}$$

$$\begin{aligned} &Q(\gamma_1, \ldots, \gamma_{N-1}|\lambda_1, \ldots, \lambda_N) \\ &= \prod_{j=1}^{N-1}\prod_{k=1}^{N}h^{\frac{\gamma_j - \lambda_k}{i\hbar}}\Gamma\left(\frac{\gamma_j - \lambda_k}{i\hbar}\right). \end{aligned} \tag{17}$$

Then the Weyl-invariant Whittaker function for the GL(N, ℝ) Toda chain is given by recurrent formula

$$\begin{aligned} &\psi_{\lambda_1, \ldots, \lambda_N}(x_N, \ldots, x_N) \\ &= \int_C \mu^{-1}(\boldsymbol{\gamma})Q(\boldsymbol{\gamma}; \lambda)\Psi_{\boldsymbol{\gamma};\, \lambda_1 + \ldots + \lambda_N}(x_1, \ldots, x_N)d\boldsymbol{\gamma}, \end{aligned} \tag{18}$$

where the integral is taken along the horizontal lines with $Im\gamma_j > max_k\{Im\lambda_k\}$.

Proof of the Theorem. First of all, integral (18) is correctly defined. Indeed, the function

$$q(\gamma|\lambda_1, \ldots, \lambda_N) \equiv \prod_{k=1}^{N} h^{\frac{\gamma-\lambda_\hbar}{i\hbar}} \Gamma\left(\frac{\gamma-\lambda_k}{i\hbar}\right) \tag{19}$$

has the asymptotics

$$q(\gamma; \boldsymbol{\lambda}) \sim |\gamma|^{-N/2} \exp\left\{-\frac{\pi N}{2\hbar}|\gamma|\right\} \tag{20}$$

as $|\mathrm{Re}\gamma| \longrightarrow \infty$ in a finite horizontal strip, while

$$\mu^{-1}(\boldsymbol{\gamma}) \sim |\gamma_j|^{N-2} \exp\left\{\frac{\pi}{\hbar}(N-2)|\gamma_j|\right\}. \tag{21}$$

Hence, the integral in Eq. (18) is absolutely convergent due to asymptotics (9).

Let us verify that Eq. (14a) holds. Using Eq. (12), one finds

$$\begin{aligned} &A_N(\lambda)\psi_{\lambda_1, \ldots, \lambda_N}(x_1, \ldots, x_N) \\ &= \int_C \left(\lambda - \sum_{k=1}^{N}\lambda_k + \sum_{m=1}^{N-1}\gamma_m\right)\prod_{j=1}^{N-1}(\lambda-\gamma_j)\mu^{-1}(\boldsymbol{\gamma}) \\ &\times Q(\boldsymbol{\gamma}; \lambda)\Psi_{\boldsymbol{\gamma}, \lambda_1+\ldots+\lambda_N}(x_1, \ldots, x_N)d\boldsymbol{\gamma} \qquad (22) \\ &+ i^{-N}\sum_{j=1}^{N-1}\int_C\prod_{m\neq j}\frac{\lambda-\gamma_m}{\gamma_j-\gamma_m}\mu^{-1}(\boldsymbol{\gamma})Q(\boldsymbol{\gamma}; \lambda) \\ &\times \Psi_{\boldsymbol{\gamma}-i\hbar\mathbf{e}_j, \lambda_1+\ldots+\lambda_N}(x_1, \ldots, x_N)d\boldsymbol{\gamma}. \end{aligned}$$

We shift the integrations $\gamma_j \longrightarrow \gamma_j + i\hbar$ and use the functional equation

$$\mu^{-1}(\boldsymbol{\gamma} + i\hbar\boldsymbol{\delta}_j) = (-1)^N\mu^{-1}(\boldsymbol{\gamma})\prod_{m\neq j}\frac{\gamma_j-\gamma_m+i\hbar}{\gamma_j-\gamma_m}. \tag{23}$$

The second integrand in Eq. (22) has no poles in any finite horizontal strip in the upper half-plane $\mathrm{Im}\gamma_j > \max_k\{\mathrm{Im}\lambda_k\}$ [all possible poles and the appropriate zeros of the function $\mu^{-1}(\boldsymbol{\gamma})$ cancel one another]. As a consequence, the integral around the strip vanishes. Moreover, the integrand in this strip rapidly decreases as $\mathrm{Re}\gamma_j \longrightarrow \pm\infty$. Therefore, it is possible to return the shifted contour to the original one. Hence, one arrives at the relation

$$\begin{aligned} &A_N(\lambda)\psi_{\lambda_1, \ldots, \lambda_N} \\ &= \int_C\left\{\left(\lambda - \sum_{k=1}^{N}\lambda_k + \sum_{m=1}^{N-1}\gamma_m\right)\prod_{j=1}^{N-1}(\lambda-\gamma_j)Q(\boldsymbol{\gamma}; \lambda)\right. \\ &\left. + i^N\left(\sum_{j=1}^{N-1}\prod_{m\neq j}\frac{\lambda-\gamma_m}{\gamma_j-\gamma_m}\right)Q(\boldsymbol{\gamma}+i\hbar\mathbf{e}_j; \boldsymbol{\lambda})\right\} \qquad (24) \\ &\times\mu^{-1}(\boldsymbol{\gamma})\Psi_{\boldsymbol{\gamma}, \lambda_1+\ldots+\lambda_N}d\boldsymbol{\gamma}. \end{aligned}$$

The function $Q(\boldsymbol{\gamma}; \lambda)$ satisfies equations

$$\prod_{k=1}^{N}(\gamma_j-\lambda_k)Q(\boldsymbol{\gamma}; \lambda) = i^N Q(\boldsymbol{\gamma}+i\hbar\mathbf{e}_j; \boldsymbol{\lambda}) \tag{25}$$

for any $j = 1, \ldots, N-1$. Therefore, Eq. (24) takes the form

$$\begin{aligned} A(\lambda)\psi_{\lambda_1, \ldots, \lambda_N} &= \int_C\left\{\left(\lambda - \sum_{k=1}^{N}\lambda_k + \sum_{m=1}^{N-1}\gamma_s\right)\prod_{j=1}^{N-1}(\lambda-\gamma_j)\right. \\ &\left. + \sum_{j=1}^{N-1}\prod_{k=1}^{N}(\gamma_j-\lambda_k)\prod_{m\neq j}\frac{\lambda-\gamma_m}{\gamma_j-\gamma_m}\right\} \qquad (26) \\ &\times\mu^{-1}(\boldsymbol{\gamma})Q(\boldsymbol{\gamma}; \lambda)\Psi_{\boldsymbol{\gamma}, \lambda_1+\ldots+\lambda_N}d\boldsymbol{\gamma}. \end{aligned}$$

But the expression in the braces is nothing but the polynomial $\prod_{k=1}^{N}(\lambda-\lambda_k)$. Indeed, any polynomial with leading terms $F(\lambda) = \lambda^N + f_1\lambda^{N-1} + \ldots$ can be uniquely restored from its values at any $N-1$ arbitrary points $\gamma_1, \ldots, \gamma_{N-1}$, according to the interpolation formula

$$\begin{aligned} F(\lambda) &= \left(\lambda + f_1 + \sum_{m=1}^{N-1}\gamma_m\right)\prod_{j=1}^{N-1}(\lambda-\gamma_j) \\ &+ \sum_{j=1}^{N-1}F(\gamma_j)\prod_{m\neq j}\frac{\lambda-\gamma_m}{\gamma_j-\gamma_m}. \end{aligned} \tag{27}$$

In our case,

$$F(\lambda) = \prod_{k=1}^{N}(\lambda-\lambda_k) \tag{28}$$

with $f_1 = -\lambda_1 - \ldots - \lambda_N$. Hence, we obtain Eq. (14a).

Let us next consider Eq. (14b). Using Eq. (13), one obtains

$$\begin{aligned} C_N(\lambda_n)\psi_{\lambda_1, \ldots, \lambda_N} &= -e^{x_N}\int_C\mu^{-1}(\boldsymbol{\gamma})Q(\boldsymbol{\gamma}; \lambda) \\ &\times\prod_{j=1}^{N-1}(\lambda_n-\gamma_j)\Psi_{\boldsymbol{\gamma}, \lambda_1+\ldots+\lambda_N}d\boldsymbol{\gamma}. \end{aligned} \tag{29}$$

Clearly,

$$e^{x_N}\Psi_{\boldsymbol{\gamma}, \lambda_1+\ldots+\lambda_N} = \Psi_{\boldsymbol{\gamma}, \lambda_1+\ldots+\lambda_N-i\hbar} \tag{30}$$

and, therefore, Eq. (29) takes the form

$$C_N(\lambda_n)\psi_{\lambda_1,\ldots,\lambda_N} = (-1)^N\int_C \mu^{-1}(\boldsymbol{\gamma})Q(\boldsymbol{\gamma};\lambda) \times\prod_{j=1}^{N-1}(\gamma_j-\lambda_n)\Psi_{\boldsymbol{\gamma},\lambda_1+\ldots+\lambda_N-i\hbar}d\boldsymbol{\gamma}. \tag{31}$$

Evidently, the function $Q(\boldsymbol{\gamma};\lambda)$ satisfies equation

$$\prod_{j=1}^{N-1}(\gamma_j-\lambda_n)Q(\boldsymbol{\gamma};\lambda) = i^{N-1}Q(\boldsymbol{\gamma};\lambda-i\hbar\mathbf{e}_n). \tag{32}$$

Hence, we proved that function (18) obeys relations (14).

The final step is to prove that function (18) is the genuine Whittaker function. The integrand in Eq. (18) decreases exponentially as $\gamma_j \longrightarrow -i\infty$ ($j = 1,\ldots, N-1$) and, as a consequence, the integrals over large semicircles in the lower half-plane vanish. Using the Cauchy formula for calculating integral (18) in the asymptotic region $x_{k+1} \gg x_k$ ($k = 1, \ldots, N-1$), one can easily see that the asymptotics of the function $\psi_{\lambda_1,\ldots,\lambda_N}$ is expressed precisely in terms of the corresponding Harish–Chandra functions (see, e.g., [4]):

$$\psi_{\boldsymbol{\lambda}}(\mathbf{x}) = \sum_{s\in W}\hbar^{-2i(s\boldsymbol{\lambda},\rho)/\hbar}\prod_{j<k}\Gamma\left(\frac{s\lambda_j-s\lambda_k}{i\hbar}\right)e^{\frac{i}{\hbar}(s\boldsymbol{\lambda},\mathbf{x})} + O(\max\{e^{x_k-x_{k+1}}\}_{k=1}^{N-1}) \tag{33}$$

(in this formula, the summation is over the Weyl group). Hence, we construct exactly the Weyl-invariant Whittaker function. Moreover, using the Stirling formula for the Γ-functions, it is easy to see that asymptotics (15) holds. The theorem is proved.

The Mellin–Barnes representation. *Theorem 2. Let a set $\|\gamma_{jk}\|$ be a lower triangular $N\times N$ matrix. The solution to Eq. (14) can be written (up to an unessential numerical factor) in the form of multiple Mellin–Barnes integrals*:

$$\psi_{\gamma_{N1},\ldots,\gamma_{NN}}(x_1,\ldots,x_N) = \int_C\prod_{n=1}^{N-1}\frac{\prod_{j=1}^{n}\prod_{k=1}^{n+1}\hbar^{\frac{\gamma_{nj}-\gamma_{n+1,k}}{i\hbar}}\Gamma\left(\frac{\gamma_{nj}-\gamma_{n+1,k}}{i\hbar}\right)}{\prod_{\substack{j,k=1\\ j<k}}^{n}\left|\Gamma\left(\frac{\gamma_{nj}-\gamma_{nk}}{i\hbar}\right)\right|^2} \times\exp\left\{\frac{I}{\hbar}\sum_{n,k=1}^{N}x_n(\gamma_{nk}-\gamma_{n-1,k})\right\}\prod_{\substack{j,k=1\\ j\le k}}^{N-1}d\gamma_{jk}, \tag{34}$$

where the integral should be understand as follows: we first integrate with respect to γ_{11} along the line $\mathrm{Im}\gamma_{11} > \max\{\mathrm{Im}\gamma_{21}, \mathrm{Im}\gamma_{22}\}$, then we integrate over the set $(\gamma_{21}, \gamma_{22})$ along the lines $\mathrm{Im}\gamma_{2j} > \max_m\{\mathrm{Im}\gamma_{3m}\}$, and so on. The last integrations should be performed over the set of variables $(\gamma_{N-1,1}\ldots, \gamma_{N-1,N-1})$ along the lines $\mathrm{Im}\gamma_{N-1,k} > \max_m\{\mathrm{Im}\gamma_{N,m}\}$ The proof is a straightforward application of recurrent relations (18), starting with the trivial Whittaker function $\psi_{\gamma_{11}}(x_1) = \exp\left\{\frac{i}{\hbar}\gamma_{11}x_1\right\}$.

We are deeply indebted to E. Sklyanin for drawing our attention to the possibility of recurrent reconstruction of the eigenfunction for the open Toda chain. We thank M. Semenov-Tyan-Shanskiĭ for stimulating discussions.

D. Lebedev would like to thank F. Smirnov and LPTHE, Université Pierre et Marie Curie for hospitality, where the work was partially done. This work was supported in part by the INTAS (grant no. 97-1312), the Russian Foundation for Basic Research [project nos. 98-01-00344 (S. Kharchev) and 98-0100328 (D. Lebedev)], and by grant no. 96-15-96455 for the Support of Scientific Schools.

REFERENCES

1. S. Kharchev and D. Lebedev, hep-th/9910265; Lett. Math. Phys. (in press).
2. H. Jacquet, Bull. Soc. Math. Fr. **95**, 243 (1967).
3. G. Schiffmann, Bull. Soc. Math. Fr. **99**, 3 (1971).
4. M. Hashizume, J. Math. Soc. Jpn. **5**, 394 (1979); Hiroshima Math. J. **12**, 259 (1982).
5. E. Sklyanin, Lect. Notes Phys. **226**, 196 (1985).
6. B. Kostant, in *Proceedings of SRC/LMS Research Symposium, Representation Theory of Lie Groups, Oxford, 1977*, London Math. Soc. Lecture Notes **34**, p. 287.
7. M. Semenov-Tyan-Shanskiĭ, Preprint No. R-3-84, LOMI, Leningrad, 1984; *Encyclopaedia of Mathematical Sciences. Vol. 16. Dynamical Systems VII* (Springer-Verlag, Berlin, 1994), Chap. 3, p. 226.

JETP Letters, Vol. 71, No. 6, 2000, pp. 239–241. From Pis'ma v Zhurnal Éksperimental'noĭ i Teoreticheskoĭ Fiziki, Vol. 71, No. 6, 2000, pp. 344–347.

FIELDS, PARTICLES, NUCLEI

Low-Energy Theorems and the Dirac Operator Spectral Density in QCD[1]

A. Gorsky

Institute of Theoretical and Experimental Physics, Bol'shaya Cheremushkinskaya ul. 25, Moscow, 117259 Russia

Received February 21, 2000

We discuss the spectral density of the massless Dirac operator at small eigenvalues and quark masses compatible with the restrictions imposed by the low-energy theorems in QCD. The sum rule for its derivative with respect to the quark mass is found. © *2000 MAIK "Nauka/Interperiodica".*

PACS numbers: 12.38.-t

1. A search for the universal characteristics of QCD in the strong-coupling regime remains the important problem of clarifying the structure of QCD vacuum. Among the most important universal objects is the spectral density of the massless Dirac operator, whose behavior near the zero eigenvalue provides the pattern for spontaneous symmetry breaking. The Banks–Casher relation [1] states that the density at the origin is fermionic condensate $\langle \bar{q}\, q\rangle = -\pi\rho(0)$, where

$$\hat{D}q = \lambda q, \quad \rho(\lambda) = \langle V^{-1}\sum \delta(\lambda - \lambda_n)\rangle_A. \qquad (1)$$

V is the Euclidean volume, and averaging is over the gluon ensemble. Generalization of the Banks–Casher relation for the moments of density in a finite volume was obtained in [2]. The obvious question arises as to the behavior of the spectral density for small masses and eigenvalues. In perturbation theory, density behaves as $\rho(\lambda) = c\lambda^3$; hence, the linear and quadratic terms have a nonperturbative nature. It can be expected to describe the critical behavior of the system at zero temperature and, possibly, define a universality class. Note that the universality properties of the spectral density allow the matrix model technique to be applied to an analysis of its behavior in a finite volume (see [3] for the review).

It is natural to relate the characteristics of spectral density to other universal objects in QCD. The best candidates are the low-energy theorems for the zero-momentum QCD correlators in different channels which follows from the chiral Ward identities [4, 5]. The first attempt [6] to get information about the spectral density behavior involved $\int dx \langle S^i(x)S^j(0)\rangle$ isovector scalar correlator. It was claimed that it yields the term linear in λ that vanishes for $N_f = 2$. Recently, two other sum rules arising from the correlators

$$\int dx \langle A^i(x)A^j(0) - V^i(x)V^j(0)\rangle$$

[7] and

$$\int dx \langle S^i(x)S^j(0) - \delta^{ij}P^0(x)P^j(0)\rangle$$

[8] were obtained, but no additional information about the spectral density was extracted. Let us note that the analysis in [6] was questionable, since there was some contradiction between the spectral densities derived from two- and three-point correlators.

In this note, we discuss the complete set of restrictions imposed by low energy theorems for the two-point and three-point correlators on the spectral density. Correlators in the scalar and pseudoscalar channels yield the information on the spectral density itself, while those in the vector and axial channels are relevant only to the correlations of the eigenvalues.

2. Let us consider the correlators in the isovector and isoscalar scalar and pseudoscalar channels in the $N_f = 2$ case. In what follows, we will discuss only correlators which are free from the nonuniversal high-energy contributions. A complete list of such low-energy theorems for two-, three-, and four-point correlators can be found in [4]. Corresponding correlators can be expressed in terms of the spectral density as follows;

$$\int dx \langle \delta^{ij}S^0(x)S^0(0) - P^i(x)P^j(0)\rangle = -\frac{G_\pi^2\delta_{ij}}{M_\pi^2} + \delta_{ij}\frac{B^2}{8\pi^2}(l_3 - 4l_4 + 3) = -\delta_{ij}\left(\int \frac{8m^2\rho(\lambda, m)}{(\lambda^2 + m^2)^2} - 4m\int \frac{\partial_m\rho(\lambda, m)}{(\lambda^2 + m^2)}\right), \qquad (2)$$

[1] This article was submitted by the author in English.

0021-3640/00/7106-0239$20.00

$$\int dx\langle S^i(x)S^j(0)-\delta_{ij}P^0(x)P^0(0)\rangle = -\delta_{ij}8B^2l_7$$
$$= -\delta_{ij}\left(\int\frac{8m^2\rho(\lambda,m)}{(\lambda^2+m^2)^2}-4\frac{\left\langle\int dxQ(x)Q(0)\right\rangle}{m^2V}\right), \quad (3)$$

$$\int dx\langle P^3(x)P^0(0)\rangle = \frac{G_\pi\tilde{G}_\pi}{M_\pi^2} = 8(m_u-m_d)m$$
$$\times\int\frac{\rho(\lambda,m)}{(\lambda^2+m_u^2)^2}-\frac{4(m_u-m_d)\left\langle\int Q(x)Q(0)\right\rangle}{m^3V}, \quad (4)$$

$$G_\pi = 2F_\pi B = \frac{F_\pi m_\pi^2}{m};\quad \tilde{G}_\pi = -(m_u-m_d)\frac{4B^2l_7}{F_\pi}.$$

The sum rule arising from the last low-energy theorem exactly coincides with the one coming from correlator (3). Low-energy constants l_3, l_4 behave as $\log m$ at small quark masses, while the constant l_7 contains no chiral logarithms [4].

We can add here the low-energy theorem for the three-point correlator

$$\int dxdy\langle S^0(x)P^i(y)P^k(0)\rangle = \frac{\delta^{ik}G_\pi^3}{M_\pi^4F_\pi}$$
$$-\delta_{ik}\frac{B^2G_\pi F_\pi}{8\pi^2M_\pi^2}(l_3-4l_4+3) = \delta^{ij}\frac{d}{dm}\int\frac{2\rho(\lambda,m)}{\lambda^2+m^2}. \quad (5)$$

It appears that the sum rules resulting from low-energy theorems (2) and (5) are identical.

The last low-energy theorem, which is potentially important, follows from the four-point pseudoscalar correlator

$$\int\langle P^iP^jP^kP^l\rangle = -\frac{G_\pi^4}{F_\pi^2M^8}(\delta_{ij}\delta_{kl}+\delta_{ik}\delta_{jl}+\delta_{il}\delta_{jk})$$
$$\times\left(-\frac{M^2}{F^2}+\frac{M^4(24l_4-9)}{96\pi^2F^4}+\ldots\right) = \int\frac{4\rho(\lambda,m)}{(\lambda^2+m^2)^2}+R_{ijkl}. \quad (6)$$

Unfortunately, it is more difficult to extract the information from the four-point correlator, since there is the contribution R_{ijkl} corresponding to a diagram with at least two fermionic loops that cannot be expressed in terms of the spectral density. Moreover, the sum rules are sensitive to the two-loop contribution to the four-point correlator in the chiral theory, which is unknown at the moment. Therefore, there are only two rigorous independent sum rules for the spectral density.

Combination of sum rules (2) and (3) yields the following model-independent sum rule for the mass derivative of the spectral density

$$m\int\frac{4\partial_m\rho(\lambda,m)}{(\lambda^2+m^2)} = \frac{B^2}{8\pi^2}(l_3-4l_4+3)-\frac{G_\pi^2}{M_\pi^2}$$
$$+8B^2l_7+\frac{4\left\langle\int Q(x)Q(0)\right\rangle}{m^2V}. \quad (7)$$

3. We turn now to the discussion of the restrictions imposed by the sum rules on the behavior of the density near the origin. We would like to look for the following ansatz:

$$\rho(\lambda,m) = \rho(0)+c_1\lambda\log\lambda+c_2\lambda+c_3m$$
$$+c_4m\log m+c_5m\log^2m+O(m^2,\lambda^2,m\lambda), \quad (8)$$

where c_i are the constants to be found. It appears that this ansatz is consistent with the low-energy theorems for the correlators which are free from high-energy contributions.

Apart from the sum rules above, we assume two additional model-independent restrictions on the spectral density. First, we use the universality of the $m\log m$ correction to the chiral condensate [5]. Second, there is the unambiguous statement that there are no $\log m$ contributions to the correlator $\langle S^iS^i\rangle$>. This fact has been already used to show that $c_2 = 0$ [6].

Consider first correlators (2) and (5), which give rise to identical sum rules. The leading m^{-1} singularity immediately comes from the $\rho(0)$ term, but the matching of the $\log m$ term appears to be a subtle point. It can be easily seen that the constants c_4 and c_1 do not contribute; hence, one has to assume that $c_5 \neq 0$.

The correction to the condensate looks like

$$\langle\bar{q}q\rangle_m = \langle\bar{q}q\rangle_0\left(1-\frac{3M_\pi^2\log M_\pi^2}{32\pi^2F_\pi^2}+\ldots\right), \quad (9)$$

and it is supposed that there is no $m\log^2m$ term. Hence, using the Banks–Casher formula for the condensate, we can claim that to cancel the $m\log^2m$ correction we have to assume that $c_1 \neq 0$. However, this term in the spectral density yields a divergence in the integral at the *UV*-region, raising the question of the subtraction of the perturbative contribution. The proper version of this procedure, which would allow us to make a prediction for c_1 and c_4, deserves further investigation.

To discuss the restriction on c_3, we have to expand the topological susceptibility up to the second order in the quark mass,

$$\frac{\left\langle\int Q(x)Q(0)\right\rangle}{V} = \frac{mBF_\pi^2}{2}+dB^2m^2+\ldots; \quad (10)$$

hence, the coefficient d enters our sum rules. If we substitute the expression for the spectral density and

assume that all logarithmic contributions cancel, the following model-independent relation arises:

$$c_3 = -8l_7 + 2d. \quad (11)$$

Note that the analogous relation was considered in [8], but the term on the lhs was missed.

Since the constants c_1 and c_5 cannot vanish simultaneously, the $m^2 \log m$ and $m^2 \log^2 m$ terms have to be manifest in the expansion of the topological susceptibility. Certainly, it is desirable to consider the $N_f > 2$ case when the dependence of the topological susceptibility on the quark masses is more transparent.

4. In this note, we considered the behavior of the Dirac operator spectral density around the origin. It appeared that the low-energy theorems impose strong restrictions on it but do not determine it unambigously. It would be useful to derive the complete list of the two-loop contributions to the off-shell correlators in the chiral theory, since this information provides additional restrictions on the linear terms in the spectral density, as well as on the λ^2 terms.

This work is partially motivated by an attempt to develop the interpretation of the spectral density of the Dirac operator within the brane approach. This issue was addressed for the $N = 1$ SUSY theory in [9], and quark masses fix the positions of D6 branes representing fundamental matter in "momentum" space. Therefore, to clarify the brane picture, it is necessary to elaborate the N_f dependence of the spectral density, as well as the case of the generic mass matrix. These questions will be discussed elsewhere.

I am grateful to H. Leutwyler for the hospitality in ITP at Bern University and discussions which initiated this work. I would like to thank A. Smilga for useful comments. The work was supported in part by the INTAS (grants no. 96-0482) and the Russian Foundation for Basic Research (project no. 97-02-16131).

REFERENCES

1. T. Banks and S. Casher, Nucl. Phys. B **169**, 103 (1980).
2. H. Leutwyler and A. Smilga, Phys. Rev. D **46**, 5607 (1992).
3. J. Verbarshoot, hep-th/9705125.
4. J. Gasser and H. Leutwyler, Ann. Phys. (N. Y.) **158**, 142 (1984).
5. V. Novikov, M. Shifman, A. Vaishtein, and V. Zakharov, Nucl. Phys. B **191**, 301 (1981).
6. A. Smilga and J. Stern, Phys. Lett. B **318**, 531 (1993).
7. J. Stern, hep-th/ 9801107.
8. A. Smilga, hep-th/9805214.
9. A. Gorsky, hep-th/9804020.

JETP Letters, Vol. 71, No. 6, 2000, pp. 242–245. Translated from Pis'ma v Zhurnal Éksperimental'noĭ i Teoreticheskoĭ Fiziki, Vol. 71, No. 6, 2000, pp. 348–353.

ATOMS, SPECTRA, RADIATIONS

Exciton Luminescence of Quasi-Two-Dimensional Solid Solutions

A. Klochikhin*, **, A. Reznitskiĭ, L. Tenishev**, S. Permogorov**, S. Ivanov**, S. Sorokin**, Kh. Mumanis**, R. Seisyan**, and C. Klingshirn*****

**Konstantinov Institute of Nuclear Physics, Russian Academy of Sciences, Gatchina, St. Petersburg, 188350 Russia*
***Ioffe Physicotechnical Institute, Russian Academy of Sciences, Politekhnicheskaya ul. 26, St. Petersburg, 194021 Russia*
****Universität Karlsruhe, Institute für Angewandte Physik, Karlsruhe, 76128 Germany*
e-mail: alexander.reznitsky@pop.ioffe.rssi.ru
Received December 20, 1999; in final form, February 8, 2000

Absorption and luminescence of the quantum wells formed by the (Zn–Cd)Se and (Ga–In)As solid solutions are studied in the range of exciton size-quantization ground state. The spectra observed are described by a model assuming the two-dimensional character of fluctuation states in quantum wells and the presence of a percolation threshold within the absorption contour. *© 2000 MAIK "Nauka/Interperiodica".*

PACS numbers: 71.55.Jv; 73.20.Dx; 78.66.-w

Optical spectra of the exciton states in quantum wells provide evidence that the two-dimensional exciton is affected by the potential fluctuations in the lateral plane both when a barrier is formed in a solid solution [1–3] and when the well material is a solid solution [4]. Measurements of the homogeneous broadening and the diffusivity of the exciton states [1] responsible for the inhomogeneously broadened absorption band of the GaAs/AlGaAs quantum well have shown that both characteristics strongly vary within the band. This fact suggests that the properties of exciton states drastically change within a relatively narrow energy range. The authors of [1] attributed this fact to the occurrence of a mobility threshold approximately in the center of this band.

This work presents a more detailed study of the effect of fluctuations of the composition of a quantum-well-forming solid solution on the exciton states in these systems. The optical spectra of such quantum wells are characterized by exponential decay at the long-wavelength wing of the absorption spectrum, by the composition-dependent broadening of this spectrum, and by the appearance of a luminescence band with a maximum red-shifted from the absorptance maximum. The Stokes shift and the luminescence band width also depend on the concentration of the components of a solid solution. These data enable one to assume that the broadening of the absorption spectrum and the appearance of the above-mentioned luminescence band are due to the formation of a disorder-induced tail of fluctuation states near the exciton-band edge. The influence of a random potential on the exciton state was earlier observed for three-dimensional disordered systems such as Cd(S–Se) and Zn(Se–Te) solid solutions with anionic substitution [5–8] and other amorphous and glassy systems for which the disorder energy scale is not small.

The distinctive feature of the quantum wells in solid solutions is that the fluctuation effects occur even in systems with atomic substitution in the cationic sublattice. It is known that the fluctuation states in three-dimensional solid solutions with cationic substitution, such as (Zn–Cd)Se and (Ga–In)As, do not play a significant role in the recombination processes even at low temperatures [5, 9]. One can naturally assume that this distinction is caused by the two-dimensional character of localization of carriers in quantum wells. The two-dimensionality of localization can be substantiated if the energy range of fluctuation states is much smaller than the size-quantization energy. In this case, in describing the fluctuation states, one can restrict oneself by considering the exciton motion in a two-dimensional ground-state band. This moderates the conditions for the occurrence of an observable fluctuation-state tail, as compared to the three-dimensional case [6–8].

A thin layer of a solid solution inserted into a broader band matrix can be regarded as a quantum well if the size-quantized level appears in the layer and regularly shifts both with changing concentrations of components, i.e., mean-potential level in the quantum well, and upon the variation of well width. The very notion of mean potential for a well formed in a solid solution assumes a clear physical meaning if the resulting states encompass macroscopic fragments of the lateral plane. At the same time, such a situation implies the occurrence of a quantum percolation [19–12], much as the classical percolation occurs upon the formation of the clusters encompassing the whole crystal. The literature data (e.g., [12]) indicate that the quantum percolation

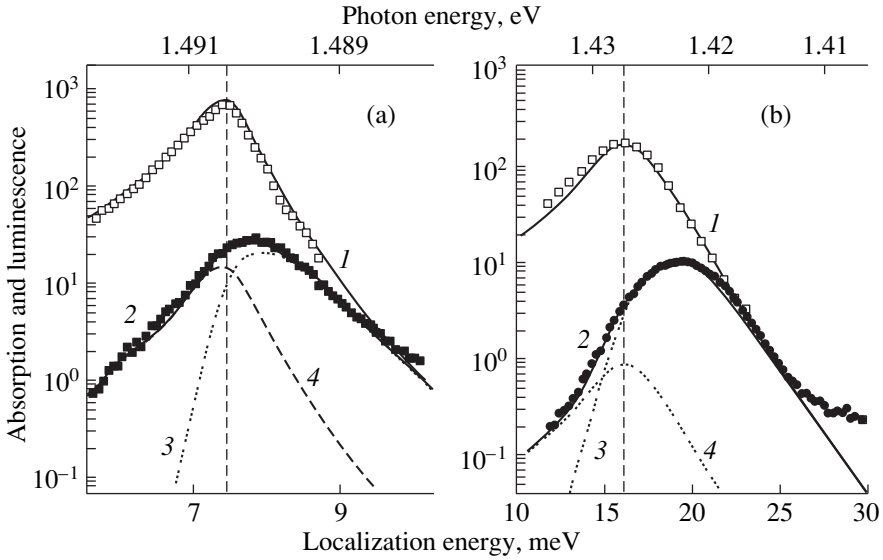

Fig. 1. Experimental absorption and luminescence spectra of the $Ga_{1-c}In_cAs$ quantum wells (open and dark circles, respectively): c = (a) 0.033 and (b) 0.16. Localization energy (lower scale) is measured from the size-quantization level in the fluctuationless well (see text). The vertical dashed line indicates the mobility threshold.

threshold is slightly shifted to higher concentrations of the active component, as compared to the appropriate classical model. For percolation through the nearest neighboring sites or through the bonds between the nearest neighbors, the quantum well in the square lattice is expected to form at concentrations of the narrow-band component $c > 0.59$ or $c > 0.5$, respectively. In reality, according to the estimates [13], the size-quantization levels appear in the systems of interest at concentrations at least an order of magnitude lower than the indicated ones. The occurrence of percolation at concentrations as small as those indicated above means that the microscopic percolation mechanism is associated with the overlap between the localized-state wave functions with radius sizably larger than the lattice constant.

It was thus of interest to reveal the concentration dependence for the number of localized states and for the Uhrbach energy in the spectrum of fluctuation states. In three-dimensional solid solutions, the total number of fluctuation states and the Uhrbach parameter are greatest when the concentration of the narrow-band component approaches the critical value corresponding to the nearest site-percolation threshold, whereupon they rapidly decrease with an increase in the concentration [5]. By analogy, one could expect that the fluctuations in a quasi-two-dimensional system would also have the strongest effect when the concentration of the narrow-band component falls between the critical values for the three- and two-dimensional lattices. However, there is an additional reason for the occurrence of concentration dependence of the above-mentioned quantities in a quasi-two-dimensional system. In such systems, the perturbation $\delta U(z)$ introduced by the atomic potential of the narrow-band component is expressed as a matrix element of this potential, with the transverse-motion ground-state wave functions $\phi_0(z)$,

$$\{\delta U\}_{00} = \int_{-\zeta/2}^{\zeta/2} \phi_0(z)\delta U(z)\phi_0(z)dz, \qquad (1)$$

where ζ is the potential-well width. If the radius a_U of the perturbing potential is shorter than the characteristic length of exponential decay of the wave function $\phi_0(z)$, then

$$\{\delta U\}_{00} \approx \phi_0^2(0)\delta U(0)a_U. \qquad (2)$$

The perturbation magnitude is $\delta U(z) = (U(z) - \bar{U})$, where $\bar{U}$ is the potential mean value in the well. As the concentration of the attraction atomic centers increases, $\bar{U}$ tends to the limiting value equal to the potential value for the narrow-band component of a solid solution. As in the three-dimensional case [6–8], this should reduce the $\delta U(z)$ magnitude. At the same time, the lowering of the potential mean level brings about an increase in the quantum-well depth and lowering of the size-quantization ground-state energy and, as a result, an increase in the $\phi_0^2(z)$ value in the quantum well. This factor can lead to a considerable rise in the magnitude of perturbation potential (2), as distinct from the three-dimensional situation.

In this work, we studied the optical spectra of the (Ga–In)As/GaAs and (Zn–Cd)Se/ZnSe quantum wells. The experimental data on the luminescence and absorption of the (Ga–In)As/GaAs system are presented in

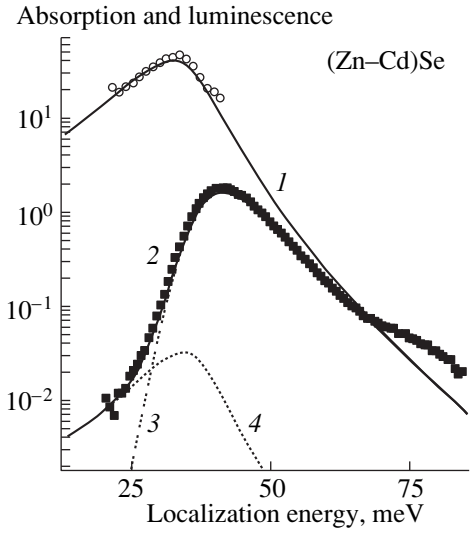

Fig. 2. Luminescence (dark circles) and luminescence excitation (open circles) spectra of a sample with 0.5-monolayer CdSe and ZnSe inserts. Notations as in Fig. 1.

Fig. 1 for two comparatively low In concentrations of 3.3 and 16.1%. The corresponding samples were comprised of 30 (Ga–In)As quantum wells of widths 7.5 and 9.3 nm separated by the GaAs barriers of widths 33 and 90 nm. One can see from Fig. 1 that the range of fluctuation states and the Stokes shifts of the luminescence bands relative to the absorption bands increase with increasing In concentration.

Similar structures were observed for the luminescence and luminescence excitation spectra of a sample comprised of 11 quantum wells formed by the 0.5-monolayer CdSe and ZnSe inserts with a period of 5 nm (Fig. 2). With allowance made for the fact that, in reality, Cd is distributed among four to six monolayers [14], its mean concentration in the well is equal to ca. 10%.

To analyze the shapes and mutual arrangement of the absorption and luminescence spectra of the structures studied, we assume that the absorption band is formed by two types of states that qualitatively differ in the ability to relax with energy transfer. This assumption is valid if the quantum percolation threshold occurs within the absorption contour. We use the classical continuous two-dimensional percolation theory for the quantitative description of the contributions of these two different types of fluctuation states to absorption and luminescence. As in the three-dimensional case [6–8], we assume that the exciton spectral density is formed by fluctuation states that can be divided into two types: the major part includes mobile states capable of relaxing with energy transfer to the lattice, while the spatially isolated localized "emitting" states incapable of undergoing radiationless transitions at $T = 0$ comprise the minor portion of states.

In the zeroth approximation, the fluctuation states lying below a certain energy ω_0 are regarded as spatially isolated and chaotically distributed over the quantum-well plane. The localization energy is taken to be positive and measured from the size-quantization level in the ideal quantum well without fluctuations. Let us introduce a unified geometrical size $R_{int}/2$ for all the fluctuation potential wells with localization energies $\omega > \omega_0$ such that if any one of these potential wells or their complex is separated from all other fluctuation wells with higher localization energy by a distance larger than R_{int}, then the state is considered spatially localized. The boundary energy ω_0 is chosen on the condition that $\mathcal{N}(\omega_0)a_{\omega_0}^2 < 1$, where $\mathcal{N}(\omega_0)$ is the integrated density of states with the localization energy above ω_0 and $a_{\omega_0} = \sqrt{\hbar^2/2M\omega_0}$ is the radius of the wave function for the state with localization energy ω_0. The mobility threshold ω_{ME} of such a system is assumed to lie at localization energies higher than ω_0.

The continuous percolation theory allows one to determine the number of potential wells which have a given localization energy and do not overlap with the higher energy states, as well as the number of superclusters, i.e., isolated pairs, triads, etc. of wells whose ground states also have no way of relaxing. As a result, one can derive the relation between the numbers of isolated and mobile states occurring in a wide energy range. The dependence of the contribution from the isolated wells and pair ground states on the localization energy can be represented as

$$P(\omega) = [\exp\{-2\mathcal{P}(\omega)\} + \mathcal{P}(\omega)\exp\{-2.841\mathcal{P}(\omega)\}], \quad (3)$$

where $\mathcal{P}(\omega) = \frac{1}{2}[R_{int}/\overline{r(\omega)}]^2$ and

$$\overline{r(\omega)} = \left(\frac{1}{\pi}\frac{1}{\mathcal{N}(\omega)}\right)^{1/2}.$$

The integrated density of states $\mathcal{N}(\omega)$ gives the concentration of potential wells with localization frequency bounded by the ω value on one side and by the Lifshitz boundary on the other [15]. The first term in Eq. (3) is the exact concentration of the isolated single states, and the second one is the extrapolation of a power series obtained in [16] for the isolated pairs. We used in our calculations the $\mathcal{P}(\omega_{ME}) = 2.3$ value for the density of exciton states at the percolation threshold. As in the three-dimensional case, the isolated states dominate below the percolation threshold, where their number reaches a maximum and then exponentially decreases with decreasing ω.

The spatially isolated single-cluster states dominate the luminescence band, while the ground states of superclusters give rise to a rapidly converging (by vir-

tue of additional exponentially small factors) series of correction terms [6–8]. At the same time, all states, irrespective of their ability to relax, contribute to the optical absorption.

Ignoring the exciton–phonon interaction, which is weak in the systems of interest, and taking into account the relation between the emission probability and the coefficient $\alpha^0_{1s}(\omega)$ of phononless absorption for the transition to the exciton 1*s* state, one can represent the luminescence spectrum in the form

$$I^0_{1s}(\omega) \sim \alpha^0_{1s}(\omega)\tau_{rad} \times \{P(\omega) + \tau_{rel}/\tau_{rad}[1 - P(\omega)]\}, \quad (4)$$

where the first term in braces, $P(\omega)$, is described by an expression of type (3); it allows for the contribution of the isolated fluctuation-well states with localization energy ω and the supercluster ground states with energy ω. The second term stands for emission from the states capable of undergoing nonradiative relaxation, so that their contribution is proportional to the τ_{rel}/τ_{rad} ratio of the relaxation and radiative recombination times. All things being the same, the contribution of the relaxing states to the emission is determined by the energies transferred in the radiationless relaxation processes, i.e., by the energy range of fluctuation states.

Figures 1 and 2 present the experimental data and the calculated absorption and luminescence spectra (curves *1* and *2*, respectively), as well as the contributions of the emitting (curve *3*) and relaxing (curve *4*) exciton states to the luminescence spectrum. One can see by comparing the data in Figs. 1a and 1b that the contribution of the relaxing states to the emission decreases with increasing In concentration. A plausible explanation for this result is that the rise in the In concentration brings about elongation of the tail of fluctuation states and, as a consequence, an increase in the energy of acoustic phonons assisting in the energy transfer to the lattice in the course of relaxation processes, eventually leading to a higher relaxation probability. It is worth noting that, similar to the GaAs–AlGaAs system [1], the percolation threshold obtained upon modeling optical spectra in all cases nicely coincides with the absorptance maximum. Such a coincidence can be due to the fact that in the vicinity of the percolation threshold the characteristic sizes of the localized exciton wave functions are comparable with the light wavelength, while the mobile above-threshold states can be approximately characterized by a wavevector comparable in magnitude with the photon wavevector.

Note in conclusion that the optical spectra of both systems studied are described within the framework of a unified approach, although the energy scale of the fluctuation potential δU_{00} for (Zn–Cd)Se turns out to be larger than for (Ga–In)As by a factor of 2–2.5. This approximately correlates with the ratio of the $\phi^2_0(0)$ values in these wells and is due to the fact that the exciton localization energy in the (Zn– Cd)Se quantum well $\delta E = E^G_{\mathrm{ZnSe}} - E^{1s}_{(\mathrm{Zn–Cd})\mathrm{Se}}$ is larger than the corresponding value in the (Ga–In)As samples studied.

This work was supported by the Russian Foundation for Basic Research (project no. 97-02-18138) and the Scientific and Technical Program “Physics of Solid-State Nanostructures” (grant no. 99-1114).

REFERENCES

1. J. Hegarty, L. Goldner, and M. D. Sturge, Phys. Rev. B **30**, 7346 (1984).
2. T. Takagahara, Phys. Rev. B **32**, 7013 (1985).
3. U. Jahn, M. Ramsteiner, R. Hey, *et al.*, Phys. Rev. B **56**, R4387 (1997).
4. Fang Yang, M. Wilkinson, E. J. Austin, *et al.*, Phys. Rev. Lett. **70**, 323 (1993).
5. S. Permogorov and A. Reznitsky, J. Lumin. **52**, 201 (1992).
6. A. A. Klochikhin, S. A. Permogorov, and A. N. Reznitskiĭ, Fiz. Tverd. Tela (St. Petersburg) **39**, 1170 (1997) [Phys. Solid State **39**, 1035 (1997)].
7. A. A. Klochikhin, S. A. Permogorov, and A. N. Reznitskiĭ, Zh. Éksp. Teor. Fiz. **120**, 1039 (1999) [JETP **88**, 574 (1999)].
8. A. Klochikhin, A. Reznitsky, S. Permogorov, *et al.*, Phys. Rev. B **59**, 12947 (1999).
9. S. Permogorov, A. Yu. Naumov, L. N. Tenishev, *et al.*, Fiz. Tverd. Tela (St. Petersburg) **37**, 2466 (1995) [Phys. Solid State **37**, 1350 (1995)].
10. Y. Shapir, A. Aharony, and A. B. Harris, Phys. Rev. Lett. **49**, 486 (1982).
11. Y. Meir, A. Aharony, and A. B. Harris, Europhys. Lett. **10**, 275 (1989).
12. I. Chang, Zvi Lev, A. B. Harris, *et al.*, Phys. Rev. Lett. **74**, 2094 (1995).
13. S. V. Ivanov, A. A. Toropov, T. V. Shubina, *et al.*, J. Appl. Phys. **83**, 3168 (1998).
14. R. N. Kyutt, A. A. Toropov, S. V. Sorokin, *et al.*, Appl. Phys. Lett. **75**, 373 (1999).
15. I. M. Lifshits, Usp. Fiz. Nauk **83**, 617 (1964) [Sov. Phys. Usp. **7**, 549 (1965)].
16. S. W. Haan and R. Zwanzig, J. Phys. A **10**, 1547 (1977).

Translated by V. Sakun

JETP Letters, Vol. 71, No. 6, 2000, pp. 246–249. Translated from Pis'ma v Zhurnal Éksperimental'noĭ i Teoreticheskoĭ Fiziki, Vol. 71, No. 6, 2000, pp. 354–358.

ATOMS, SPECTRA, RADIATIONS

Hard X Radiation and Fast Particles in Laser Plasma Experiments at Laser Intensities of up to 5×10^{18} W/cm^2 on the Target Surface

V. G. Borodin*, O. N. Gilev, A. L. Zapysov**, V. M. Komarov*, V. A. Lykov**, V. A. Malinov*, V. M. Migel'*, N. V. Nikitin*, V. G. Pokrovskiĭ**, V. A. Pronin**, V. N. Saprykin**, A. V. Charukhchev*, and V. N. Chernov***

**Russian Federal Nuclear Center–All-Russia Research Institute of Technical Physics, P.O. 245, Snezhinsk, Chelyabinsk region, 456770 Russia*

***Research Institute of Complex Tests of Optical-Electronic Devices and Systems, Vavilov State Optical Institute, All-Russia Scientific Center, Sosnovy Bor, Leningrad region, Russia*

e-mail: cher@sbor.ru

Received April 1, 1999

Results are presented from an investigation of the hard X-ray spectrum and the parameters of fast particles in experiments on the interaction of laser pulses with solid targets in the PROGRESS-P facility at laser intensities of up to 5×10^{18} W/cm^2 on the target surface. The maximum energy of fast electrons obtained from direct measurements is found to be 8–10 MeV. © *2000 MAIK "Nauka/Interperiodica".*

PACS numbers: 52.40.Nk; 52.50.Jm; 52.25.Nr

In the interaction of ultrashort pico- and subpicosecond laser pulses with intensities $>10^{17}$ W/cm^2 with solid targets, the laser pump wave energy is converted directly into the energy of plasma electrons mainly via nonlinear collisionless processes [1, 2]. The electrons accelerated in such a manner give rise to the fluxes of fast ions and hard X-ray (HXR) photons whose energy may be as high as several tens of megaelectronvolts [3]. Plasma sources of such particles and photons open up unique opportunities for initiating nuclear reactions, creating compact neutron sources and artificial radioactive sources, and producing various isotopes [4]. In this connection, it becomes relevant to study the parameters of laser-produced HXR photons and of the particles accelerated by the laser field.

The experiments were carried out with the Progress-P picosecond laser with Nd-glass chirped pulse amplification [5]. A schematic of the measurements is shown in Fig. 1.

The laser light (λ = 1053 nm), whose energy in the interaction chamber amounted to 16 J, the pulse duration being about 1.4–1.5 ps, was focused into a focal spot ≤ 7 μm in diameter on the target by an f/1.1 on-axis parabolic mirror (the laser beam diameter was 190 mm). The fraction of energy in the spot was 50% of the total laser energy. The main pulse was preceded by an amplified luminescence prepulse with a duration of about 5 ns, the prepulse intensity being $\leq 10^{-8}$ of the main pulse intensity. At 20 ps before the main pulse, the relative prepulse intensity was $<10^{-3}$, which is an upper limit determined by the measurement technique. The experiments were carried out within 40–60 degrees of normal incidence with both *p*- and *s*-polarized light and with targets made of different materials.

In the energy range 15–90 keV, the HXR spectrum was measured by the method of selective filters (made of Zr, Rh, Cd and Gd, and Pb) with jumplike characteristics of *K*-shell absorption in this photon energy range; and, in the energy range above 1.5 MeV, the HXR spectrum was measured by the method of "gray" filters (made of Pb) [6]. Preliminary measurements revealed that, in the target chamber, there were not only X-ray photons but also fast electrons escaping from the target plasma. Since HXR detectors are very sensitive to such electrons (whose energy was as high as several megaelectronvolts), we placed a protecting Be filter (with a mass thickness of 3.5 g/cm^2) at a distance of 15–20 cm from the detectors. Such a filter, which reduces the X-radiation intensity by a factor of only 1.5 to 2, absorbs all electrons with energies of up to 10 MeV. X-ray photons with energies ≤70 keV were recorded by semiconductor detectors, and X-ray photons with higher energies were recorded by scintillation (CsI + Tl) detectors. The detectors were placed inside a Pb container, which protected them from the scattered photons and particles.

Fast electrons were detected simultaneously with the measurement of the HXR spectrum by the method of gray filters, which were also made of Pb. Near the HXR detector, we positioned an additional detector with a Pb filter and without a Be filter. As a result, the additional detector shielded by a Pb filter recorded both

electrons and X-ray photons, while the HXR detector protected by both Be and Pb filters monitored only X radiation. In some experiments, such pairs of detectors were placed behind the target.

The X-radiation and electron fluxes through the target were visualized with an RF-3 X-ray photo film loaded into a special film cassette that was positioned at a distance of 5 cm behind the target. The film, sensitive to X-ray photons with energies of up to 60 keV, was protected from laser light by 0.25-mm thick Al foil. Different ranges of X-ray energy were selected with the help of additional Pb strips of different thicknesses, which were glued to the foil.

Soft X-ray imaging was done with a multiframe pinhole camera [6]; the holes with diameters from 5 to 15 μm were protected by different cassette filters.

Fast ions (with velocities $\geq 10^8$ cm/s) escaping from the target plasma in different directions were recorded by the time-of-flight method with the help of an array of ion collectors [7]. The sensitivity of the collector technique was such that we could measure the current produced by ions with velocities lower than 10^9 cm/s. The collectors were arranged around the target so as to simultaneously detect the ions that flew away from the target in the direction nearly orthogonal to its surface and in the specular direction with respect to the incident laser light. In our experiments, the collectors served to study the spatial distribution of fast ions flying away from the target and (in combination with plasma calorimeters) to estimate the mean charge-to-mass ratio of the plasma ions [7].

Figure 2 shows the results of measuring the HXR spectrum in several experiments with Al and Sn targets, the laser intensity on the target surface being $I \approx 1.5$–5×10^{18} W/cm^2. The results presented were processed under the assumption that laser-produced HXR fluxes are isotropically emitted into a 4π solid angle.

All of the spectra in Fig. 2 are characterized by two different temperatures. Another common feature of the spectra is that the lower the energy of the relatively soft (≤40 keV) X-ray photons, the lower the spectral intensity. A significant reduction (by a factor of more than 60) in the soft X-radiation intensity can also be inferred from the fact that the imaging of soft X-ray photons with a mean energy of 0.25 keV was not available with a multiframe pinhole camera. Such behavior of the spectra in the soft X-ray range differs markedly from that revealed in our previous experiments [6], in which the laser light intensity at the target surface was lower ($I \approx 10^{17}$ W/cm^2) and the spectral intensity was found to increase with decreasing photon energy (at least in the energy range above 0.24 keV).

In monitoring HXR emission spectra from an Sn target, the detector with a Cd filter recorded, along with the continuous spectrum, the K_αSn line (25.3 keV) emission produced in the interaction of fast electrons with a cold target material. In processing the signals

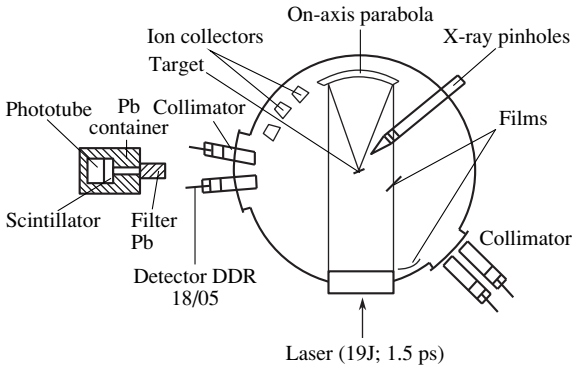

Fig. 1. Schematic of the diagnostic complex in the target chamber.

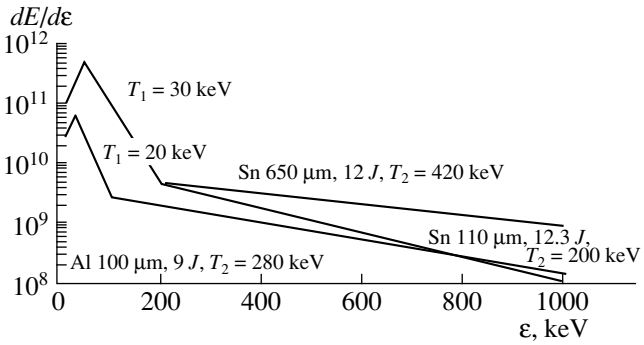

Fig. 2. HXR spectrum for Al and Sn targets at $I \approx 5 \times 10^{18}$ W/cm^2.

from detectors with different filters simultaneously, it is possible to single the signal associated with the K_αSn line out of the signal captured by the detector with a Cd filter and to calculate the energy yield of this line relative to the laser energy on the target.

Some results of measuring the electron temperature and HXR yield are summarized in the table.

The HXR yield obtained from the spectral measurements was used to estimate the yield of fast electrons with energies higher than 15 keV. For Sn targets, the yield of fast electrons was found to be 0.015–0.04 of E_{las}.

The yields of fast electrons in different spectral ranges were determined using detectors with Pb filters of mass thicknesses 1.26, 3.33, and 8.84 g/cm^2. The detector with the filter of mass thickness 1.26 g/cm^2 measured the yield of electrons with energies >2.7 MeV, the detector with the filter of mass thickness 3.33 g/cm^2 monitored the yield of electrons with energies >7.6 MeV, and the detector with the filter of mass thickness 8.84 g/cm^2 captured the yield of electrons with energies >22 MeV. As in the measurements of HXR spectra, the contribution to the detector signal from the HXR photons that passed through the corre-

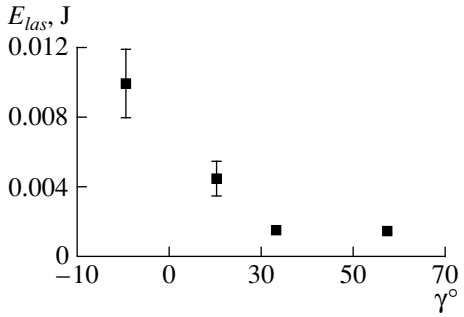

Fig. 3. Spatial distribution of the escaping fast ions for an Al target at $I \approx 5 \times 10^{18}$ W/cm^2. The abscissa is the angle at which an ion escapes from the target plasma with respect to the normal to the target surface, and the ordinate is the fraction of laser energy that is carried away by the fast ions.

sponding filter was determined with the help of an additional detector shielded not only by a Pb filter but also by a Be filter of mass thickness 3.5 g/cm^2. For the detector with a filter of mass thickness 1.26 g/cm^2, this contribution was found to be smaller than 10%; and for the detector with a filter of mass thickness 3.33 g/cm^2, it was found to vanish.

In all measurements of the electron yield, we recorded no signals from the detector with a Pb filter of mass thickness 8.84 g/cm^2. This indicates that no electrons with energies above 22 MeV were produced. Note also that the signals from the detectors positioned on different sides of the target differed by no more than a factor of 2.

In order to construct the HXR spectrum and the spatial distribution of fast electrons escaping from the target plasma in different directions, it is necessary to carry out experiments with a larger number of measurement channels. The data from our experiments allowed us to obtain only rough estimates for both the fraction of electrons with energies higher than 2.7 MeV and the energy that they carried away from the target. In experiments with an Sn target of thickness 650 μm at E_{las} = 12 J (see table), the number of such electrons was estimated to be about 1.5×10^9 and the energy carried by them was about 12×10^{-3} J.

Ion measurements were performed mostly in experiments with Al targets. Our previous measurements and the estimates carried out by analogy with [7] showed that the fast ion component consisted primarily of protons with a maximum velocity of about 10^9 cm/s and maximum energy of about 0.55 MeV.

The appearance of protons (and C ions) in the plasma of an Al target is attributed to the adsorption of water vapor and/or the chemical consequences of polishing the target surface. The measurements of fast ions escaping from the target plasma in different directions (Fig. 3) showed that the ion fluxes were directed preferentially along the normal to the target.

Integrating the ion spectra, we found that the coefficient of the conversion of laser energy into the energy of fast ions with velocities higher than 10^8 cm was 1–3%. Note that this was a lower limit on the conversion coefficient, because the relevant estimates were made under the assumption that the fast ion component consisted only of protons.

Thus, the results of our experiments on irradiating solid targets by picosecond laser pulses with laser light intensities on the target surface in the range up to 5×10^{18} W/cm^2 can be summarized as follows.

We have measured the HXR spectra in the photon energy range 20–1000 keV. The spectra are characterized by two temperatures: the first temperature is 20–30 keV, and the second temperature is 200–400 keV. We have revealed that, in the photon energy range below 40 keV, the spectral intensity decreases with decreasing photon energy.

We have demonstrated the effectiveness of recording fast electrons escaping from the target plasma in different directions by the technique based on semiconductor detectors protected with gray filters made of Pb. Such detectors can be mounted right on the target chamber or can be placed near the chamber.

We have revealed the presence of fast electrons escaping from the plasma with energies above 8 MeV.

Direct measurements of the electron temperature in experiments with an Sn target of thickness 650 μm at E_{las} = 12 J allowed us to estimate both the number of fast electrons with energies higher than 2.7 MeV ($\approx 1.5 \times 10^9$) and the energy they carry away from the target plasma ($\approx 2 \times 10^{-3}$ J).

Table

Target material, thickness, μm	Energy on the target, E_{las}, J	Intensity on the target, I, W/cm^2	Temperature of fast electrons		Relative HXR yield, E_x/E_{las}, for different photon energies		Relative yield of the K_α line, $E_{K\alpha}/E_{las}$
			T_1	T_2	>20 keV	>200 keV	
Sn, 650	12	4.4×10^{18}	30	420	3.9×10^{-4}	2.7×10^{-5}	8.5×10^{-5}
Sn, 110	12.3	5×10^{18}	30	200	3.8×10^{-4}	2.8×10^{-5}	6.5×10^{-5}
Sn, 650	3	1.5×10^{18}		270		1×10^{-5}	9.5×10^{-5}
Al, 100	9.1	3.5×10^{18}	20	280	4.4×10^{-4}	1×10^{-5}	

Using the measured HXR spectra, we have found that the coefficient of the conversion of laser energy into the energy of fast electrons in the range above 15 keV is 1.5–4%.

We have demonstrated experimentally that fast ions escape from the target plasma preferentially along the normal to the target surface. The fraction of laser energy that is converted into the energy of fast ions is found to be 1–3%.

REFERENCES

1. A. A. Andreev, A. A. Mak, and V. E. Yashin, Kvantovaya Élektron. (Moscow) **24**, 99 (1997).
2. H. Ruhl, Y. Sentoku, K. Mima, *et al.*, Phys. Rev. Lett. **82**, 743 (1999).
3. F. N. Beg and A. R. Bell, Phys. Plasmas **4**, 447 (1997).
4. V. Yu. Bychenkov, V. T. Tikhonchuk, and S. V. Tolokonnikov, Zh. Éksp. Teor. Fiz. **115**, 2080 (1999) [JETP **88**, 1137 (1999)].
5. V. G. Borodin, V. M. Komarov, V. A. Malinov, *et al.*, Kvantovaya Élektron. (Moscow) **29**, 101 (1999).
6. A. L. Zapysov, V. G. Borodin, O. N. Gilev, *et al.*, Fiz. Plazmy **24**, 157 (1998) [Plasma Phys. Rep. **24**, 136 (1998)].
7. A. A. Andreev, V. M. Komarov, and A. G. Samsonov, Kvantovaya Élektron. (Moscow) **19**, 709 (1992).

Translated by O. Khadin

JETP Letters, Vol. 71, No. 6, 2000, pp. 250–254. From Pis'ma v Zhurnal Éksperimental'noĭ i Teoreticheskoĭ Fiziki, Vol. 71, No. 6, 2000, pp. 359–365.

CONDENSED MATTER

Spin-Glass Transition in a Kondo Lattice with Quenched Disorder[1]

M. N. Kiselev*, ** and R. Oppermann*, ***

** Institüt für Theoretische Physik, Universität Würzburg, D-97074 Würzburg, Germany*

*** Russian Research Center Kurchatov Institute, pl. Kurchatova 1, Moscow, 123182 Russia*

**** University of Oxford, Department of Physics, OX1 3NP Oxford, UK*

Received January 24, 2000; in final form, February 18, 2000

We use the Popov–Fedotov representation of spin operators to construct an effective action for a Kondo lattice model with quenched disorder at finite temperatures. We study the competition between the Kondo effect and frozen spin order in Ising-like spin glass. We present the derivation of new mean-field equations for the spin-glass order parameter and analyze the effects of screening of localized spins by conduction electrons on the spin-glass phase transition. © *2000 MAIK "Nauka/Interperiodica".*

PACS numbers: 75.20.Hr; 75.10.Nr; 75.30.Mb

One of the most interesting questions of physics of heavy-fermion compounds is the competition between Kondo screening of localized spins by conduction electrons (CE) and ordering of these spins due to Ruderman–Kittel–Kasuya–Yosida (RKKY) interaction (see, e.g., [1]). The screening is attributed to the Kondo effect, viz., the resonance scattering of an electron on a magnetic atom with simultaneous change of the spin projection. In dilute alloys such scattering results in a sharp resonance at the Fermi level with characteristic energy width $\epsilon \sim T_K \sim \epsilon_F \exp(-\alpha^{-1})$, where T_K is the Kondo temperature, J is the coupling constant, ρ is the density of states of CE at the Fermi level, and $\alpha = \rho J$. As was recently discussed (see, e.g., [2, 3]), such competition can be responsible for the non-Fermi-liquid behavior observed in some heavy-fermion compounds. Most of such materials share two characteristics: proximity to the magnetic region of an appropriate phase diagram (usually temperature vs. pressure or chemical composition) and disorder due to chemical substitution. In many respects, the concentrated Kondo systems, e.g., the lattice of magnetic atoms interacting with CE "bath" [Kondo lattice (KL)], show striking similarities to dilute Kondo systems. The Kondo temperature in these systems is a characteristic crossover temperature at which spins transform their local properties to some itinerant Fermi-liquid behavior determining the low-temperature regime of heavy-fermion compounds. Non-Fermi-liquid behavior in a heavy-fermion system is then mainly attributed to reducing the Kondo temperature and possibly even suppressing it to zero. In turn, the magnetic or spin glass (SG) transition can also be suppressed due to the interplay between Kondo scattering and spin–spin interaction. Thus, such an interplay can result in a quantum phase transition [2] when both Kondo and magnetic temperatures are equal to zero at some finite doping. The role of chemical substitution in this case is to "tune" the Fermi level of a metallic system providing sharp Kondo resonance.

The problem of competition between the RKKY and Kondo interactions in a clean system was studied for the first time by Doniach [4] in the "Kondo necklace" model. The transition typically takes place between a paramagnetic metal and a magnetic (usually AFM) metal. In this case, there are two possibilities: the compound will have long-range magnetic order when the RKKY interaction is sufficiently large compared with the Kondo interaction, or the compound will be paramagnetic due to the quenching of magnetic moments of the rare earth atoms and the ground state has the features of a Kondo-singlet state. Nevertheless, in the region $T^M_{\mathrm{RKKY}} \sim T_K$ the competition between magnetic and Kondo interactions results in a dramatic change in the "naive" Doniach diagram (see [5]). Namely, both Kondo and magnetic temperatures are strongly suppressed and a spin-liquid state (e.g., of resonance valence bond type [6]) occurs.

The goal of this letter is to present some results concerning the competition between the Kondo effect and Ising-like SG transition, which is in many aspects similar to the magnetic instability. We study mechanisms of suppressing the SG transition and effects of screening in a disordered environment. In this paper, we consider the high-temperature regime of the KL model. We leave aside the issue of the ground-state properties and especially the question whether the non-Fermi-liquid behavior is a generic feature of vicinity to a quantum phase transition for a future publication.

[1] This article was submitted by the authors in English.

The Hamiltonian of the KL model with additional quenched randomness of exchange interaction between localized spins is given by

$$H_{KL} = \sum_{k\sigma}\varepsilon_k c^\dagger_{k\sigma}c_{k\sigma} + J\sum_i\left(\mathbf{s}_i\mathbf{S}_i + \frac{1}{4}n_iN_i\right) - \sum_{ij} I_{ij}(S^z_iS^z_j + \lambda S^+_iS^-_j). \quad (1)$$

The system under consideration is a periodic lattice of magnetic atoms modeled by f orbitals interacting with metallic background spin density operator $\mathbf{s}_i = \frac{1}{2}c^\dagger_{i\alpha}\boldsymbol{\sigma}_{\alpha\alpha'}c_{i\alpha'}$. The first term in Hamiltonian (1) describes the kinetic energy of CE, and the second stands for the Kondo coupling ($J > 0$). We denote $n_i = \sum_\sigma c^\dagger_{i,\sigma}c_{i,\sigma}$ as the CE density operator. The identity $N_i = 1$ describes the half-filled f-electron shell. Quenched independent random variables I_{ij} with distribution $P(I_{ij}) \sim \exp(-I^2_{ij}N/2I^2)$ stand for direct spin–spin interaction [7]. We assume that this random interaction is of RKKY origin,[2] namely, for d-dimensional system $I \sim \alpha^2\epsilon_F l^{-d}$, where l is the lattice constant in the magnetic sublattice. The magnetic effects can also be included in our approach by introducing the nonzero standard deviation $\Delta I = \bar{I}_{\mathrm{RKKY}}$ into the distribution $P(I_{ij})$, which, in turn, can result in additional competition between SG and AFM (or, rarely, FM) states. For simplicity, we neglect these effects in this letter and concentrate on the interplay between the Kondo interaction and the effects of bond disorder. Since the indirect RKKY interaction through CE is mostly determined by "fast" electrons with characteristic energies $\epsilon \sim \epsilon_F \gg T_K$, we also neglect the Kondo renormalizations of RKKY exchange.

As has been well known for a long time, the spin $S = 1/2$ matrices can be exactly replaced by bilinear combination of Fermi operators

$$S^z_i = \frac{1}{2}(f^\dagger_{i\uparrow}f_{i\uparrow} - f^\dagger_{i\downarrow}f_{i\downarrow}),$$

$$S^+_i = f^\dagger_{i\uparrow}f_{i\downarrow}, \quad S^-_i = f^\dagger_{i\downarrow}f_{i\uparrow}.$$

Nevertheless, most fermionic representations of spin are not free of constraint problem. For this reason, the dimensionality of space in which these operators act is always greater than the dimensionality of the spin matrices. Elimination of unphysical states is a serious problem which makes the diagrammatic techniques quite complicated. Moreover, in most cases, the analytic continuation of Feynman diagrams becomes extremely difficult. To avoid the main difficulties related to constraint, the new representation for spin operators was proposed in the long-forgotten paper of Popov and Fedotov [9]. In this representation the partition function of the problem containing spin operators (H_S) can be easily expressed in terms of new fermions with imaginary chemical potential (H^f_S):

$$Z_S = \mathrm{Tr}e^{-\beta H_S} = i^N\mathrm{Tr}\exp\{-\beta(H^f_S + i\pi N_f/2\beta)\},$$

$$N_f = \sum_{i\sigma} f^\dagger_{i\sigma}f_{i\sigma}, \quad \beta = 1/T.$$

As a result, there is no constraint, the unphysical states are eliminated, and the standard Matsubara–Abrikosov–Gor'kov diagrammatic technique is obtained [9–11].

We sketch our derivation of the effective action and of resulting mean-field equations for the KL model in order to make explicit the approximations adopted and the physics underlying these approximations. To construct the path-integral representation for the partition function, the new Grassmann variables $c^\dagger_{i\alpha} \longrightarrow \bar{\Psi}_{i\sigma}$, $c_{i\sigma} \longrightarrow \Psi_{i\sigma}$ for CE with chemical potential μ and $f^\dagger_{i\alpha} \longrightarrow \bar{a}_{i\sigma}$, $f_{i\alpha} \longrightarrow a_{i\alpha}$ for Popov–Fedotov spin operators ($S = 1/2$) are introduced. The Euclidean action for the KL model is given by

$$\mathcal{A} = \int_0^\beta d\tau\left(\sum_{i\alpha}[\bar{\Psi}_{i\alpha}(\tau)(\partial_\tau + \mu)\Psi_{i\alpha}(\tau) + \bar{a}_{i\alpha}(\tau)(\partial_\tau - i\pi T/2)a_{i\alpha}(\tau)] - H_{int}(\tau)\right), \quad (2)$$

where the generalized Grassmann fields satisfy the following boundary conditions: $\Psi_{i\alpha}(\beta) = -\Psi_{i\alpha}(0)$, $\bar{\Psi}_{i\alpha}(\beta) = -\bar{\Psi}_{i\alpha}(0)$, $a_{i\alpha}(\beta) = ia_{i\alpha}(0)$, $\bar{a}_{i\alpha}(\beta) = -i\bar{a}_{i\alpha}(0)$.

In this paper, we consider $\lambda = 0$, which corresponds to the Sherrington–Kirkpatrik [12] spin-glass model. Such an anisotropy of RKKY interaction can be associated, e.g., with lattice geometry. In the case of the Ising-like model, the dynamical fluctuations in the spin subsystem appear only due to the interaction with conduction electrons and, in the high temperature regime $T \sim T_{\mathrm{SG}}$, can be neglected. To study the influence of Kondo scattering on the SG transition temperature T_{SG}, we use standard replica trick $\Psi_i(\tau) \longrightarrow v^a_i(\tau)$, $a_i(\tau) \longrightarrow \varphi^a_i(\tau)$, $a = 1, \ldots, n$. Then the free energy of the model

[2] It has been pointed out in [8] that the presence of nonmagnetic impurities makes the RKKY interaction a random interaction even in the case of regular arrangement of magnetic moments.

can be calculated (see, e.g., [13]) by taking the formal limit $n \longrightarrow 0$ in

$$\langle Z^n \rangle_{av} = \prod \int dI_{ij} P(I_{ij}) \prod D[\varphi^a_{i,\sigma} \nu^a_{i,\sigma}] \times \exp\left(\mathcal{A}_0[\nu^a, \varphi^a] - \int_0^\beta d\tau H_{int}(\tau) \right), \quad (3)$$

where $\mathcal{A}_0$ corresponds to noninteracting fermions.

As we already mentioned, to consider the competition between the Kondo scattering and the trend of disorder, we assume that the magnetic temperature $T^M_{\mathrm{RKKY}} \ll T^*$, where T^* stands for a characteristic temperature corresponding to the Kondo temperature in the lattice. This assumption allows one to decouple the Kondo interaction term $H^K_i = -\frac{J}{2} \bar{\nu}^a_{i,\sigma} \varphi^a_{i,\sigma} \bar{\varphi}^a_{i,\sigma'} \nu^a_{i,\sigma'}$ in each site by the replica-dependent Hubbard–Stratonovich field ψ^a_i [14]. Performing the average over the random potential in (3) results in

$$\langle Z^n \rangle_{av} = \prod \int D[\nu^a, \varphi^a, \psi^a] \exp\left(\mathcal{A}_0 + \frac{I^2}{4N} \mathrm{Tr}[X^2] + \int_0^\beta d\tau \sum_{i,a,\sigma} \left\{ \psi^a_i \bar{\nu}^a_{i\sigma} \varphi^a_{i\sigma} + \psi^{a*}_i \bar{\varphi}^a_{i\sigma} \nu^a_{i\sigma} - \frac{2}{J} |\psi^a_i|^2 \right\} \right) \quad (4)$$

with

$$X^{ab}(\tau, \tau') = \sum_i \sum_{\sigma,\sigma'} \bar{\varphi}^a_{i,\sigma}(\tau) \sigma \varphi^a_{i,\sigma}(\tau) \bar{\varphi}^b_{i,\sigma'}(\tau') \sigma' \varphi^b_{i,\sigma'}(\tau').$$

The next step is to perform the Gaussian integration over the replica-dependent Grassmann field ν^a describing CE and to decouple the eight-fermion term $\mathrm{Tr}[X^2]$ with the help of Q matrices (see details in [10]). As a result, the partition function is given by

$$\langle Z^n \rangle_{av} = \int D[Q] \exp\left(-\frac{1}{4} (\beta I)^2 N \mathrm{Tr}[Q^2] + \sum_i \ln \left\{ \prod \int D[\varphi^a, \psi^a] \times \exp\left[\sum_a \sum_{\{\omega\}} \bar{\varphi}^a_{i,\sigma} \mathcal{G}^{-1}_a \varphi^a_{i\sigma} + \frac{1}{2} (\beta I)^2 \mathrm{Tr}[QX] \right] \right\} \right), \quad (5)$$

where $\mathcal{G}^{-1}$ is the inverse Green's function for Popov–Fedotov fermions depending on Matsubara frequencies $\omega_n = 2\pi T(n + 1/4)$ (see details in [9]),

$$\mathcal{G}^{-1}_a = i\omega_{n_1} \delta_{\omega_{n_1}, \omega_{n_2}} - T \sum_\epsilon \psi^{a*}_i(\epsilon_l + \omega_{n_1}) \times G_0(-i\nabla_i, \epsilon_l) \psi^a_i(\epsilon_l + \omega_{n_2}), \quad (6)$$

and $G_0(-i\nabla, \epsilon_l) = (i\epsilon_l - \varepsilon(-i\nabla) + \mu)^{-1}$ stands for the CE Green's function $\epsilon_l = 2\pi T(l + 1/2)$.

We are still left with a term of fourth order residing in $\mathrm{Tr}[QX]$ and cannot evaluate the Grassmann integral directly. Consequently, a second decoupling is needed. To perform it, we stress that we do not intend to deal with dynamical behavior here and confine ourselves by high temperature regime in the vicinity of the SG transition such that the lowest Matsubara frequency is sufficient. Assuming this and recalling that the spatial fluctuations are suppressed by the choice of infinite-range interaction [12], one can consider Q as a constant saddle-point matrix under condition $Q = Q^T$. The elements of this matrix will later be determined self-consistently from the saddle-point condition. Assuming that the elements of Q are $Q^{aa}_{SP} = \tilde{q}$ and $Q^{a \neq b}_{SP} = q$, one can decouple the $\mathrm{Tr}[QX]$ term by introducing replica-independent z and replica-dependent y^a fields and map the KL problem with disorder onto an effective one-site interacting spin system coupled to an external local replica-dependent magnetic field:

$$\langle Z^n \rangle_{av} = \exp\left(-\frac{1}{4} (\beta I)^2 N (n\tilde{q}^2 + n(n-1)q^2) + \sum_i \ln \left[\prod \int D[\varphi^a, \psi^a] \int_z^G \int_{y^a}^G \exp(\mathcal{A}[\varphi^a, \psi^a, y^a, z]) \right] \right), \quad (7)$$

where $\int_z^G f(z)$ denotes $\int_{-\infty}^{\infty} dz/\sqrt{2\pi} \exp(-z^2/2) f(z)$,

$$\mathcal{A}[\varphi^a, \psi^a, y^a, z] = \sum_{a,\sigma} \bar{\varphi}^a_\sigma [\mathcal{G}^{-1}_a - \sigma H(y^a, z)] \varphi^a_\sigma - \frac{2}{J} \sum_\omega |\psi^a(\omega)|^2 \quad (8)$$

and $H(y^a, z) = I\sqrt{q}\, z + I\sqrt{\tilde{q} - q}\, y^a$ is the effective local magnetic field. Note that the variable $q = \langle S^a_i S^b_i \rangle$ corresponds to the Edwards–Anderson SG order parameter when the limit $n \longrightarrow 0$ is taken. Nevertheless, the diagonal element $\tilde{q}$ can be set to neither zero nor one, in contrast to the classical Ising glass theory, because of dynamical effects due to the interaction with the CE bath. To take into account this interaction, we include a replica-dependent magnetic field into the bare Green's function $\mathcal{G}^a_{0\sigma} = (i\omega_n - \sigma H(y^a, z))^{-1}$ and perform the inte-

gration over Popov–Fedotov Grassmann variables with the help of the expression

$$\begin{aligned}\mathrm{Tr}\ln(\mathcal{G}_a^{-1} - \sigma H) &= \ln(2\cosh(\beta H)) \\ &+ \mathrm{Tr}\sum_{m=1}^{\infty}\frac{(-1)^{m+1}}{m}(\mathcal{G}_{0\sigma}^{a}(H)\Sigma(\psi^a))^m,\end{aligned} \tag{9}$$

where $\Sigma(\psi^a) = -T\sum_{\epsilon}\psi_i^{a*}(\epsilon + \omega_{n_1})G_0(-i\nabla_i, \epsilon)\psi_i^a(\epsilon + \omega_{n_2})$ depends on the variable ψ "responsible" for Kondo interaction. Calculating the first term in expansion (9), one gets the following expression for the effective "bosonic" action in the one-loop approximation:

$$\begin{aligned}\mathcal{A}[\psi^a, H] &= \ln(2\cosh(\beta H(y^a, z))) \\ -\frac{2}{J}\sum_n &[1 - J\Pi(i\Omega_n, H(y^a, z))]|\psi^a|^2 - O(|\psi^a|^4).\end{aligned} \tag{10}$$

The polarization operator Π in the limit $T, H \ll \epsilon_F$ is given by

$$\begin{aligned}&\Pi(i\Omega_n, H) \\ &= -\beta^{-1}\sum_{n,\mathbf{k},\sigma} G_0(\mathbf{k}, i\epsilon_n + i\Omega_n)\mathcal{G}_{0\sigma}(i\epsilon_n, H) \\ &\xrightarrow{\Omega_n = 0} \rho(0)\left[\ln\left(\frac{\epsilon_F}{\sqrt{H^2 + \pi^2\beta^{-2}/4}}\right)\right. \\ &\left. + \frac{\pi}{2\cosh(\beta H)} + O\left(\frac{H^2}{\epsilon_F^2}\right)\right].\end{aligned} \tag{11}$$

When $H = 0$, the coefficient in front of $|\psi^a|^2$ in Eq. (10) changes its sign at $T^* \sim \epsilon_F\exp(-\alpha^{-1})$. This is a manifestation of the single-impurity Kondo effect (see, e.g., [14, 15]).

One can now perform the Gaussian integration over ψ^a fields in Eq. (7) by the stationary phase method:

$$\begin{aligned}&\int D[\psi^a]\exp(\delta\mathcal{A}[\psi^a]) \\ &= \exp(-\mathrm{Tr}\ln[1 - J\Pi(i\Omega_n, H(y^a, z))]).\end{aligned}$$

After the last step, namely, integration over replica-dependent field y^a, the limit $n \longrightarrow 0$ can be taken. The free energy per site $f = \beta^{-1}\lim_{n\to 0}(1 - \langle Z^n\rangle_{av})/nN$ is given by

$$\begin{aligned}\beta f(\tilde{q}, q) &= \frac{1}{4}(\beta I)^2(\tilde{q}^2 - q^2) \\ &- \int_z^G \ln\left(\int_y^G \frac{2\cosh(\beta H(y, z))}{1 - J\Pi(0, H(y, z))}\right).\end{aligned} \tag{12}$$

New equations for q, $\tilde{q}$ are determined by conditions $\partial f(\tilde{q}, q)/\partial\tilde{q} = 0$, $\partial f(\tilde{q}, q)/\partial q = 0$:

$$\begin{aligned}&\frac{1}{2}(\beta I)^2\tilde{q} = \int_z^G \frac{\partial\ln\mathcal{F}}{\partial\tilde{q}}, \quad \frac{1}{2}(\beta I)^2 q = -\int_z^G \frac{\partial\ln\mathcal{F}}{\partial q}, \\ &\mathcal{F} = \int_y^G \frac{2\cosh(\beta H(y, z))}{1 - J\Pi(0, H(y, z))}.\end{aligned} \tag{13}$$

Eqs. (12), (13) contain the key result of the paper. They represent the solution of the KL problem with quenched disorder on a replica symmetrical level. To demonstrate some interesting physical effects described by these equations, let us consider the case $T \sim T_{SG} \geq T^*$ (Kondo high-temperature limit). Since $H(y^a, z)$ is a dynamical variable, we break the parametrical region of H to several pieces. First, when $H \gg T, T^*$, the logarithm in Eq. (11) is cut by H and there are no temperature-dependent Kondo corrections to the mean field equations. This corresponds to the limit $T^* \ll I$ providing frozen spins and preventing them from resonance scattering.[3] Nevertheless, when $T^* \sim I$, the region $H \leq T$ becomes very important. We calculate $\mathcal{F}$ expanding the rhs of Eq. (12) up to $(H/T)^2$:

$$\begin{aligned}\ln(C\mathcal{F}_{z,\tilde{q},q}) &= -\frac{1}{2}\ln(1 + \gamma u^2 r^2) + \frac{u^2}{2}\frac{r^2 - q\gamma z^2}{1 + \gamma u^2 r^2} \\ &+ \ln\left[\cosh\left(\frac{uz\sqrt{q}}{1 + \gamma u^2 r^2}\right)\right].\end{aligned} \tag{14}$$

We use the following shorthand notations: $u = \beta I$, $\gamma = 2c/\ln(T/T^*)$, $r^2 = \tilde{q} - q$, and $C = 2c\alpha/\gamma$ with $c = \pi/4 + 2/\pi^2 \sim 1$. We note again that when $J = 0$, which corresponds to the absence of Kondo interaction,

$$\mathcal{F}(z, \tilde{q}, q) = \exp\left(\frac{1}{2}(\beta I)^2(\tilde{q} - q)\right)\cosh(\beta I z\sqrt{q})$$

and the standard Sherrington–Kirkpatrik equation [12] takes place, providing, e.g., an exact identity $\tilde{q} = 1$.

In the vicinity of the phase-transition point, Eq. (13) reads

$$\begin{aligned}\tilde{q} &= 1 - \frac{2c}{\ln(T/T^*)} + O\left(\frac{1}{\ln^2(T/T^*)}\right), \\ q &= \int_z^G \tanh^2\left(\frac{\beta I z\sqrt{q}}{1 + 2c(\beta I)^2(\tilde{q} - q)/\ln(T/T^*)}\right) \\ &+ O\left(\frac{q}{\ln^2(T/T^*)}\right).\end{aligned} \tag{15}$$

[3] We also note that when $T^* \gg I$ the SG transition does not happen.

These equations describe a second-order transition in an SG Ising-like Sherrington–Kirkpatrik[4] system coupled with a CE bath in the presence of Kondo scattering. Taking the limit $q \longrightarrow 0$, we estimate the temperature of SG transition $(T_{SG}/I)^2 = 1 - 4c/\ln(T_{SG}/T^*) - \ldots < 1$. Thus, the Kondo-scattering resonance results in depression of the SG-transition temperature due to the screening effects in the same way as magnetic moments and one-site susceptibility are screened in the single-impurity Eq. Kondo problem [15]. This screening shows up at large time scale $t \geq 1/T^*$ and affects both diagonal and nondiagonal elements of the Q matrix. Moreover, $\tilde{q}$ becomes partially screened well above the SG transition point. Recalling that $H \sim Iy\sqrt{\tilde{q}}$, one can see that our assumption $H/T \leq 1$ is consistent with Eq. (15) even if $T \sim T_{SG}$. It is necessary to note that a growing SG order parameter in Eqs. (10)–(11) suppresses the Kondo effect and also provides a broader validity domain for Eq. (15). We leave the self-consistent analysis of Eqs. (12), (15) for a future detailed publication.

In conclusion, we have considered the Kondo high-temperature limit (in a sense of $T > T^*$) of a KL model with quenched disorder. We derived new mean field equations for the SG transition in the presence of strong Kondo scattering and have shown that the partial screening of both diagonal and nondiagonal elements of the Q matrix takes place. As a result, the temperature of SG transition is strongly suppressed when Ising and Kondo interactions are of the same order of magnitude.

We thank F. Bouis, B. Coqblin, K. Kikoin, and P. Pfeuty for useful discussions. This work is supported by the SFB410 (II-VI semiconductors). One of us (MNK) is grateful to the Alexander von Humboldt Foundation for support during his stay in Germany.

[4] When an Ising system described by Eq. (1) with nearest neighbor interaction is treated with the mean-field theory, equations identical to Eq. (13) are obtained with $\sqrt{Z}\,I$ replacing I, where Z is the average number of neighbors.

REFERENCES

1. N. Grewe and F. Steglich, in *Handbook of the Physics and Chemistry of Rare Earths*, Ed. by K. A. Gschneider, Jr., and L. Eyring (Elsevier, Amsterdam, 1991), Vol. 14, p. 343.
2. A. Rosch, A. Schröder, O. Stockert, and H. V. Löhneysen, Phys. Rev. Lett. **79**, 159 (1997).
3. A. Schröder, G. Aeppli, E. Bucher, *et al.*, Phys. Rev. Lett. **80**, 5623 (1998).
4. S. Doniach, Physica B (Amsterdam) **91**, 231 (1977).
5. K. A. Kikoin, M. N. Kiselev, and A. S. Mishchenko, Pis'ma Zh. Éksp. Teor. Fiz. **60**, 583 (1994) [JETP Lett. **60**, 600 (1994)]; Zh. Éksp. Teor. Fiz. **112**, 729 (1997) [JETP **85**, 399 (1997)]; J. R. Iglesias, C. Lacroix, and B. Coqblin, Phys. Rev. B **56**, 11820 (1997).
6. P. Coleman and N. Andrei, J. Phys.: Condens. Matter **1**, 4057 (1989).
7. S. Sachdev, N. Read, and R. Oppermann, Phys. Rev. B **52**, 10286 (1995); A. Sengupta and A. Georges, *ibid.* **52**, 10295 (1995).
8. A. Yu. Zyuzin and B. Z. Spivak, Pis'ma Zh. Éksp. Teor. Fiz. **43**, 185 (1986) [JETP Lett. **43**, 234 (1986)]; L. N. Bulaevskiĭ and S. V. Panyukov, Pis'ma Zh. Éksp. Teor. Fiz. **43**, 190 (1986) [JETP Lett. **43**, 240 (1986)].
9. V. N. Popov and S. A. Fedotov, Zh. Éksp. Teor. Fiz. **94**, 193 (1988) [Sov. Phys. JETP **67**, 535 (1988)].
10. R. Oppermann and A. Muller-Groeling, Nucl. Phys. B **401**, 507 (1993).
11. F. Bouis and M. Kiselev, Physica B (Amsterdam) **259**–**261**, 195 (1999).
12. D. Sherrington and S. Kirkpatrik, Phys. Rev. Lett. **35**, 1972 (1975).
13. K. Binder and A. P. Young, Rev. Mod. Phys. **58**, 801 (1986).
14. N. Read and D. M. Newns, J. Phys. C **16**, 3273 (1983).
15. A. M. Tsvelik and P. B. Wiegmann, Adv. Phys. **32**, 453 (1983).

JETP Letters, Vol. 71, No. 6, 2000, pp. 255–258. Translated from Pis'ma v Zhurnal Éksperimental'noĭ i Teoreticheskoĭ Fiziki, Vol. 71, No. 6, 2000, pp. 366–371.

CONDENSED MATTER

Electrostatic Potential, Energy Spectrum, and Fano Resonances in a Ballistic Ring Interferometer Based on an AlGaAs/GaAs Heterojunction

O. A. Tkachenko*, V. A. Tkachenko*, D. G. Baksheev*, Z. D. Kvon*, and J. C. Portal**

** Institute of Semiconductor Physics, Siberian Division, Russian Academy of Sciences, pr. Akademika Lavrent'eva 13, Novosibirsk, 630090 Russia*

Novosibirsk State University, ul. Pirogova 2, Novosibirsk, 630090 Russia

e-mail: bd@isp.nsc.ru

*** Grenoble High Magnetic Fields Laboratory, MPI-FKF and CNRS, B.P.166 F-38042 Grenoble, France*

Received February 4, 2000

For a ballistic ring interferometer based on high-mobility two-dimensional electron gas in an AlGaAs/GaAs heterojunction, the electrostatic potential and the energy spectrum are determined. It is shown that the splitting points in such an interferometer have the form of triangular potential wells. Calculation is performed for the two-dimensional electron transmission through the ring, and the Fano resonances caused by the coupling of the transmitted waves with the levels of higher transverse modes in triangular wells are predicted. These resonances are observed in the experiment. © *2000 MAIK "Nauka/Interperiodica".*

PACS numbers: 07.60.Ly; 73.23.Ad; 73.20.Dx; 73.50.-h

Since the pioneering publications [1, 2], the theoretical and experimental studies of ring interferometers have been continued for more than 15 years. Of special interest are the studies of semiconductor interferometers based on high-mobility two-dimensional electron gas in AlGaAs/GaAs heterojunctions [2–6]. These devices make it possible to observe the interference of ballistic electrons in the regime of a small number of propagating modes (down to a single one). In this paper, we consider the operation of such an interferometer as a quantum transistor in zero magnetic field.

Until recently, the analysis of the transport properties of ballistic ring interferometers was based on an idealized one-dimensional model that did not take into account the real profile of the potential (see [1, 7]). According to this model, uniform conductance oscillations without any additional modulation should only be observed in an open symmetric ring upon changing the Fermi energy. The origin of these oscillations can be understood in the framework of the Fabry–Perot two-mirror interference pattern, where the role of semitransparent mirrors is played by the points of ring connection with the input and output quantum wires. It is evident that real interferometers fabricated on the basis of GaAs/AlGaAs heterojunctions cannot be adequately described by one-dimensional models, because the latter allow neither for the finite width of the channels nor for the real profile of the electrostatic potential. The inadequacy of the one-dimensional model is particularly evident from the fact that the channel-splitting point in this model is a geometric one, while in a real structure it is formed by smooth electrostatic fields.

The interferometer model proposed in this paper is free of the above-mentioned disadvantages of the one-dimensional description. It is based on the solution of a three-dimensional electrostatic problem for the real structure and geometry of a ballistic interferometer. The electrostatic potential in the plane of a 2D gas was calculated and used for solving the 2D Schrödinger equation and determining the interferometer conductance. It was found that the presence of triangular quantum dots at the channel-splitting points is a fundamental feature of interferometers. The calculation of the transmissivity of such an interferometer shows that a variation in the Fermi energy is accompanied by the appearance of large-scale Fano-type conductance resonances [8] due to the scattering by the levels of the triangular dots. As a result, the ring conductance is a superposition of high-frequency oscillations, which correspond to transmission through the one-dimensional ring levels, and large-scale dips and peaks caused by the Fano resonances. Such conductance behavior is experimentally observed for ballistic rings based on a high-mobility 2D gas in a GaAs/AlGaAs heterojunction.

The calculations were performed for a ring structure with the cross section shown in Fig. 1a. Such structures are fabricated by electron-beam lithography and subsequent plasma-chemical etching [9, 10]. The upper part of the structure is occupied by a metal gate controlling the electron density in the ring. All interferometer

0021-3640/00/7106-0255$20.00

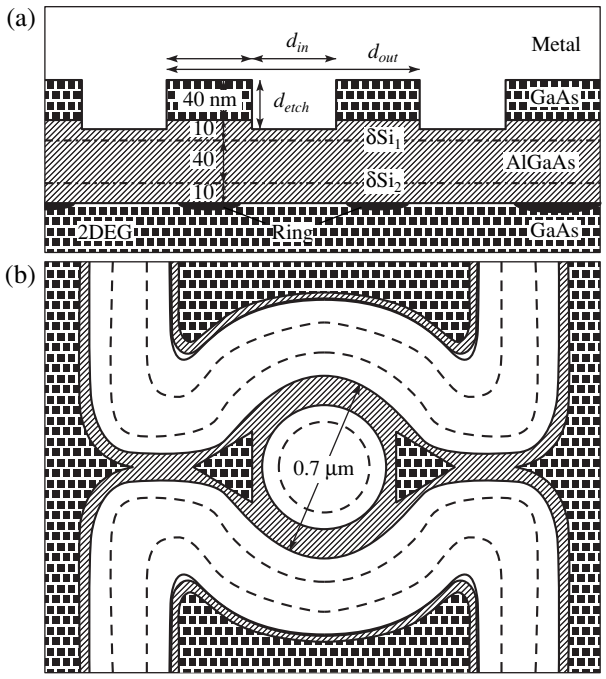

Fig. 1. (a) Cross section of the structure along the ring diameter. The dot-and-dash lines show the delta-doped layers with concentrations 2×10^{12} cm^{-2} (δSi_1) and 10^{12} cm^{-2} (δSi_2). The continuous gate is shown by hatching. The electron gas (shown by the thick black line) has the concentration in the reservoirs $n_s = 6 \times 10^{11}$ cm^{-2}. (b) Profile of the electrostatic potential in the ring interferometer. The dashed lines indicate the etch areas. At the ring input and output, two open triangular quantum dots of characteristic size ~200 nm appear.

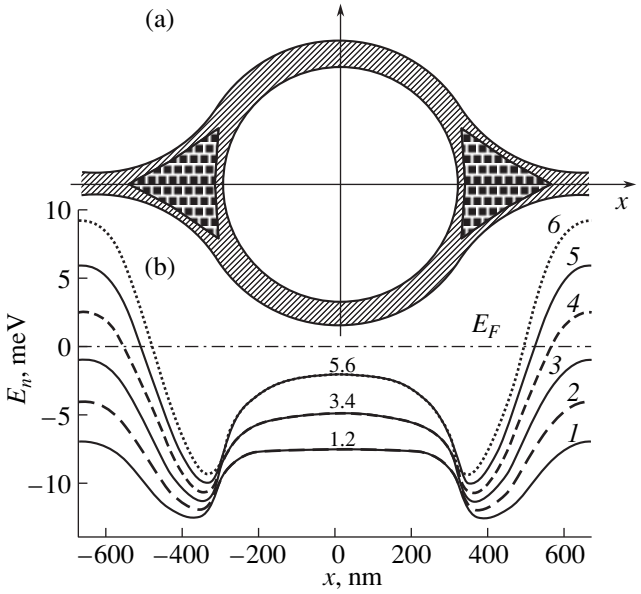

Fig. 2. (a) Section of the interferometer between the barriers in the input/output channels. (b) Energy levels $E_n(x_j)$ of the confining potential $U(x_j, y)$ in the ring interferometer. The plot shows the six lowest one-dimensional subbands $E_n(x)$.

parameters used in the calculations were chosen in accordance with the experiment.

The electrostatic potential $\phi(x, y, z)$ was determined by solving the three-dimensional Poisson equation $\nabla(\epsilon\nabla\phi) = -\rho(\phi)$, where $\epsilon(x, y, z)$ is the permittivity and the charge density ρ includes the distribution of both ionized Si impurities in the $Al_xGa_{1-x}As$ layer and electrons at the AlGaAs/GaAs heteroboundary. The electron distribution was determined self-consistently in the Thomas–Fermi approximation. The boundary conditions at the semiconductor surface corresponded to the Fermi level positioning at the band-gap center at zero gate voltage. In the bulk of the structure, the boundary conditions were determined on the assumption of a *p*-type background doping. The Poisson equation was solved by the Chebyshev cyclic method [11].

Figure 1b shows the distribution of the electrostatic potential in the plane of a 2D gas. The dashed lines indicate the etched areas, white color corresponds to the areas free from electrons, and gray color corresponds to the areas occupied by electrons. The thick line corresponding to the Fermi level defines narrow ballistic channels that form the ring interferometer. At the splitting points where the input and output channels split in two, the channels are broadened, leading to the appearance of fairly deep potential wells of triangular shape (quantum dots) at the ring input and output. These wells are retained when the structure parameters vary over wide limits. Hence, the presence of such wells is a universal property of semiconductor ring interferometers.

The calculated profile of the electrostatic potential was used for determining one-dimensional subbands $E_n(x)$ (Fig. 2); i.e., a one-dimensional Schrödinger equation with confining potential $U(x_j, y)$ was solved along the *y*-axis and the energy levels $E_n^{(j)}$ and wave functions $\xi_n^{(j)}(y)$ were determined for every cross-section $x = x_j$ of the interferometer. In the quantum wires forming the ring, the potential profile in the cross section is nearly parabolic and the energy levels are approximately equidistant as in an oscillator. In the ring area, the energy levels are twofold degenerate, because the potential wells of the two ring arms are identical and separated by a wide barrier. Therefore, the one-dimensional subbands are grouped in pairs inside the ring. Since the width of quantum wires connecting the ring with leads is the same as the width of the ring channel in the interferometers under study, the number of subbands occupied by electrons in the ring area is approximately twice that in the input/output channels. One can see from Fig. 2b that subbands *3* and *4* in the ring become populated even before the opening of the second mode in the input/output channel. This is also reflected in the transport.

In the example presented above, the one-dimensional subbands $E_n(x)$ with numbers $n > 3$ are closed for

the transmission of particles with the Fermi energy E_F (because $E_n > E_F$ in the input/output constrictions). However, in the regions of triangular dots, about ten one-dimensional subbands occur below the Fermi level, and these subbands form potential wells with a set of discrete levels. This means that the splitter, which is assumed to be nonreflecting or partially reflecting in simple one-dimensional models, has a complex internal structure. At the points of the channel junctions, intense mixing of different transverse quantization modes takes place. As a result, the electrons transmitted through the ring by the first, second, or third mode can be scattered by the levels of higher transverse modes. In the conductance, this effect manifests itself in the form of asymmetric peak–dip profiles similar to the Fano resonances (Fig. 3) caused by the interference of the resonance and nonresonance transmission channels.

The coefficient of electron transmission through the interferometer in zero magnetic field was calculated by the *S*-matrix method [12]. This method is numerically stable and enables one to analyze the contributions of different transverse modes to the conductance. It is commonly used for simplified calculations of the transport through channels with rigid walls and a piecewise constant potential (see, e.g., [13]). In the case under study, the transmissivity was determined for the realistic potential profile by using the calculated energies of one-dimensional subbands $E_n^{(j)} = E_n(x_j)$ and the transition matrix elements $(C_j)_{mn} = \int \xi_m^{(j)}(y)\xi_n^{(j+1)}(y)dy$, where $\xi_n^{(j)}(y)$ is the wave function of the level $E_n^{(j)}$ within the constant-potential interval (x_j, x_{j+1}). Then the wave function can be written as a sum of the components corresponding to different transverse modes:

$$\Psi(x, y) = \sum_{n=1}^{M} (k_n^{(j)})^{-1/2} [a_n^{(j)} \exp\{ik_n^{(j)}(x - x_j)\} + b_n^{(j)} \exp\{ik_n^{(j)}(x - x_{j+1})\}]\xi_n^{(j)}(y), \quad (1)$$

where $k_n^{(j)} = \sqrt{2m(E_F - E_n^{(j)})/\hbar^2}$ is the wave number corresponding to the longitudinal motion, and the summation is limited to a finite number of modes *M*. The amplitudes $a^{(j)}$ and $b^{(j)}$ at adjacent intervals are related through the scattering matrix S_j:

$$\begin{pmatrix} a^{(j+1)} \\ b^{(j)} \end{pmatrix} = S_j \begin{pmatrix} a^{(j)} \\ b^{(j+1)} \end{pmatrix}. \quad (2)$$

The total *S*-matrix describing the scattering from the whole structure is a combination of the matrices S_j [12]:

$$S = S_0 \otimes S_1 \otimes \ldots \otimes S_N = \begin{pmatrix} t & r \\ r' & t' \end{pmatrix}, \quad (3)$$

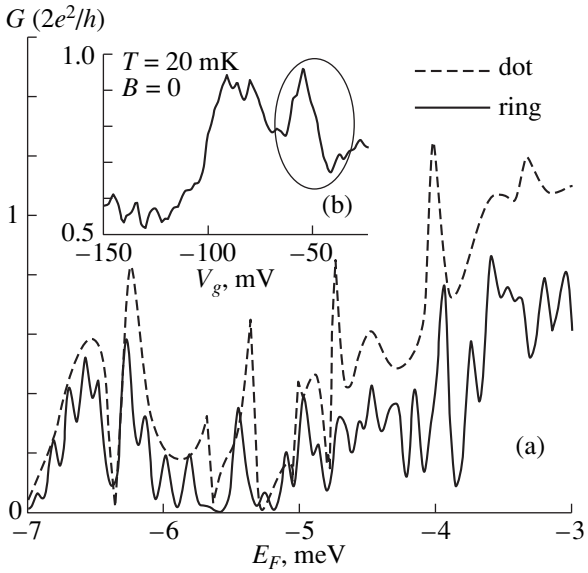

Fig. 3. (a) Modeling of 2D transport through the ring interferometer. The large-scale oscillations are caused by the resonances with the levels of triangular quantum dots, and the small-scale oscillations are caused by the resonances with the one-dimensional ring levels. For comparison, the dashed line shows the conductance of one T-junction (half of the ring). The threshold for the opening of the second mode in the input/output channels is $E_F = -4$ meV. For $-5 < E_F < -4$ meV, the third/fourth-mode motion is allowed inside the ring, resulting in the appearance of doubled frequency oscillations in the conductance. (b) Ring conductance as a function of gate voltage in zero magnetic field at temperature 20 mK. The Fano resonance is encircled.

where *t* and *t*' are the total transmission amplitudes for opposite directions and *r* and *r*' are the corresponding reflection amplitudes. The conductance of the structure is determined by the Landauer formula $G = (2e^2/h)\mathrm{Tr}[tt^+]$. Figure 3a presents the dependences of the transmissivity at the Fermi energy for the interferometer potential shown in Fig. 1b. The calculation was performed for $M = 20$ modes of the transverse motion. The result did not change upon a further increase in the number of modes. The solid line shows the transmissivity for the whole ring, and the dashed line corresponds to the transmissivity for a single "T-junction" (the calculations were performed for one half of the ring, and the transmission through the two channels was summed up at the output). A correlation between these two curves is seen. In the transmission through a single T-junction, high-amplitude dips and asymmetric peaks are observed. These are the Fano resonances caused by coupling of the transmitted waves with the levels of the higher transmission-closed one-dimensional subbands to form the potential wells in the channel-splitting region. When two T-junctions combine to form a ring interferometer, the reflection is enhanced and, in addition, high-frequency oscillations of the Fabry–Perot type appear owing to the resonances with the one-

dimensional ring levels. The suppression of the transmission because of the intersubband transitions makes the dense peaks narrow, as in the case of an isolated ring. For this reason, these peaks are blurred in the experiment (Fig. 3b) and smoothed out in the calculation. In addition, owing to the strong reflection caused by the triangular quantum dots, the conductance does not exhibit the $n(2e^2/h)$ steps, by which one can judge how many modes are open. The conductance is almost always lower than the $2e^2/h$ quantum when two or three transverse quantization modes are open (Fig. 3a). Hence, although $G < 2e^2/h$ in the measured dependences (Fig. 3b), one cannot state with assurance that the interferometer operates in a single-mode regime. Thus, the experimental dependence $G(V_g)$ reflects all the qualitative features obtained for the ring conductance by modeling: the large-scale variations caused by the Fano resonances and the oscillations having much lower amplitude and higher frequency and associated with the one-dimensional ring levels. The modeling shows that the complex-$G(V_g)$ profile strongly changes with variations in the parameters of the quantum dots within the technological tolerances. Therefore, a detailed comparison between the experimental and calculated dependences makes little sense. In the lateral quantum dots, the Fano resonances were detected only recently, and it was shown that the asymmetric profile of these resonances is highly sensitive to the gate voltages and the magnetic field [14].

Thus, it is shown in this paper that the presence of triangular quantum dots at the input and output of the device is the characteristic feature of the electrostatic potential profile in a semiconductor ring interferometer based on a 2D electron gas in an AlGaAs/GaAs heterojunction. The subbands are strongly mixed in these dots. As a result, the dependence of ring conductance on gate voltage is a superposition of high-amplitude peaks and dips (Fano resonances) and the low-amplitude high-frequency oscillations associated with the one-dimensional levels of the ring interferometer. Such conductance behavior is observed in the experiment.

This work was supported by the International Scientific Technical program FTNS (grant no. 98-1102), by the Program "Russian Universities Fundamental Research" (grant no. 1994), and by the International Scientific and Technical Program "Micro- and Macroelectronics" (grant no. 02.04.5.1).

REFERENCES

1. M. Buttiker, Y. Imry, and R. Landauer, Phys. Lett. A **96**, 365 (1983); M. Buttiker, Y. Imry, and M. Ya. Azbel, Phys. Rev. A **30**, 1982 (1984); M. Buttiker, in *SQUID'85—Superconducting Quantum Interference Devices and Their Applications*, Ed. by H. D. Haklbohm and H. Lubbig (Walter de Gruyter, New York, 1985).
2. R. A. Webb, S. Washburn, C. P. Umbach, and R. B. Leibowitz, Phys. Rev. Lett. **54**, 2696 (1985).
3. G. Timp, A. M. Chang, J. E. Cunningham, *et al.*, Phys. Rev. Lett. **58**, 2814 (1987).
4. C. J. B. Ford, A. B. Fowler, J. M. Hong, *et al.*, Surf. Sci. **229**, 307 (1990).
5. K. Ismail, S. Washburn, and K. Y. Lee, Appl. Phys. Lett. **59**, 1998 (1991).
6. A. A. Bykov, Z. D. Kvon, E. B. Olshanetsky, *et al.*, Pis'ma Zh. Éksp. Teor. Fiz. **57**, 596 (1993) [JETP Lett. **57**, 613 (1993)].
7. Jian-Bai Xia, Phys. Rev. B **45**, 3593 (1992).
8. U. Fano, Phys. Rev. **124**, 1866 (1961).
9. Z. D. Kvon, L. V. Litvin, V. A. Tkachenko, and A. L. Aseev, Usp. Fiz. Nauk **169**, 471 (1999).
10. E. B. Olshanetsky, M. Casse, Z. D. Kvon, *et al.*, in *Workbook of EP2DS-13—Electronic Properties of 2D-Systems* (Ottawa, 1999); Physica E (in press).
11. D. E. Potter, *Computational Physics* (Wiley, New York, 1973; Mir, Moscow, 1975).
12. M. Cahay, M. McLennan, and S. Datta, Phys. Rev. B **37**, 10125 (1988).
13. Y. Takagaki and D. K. Ferry, J. Phys.: Condens. Matter **4**, 10421 (1992).
14. J. Göres, D. Goldhaber-Gordon, S. Heemeyer, *et al.*, cond-mat/9912419.

Translated by E. Golyamina

JETP Letters, Vol. 71, No. 6, 2000, pp. 259–261. Translated from Pis'ma v Zhurnal Éksperimental'noĭ i Teoreticheskoĭ Fiziki, Vol. 71, No. 6, 2000, pp. 372–376.

CONDENSED MATTER

Dispersion Relation for Kink-Type Solitons in One-Dimensional Ferromagnets

E. G. Galkina and B. A. Ivanov*

Institute of Physics, National Academy of Sciences of Ukraine, pr. Nauki 144, Kiev, 258650 Ukraine
Institute for Magnetism, National Academy of Sciences of Ukraine, Kiev, Ukraine
**e-mail: vbaryakhtar@bitp.kiev.ua*
Received February 14, 2000

It is shown that the energy of a kink-type soliton in a one-dimensional ferromagnet depends periodically on the soliton momentum, the period being determined by the spin of the ferromagnet and by the character of anisotropy in it. © *2000 MAIK "Nauka/Interperiodica".*

PACS numbers: 75.10.Hk; 75.30.Ds

1. Nonlinear excitations (solitons) play an important role in the physics of low-dimensional ordered media. In particular, kink-type solitons (domain walls) must be taken into account, along with linear excitations (magnons), in describing physical properties of quasi-one-dimensional ferromagnets (see [1, 2]). In order to study consistently such ferromagnets, it is necessary to know not only the static energy of a kink but also the dispersion relation for it—that is, the energy E of a kink as a function of its momentum p. Since the Landau–Lifshitz equations, which govern the dynamics of a ferromagnet, do not possess Galilean or Lorentz invariance, the form of the dependence $E(p)$ is not obvious in advance.

In order to find this dependence, it is necessary to know the structure of a kink moving at a velocity that is not small. Presently, a solution that describes a kink having a nonzero velocity is known only for a rhombic ferromagnet, a simple model exactly integrable by the method of the inverse-scattering problem (see [2, 3]). For this case (of Walker's solution), the energy of a kink depends periodically on its momentum p, the relevant period p_0 being expressed in terms of "continuum" features of a ferromagnet, $p_0 = 2\pi M_0/g$, where M_0 is the magnetization per ferromagnet unit length, while g is the gyromagnetic ratio [2, 3].

Considering that $g = 2\mu_0/\hbar$ and $M_0 = 2\mu_0 S/a$, where S is the atom spin, a is the lattice constant, and μ_0 is the Bohr magneton, we find that the period p_0 for Walker's solution is $p_0 = 2\pi\hbar S/a$. For a magnetic bion defined as a soliton that involves a finite number of bound magnons and which can be represented as a bound state of two kinks, the period is twice as great as that, i.e., $4\pi\hbar S/a$. For the case of $S = 1/2$, this quantity coincides with the size of the Brillouin zone $p_B = 2\pi\hbar/a$. In this way, a result peculiar to discrete models of ferromagnets arises within a continuum model. Moreover, the dispersion relation for bions obtained as classical solutions to the continuum Landau–Lifshitz equations coincides with the dispersion relation for spin complexes known for the $S = 1/2$ XYZ chain of spins [3]. That the dispersion relation for the magnetic excitations in question is periodic was attributed in [3] to exact integrability of the model in the classical case and to the fact that this model represents a continuum limit of an exactly soluble discrete quantum model. However, the physics behind the emergence of results peculiar to discrete quantum theories in continuum classical models of ferromagnets has not yet been clarified.

We will show that a periodic dependence $E(p)$ is characteristic of a broad class of continuum models of ferromagnets and that this circumstance is determined by topological reasons.

2. In the continuum approximation, the dissipation-free dynamics of a ferromagnet is described by the Landau–Lifshitz equation for the normalized magnetization represented by a unit vector **m**. In terms of the angular variables specified as $m_x + im_y = \sin\theta\exp(i\varphi)$ and $m_z = \cos\theta$, the Landau–Lifshitz equation can be derived from the Lagrangian [2, 3]

$$L = \hbar S/a\int dx(1-\cos\theta)\partial\varphi/\partial t - \int dx/a\,W(\theta,\varphi), \quad (1)$$

where $W(\theta, \varphi)$ is the ferromagnet energy density. Allowing for a weak magnetic anisotropy, we can show that the energy density for a Heisenberg ferromagnet has the form

$$W(\theta,\varphi) = (Ja^2/2)[(\partial\theta/\partial x)^2 + \sin^2\theta(\partial\varphi/\partial x)^2] + W_r(\theta,\varphi), \quad (2)$$

where J is the exchange integral, while $W_r(\theta, \varphi)$ is the energy of magnetic anisotropy. The kink structure is determined by solutions of the simple-wave type—that is, $\mathbf{m} = \mathbf{m}(\xi)$ or, alternatively, $\theta = \theta(\xi)$ and $\varphi = \varphi(\xi)$ with $\xi = x - Vt$, where V is the velocity of the kink, the

boundary conditions being $\mathbf{m}(\xi \longrightarrow -\infty) = \mathbf{m}^{(-)}$ and $\mathbf{m}(\xi \longrightarrow +\infty) = \mathbf{m}^{(+)}$; here, $\mathbf{m}^{(-)}$ and $\mathbf{m}^{(+)}$ are two different, but equivalent minima of the energy $W_r(\theta, \varphi)$.

The kink momentum is determined as the total field momentum of the magnetization field; that is,

$$p = -\hbar S/a \int dx(1 - \cos\theta)\partial\varphi/\partial x. \quad (3)$$

The dynamical part of the Lagrangian in Eq. (1) and expression (3) for the momentum feature singularities that are associated with nondifferentiability of the azimuthal angle φ at the points $\theta = 0$ and π [4, 5] (this property of the variable φ plays an important role in describing the dynamics of magnetic vortices [5]). The origin of this singularity can be clarified by going over to the variable $\mathbf{M} = M\mathbf{m}$ not subjected to the condition $\mathbf{M}^2 = \text{const}$. In terms of the variable $\mathbf{M}$, the expression for the momentum can be recast into the form

$$\begin{aligned} p &= -\int dx \mathbf{A}\partial\mathbf{M}/\partial x, \\ \mathbf{A} &= (\hbar S/a)[\mathbf{e}_y M_x - \mathbf{e}_x M_y]/M(M + M_z). \end{aligned} \quad (4)$$

Here, the vector $\mathbf{A}$ has a singularity on the line specified by the equations $M_x = M_y = 0$ and $M_z = -M$.

Formally, the quantity obtained by expressing the dynamical part of Lagrangian (1) in terms of $\mathbf{M}$ and $\partial\mathbf{M}/\partial t$ [or the momentum in (4) upon the substitution $\partial\mathbf{M}/\partial t \longrightarrow -\partial\mathbf{M}/\partial x$] coincides with the Lagrangian of a charged particle in a magnetic field specified by the vector potential $\mathbf{A}$. It can be easily shown that the vector $\mathbf{B} = \text{curl}\mathbf{A} = (\hbar S/A)\mathbf{M}/M^3$ involves no singularities for $M \neq 0$. Thus, the expression in (4) for $\mathbf{A}$ describes the vector potential of a magnetic monopole occurring at the origin of coordinates. The vector potential for a monopole inevitably has a singularity on a line (Dirac string) issuing from the point at which the monopole resides and going to infinity [4]. Admissible transformations of (1) and (3) reduce to gauge transformations—that is, to changes in the orientation of the Dirac string (see [4]).

The kink momentum is not invariant under these gauge transformations. It is important, however, that the difference of the momenta between two different states appears to be a gauge-invariant quantity. Indeed, trajectories issuing from the point $\mathbf{m}^{(-)}$ and going to the point $\mathbf{m}^{(+)}$ can be associated with kinks that move at different velocities but obey identical conditions at infinity (which are specified by the points $\mathbf{m}^{(-)}$ and $\mathbf{m}^{(+)}$). In this case, the momenta of the kinks are determined by integrals of the form $\int \mathbf{A}\, d\mathbf{M}$ along these trajectories. It is clear that the difference of the momenta is determined by the integral $\int \mathbf{A}\, d\mathbf{M}$ along a closed contour. According to Stokes' integral theorem, the integral in question can be represented as the flux of the vector $\mathbf{B} = \text{curl}\mathbf{A}$ through the surface bounded by this contour $\int \mathbf{B}\, d\mathbf{S}$. Returning to the angular variables, we represent the difference of the momenta between the two states of the kink in the gauge-invariant form

$$\Delta p = (\hbar S/a)\int \sim\theta d\theta d\varphi, \quad (5)$$

where the integral is taken over that region on a sphere which is bounded by the trajectories corresponding to the two kinks in question. Thus, the dependence $V(p)$ or $E(p)$ has been reconstructed, apart from arbitrariness in choosing the reference point for the momenta.

3. Let us now consider specific models of magnets on the basis of the general considerations developed above. We have already mentioned that the simple model of the rhombic ferromagnet with $W_r = K_1 m_x^2 + K_2 m_y^2$ is the only model for which an exact solution describing a moving kink (Walker's solution; see [2, 3]) is known. The point is that the set of ordinary differential equations for $\theta = \theta(\xi)$ and $\varphi = \varphi(\xi)$, which has the form

$$\begin{aligned} Ja^2\theta'' - Ja^2\sin\theta\cos\theta(\varphi')^2 - \partial W_r/\partial\theta \\ = (V\hbar S/a)\varphi'\sin\theta, \end{aligned} \quad (6)$$

$$Ja^2(\sin\theta\varphi')' - \partial W_r/\partial\varphi = -(V\hbar S/a)\theta'\sin\theta, \quad (7)$$

where primes denote differentiation with respect to ξ, and which determines the structure of the kink, has only one first integral $Ja^2[(\theta')^2 + \sin^2\theta(\varphi')^2] - 2W_r(\theta, \varphi)$ in general and is not integrable. However, a solution at $V = 0$ can be found straightforwardly and is given by $\theta = \theta(\xi)$ and $\varphi = \varphi_0 = \text{const}$, where φ_0 is determined by the relation $\partial W(\theta, \varphi_0)/\partial\varphi_0 = 0$. In this case, we have to solve only one second-order differential equation, equation (6) for the variable θ at $\varphi = \varphi_0$, and the presence of one first integral is sufficient for constructing a general solution.

We begin our analysis by considering a magnet with anisotropy of the easy-axis type and address the case of an easy axis of order n. For $n = 2, 4, 6$, the energy of anisotropy has the form

$$W_r(\theta, \varphi) = K(\sin^2\theta) + K_{bp}\sin^n\theta\sin^2(n\varphi/2), \quad (8)$$

where the function $K(\sin^2\theta)$ contains terms of the $\sin^2\theta$, $\sin^4\theta$, ... types and has minima at $\theta = 0, \pi$, while K_{bp} is positive. The condition $\partial W/\partial\varphi = 0$ yields two sets of φ values. At a given θ, one set, $\varphi_{\min} = 2\pi m/n$, m being an integer, corresponds to a minimum of W_r, while the other, $\varphi_{\max} = 2\pi(2m + 1)/2n$, corresponds to a maximum of this function. The trajectories describing immobile kinks appear to be halves of the large circle passing through the poles $\theta = 0$ and π of the unit sphere $\mathbf{m}^2 = 1$. The trajectories characterized by the values of $\varphi = \varphi_{\min}$ and $\varphi = \varphi_{\max}$ describe energetically favorable and unfavorable kinks, respectively. All the remaining trajectories that correspond to moving kinks cover the regions between the above trajectories. [We note that,

in Walker's solution, the angle φ depends only on V at $V \neq 0$, $\varphi = \varphi(V)$, so that $\partial\varphi/\partial\xi = 0$; at $V = 0$, we have $\varphi = 0, \pi/2$. We cannot indicate any other model of a ferromagnet where the condition $\varphi = \text{const}$ is satisfied for $V \neq 0$.]

The above pattern makes it possible to reconstruct the dispersion law for a kink. We begin our consideration from some trajectory corresponding to $\varphi = \varphi_{\min}$ and assume that $p = 0$ for this trajectory. For a magnet with an easy axis of order n, the values of $p = \pm 2\pi\hbar S/an = \pm p_0/2$ will correspond to the two nearest trajectories with $V = 0$ and $\varphi = \varphi_{\max}$. Nonzero values of V are associated with trajectories passing between the sections $\varphi = \varphi_{\min}$ and $\varphi = \varphi_{\max}$. In particular, the velocity values of $\pm V_c$, where V_c is the maximum value of the kink velocity (limiting velocity), correspond to some two nonplanar trajectories. The $V = V_c$ trajectories can be reached by proceeding from either type of $V = 0$ solutions (a favorable or an unfavorable one). Thus, we can see that, in just the same way as in Walker's solution, the dependence $E(V)$ has two branches—that characterized by a higher energy and that characterized by a lower energy—which merge at the point $V = V_c$. If we assume that $p = 0$ for the $V = 0$ kink characterized by $\varphi = \varphi_{\min}$, then the momentum grows up to $p = \pm p_c$, $p_c < 2\pi\hbar S/an$ as the absolute value of the kink velocity increases to V_c. As we proceed further along the upper branch of the dependence $E(V)$, the kink velocity decreases, while the momentum increases to $p = \pm 2\pi\hbar S/an$ when the velocity approaches zero. When we go beyond the region discussed above, the momentum p grows, while the kink energy takes the same values as before—that is, we do indeed arrive at a periodic dependence $E(p)$ with a period p_0 dependent only on the atom spin S in the system and on the order n of the principal axis:

$$p_0 = 4\pi\hbar S/an. \tag{9}$$

Other models of a ferromagnet can be considered in a similar way. For example, the magnetic-anisotropy energy W_r for rhombohedral magnets involves the invariant $\cos\theta\cos 3\varphi$. In this case, the rotation of **m** is not planar even at $V = 0$. However, the function $E(p)$ is periodic, as in the above case, and the period p_0 is given by (9) with $n = 6$.

At first glance, it may seem that an immobile kink of higher energy ($\varphi = \varphi_{\max}$) is unstable with respect to a transition to the favorable kink ($\varphi = \varphi_{\min}$). An analysis revealed, however, that different momentum values correspond to these states, whence it follows that no transition between them is possible, so that both kinks are stable in the one-dimensional use. For the exactly soluble Walker model, it is well known that either of the two static kinks—that with a minimum and that with a maximum energy—is stable [3]. It should be emphasized that we mean here one-dimensional models—an unfavorable planar kink (Néel wall) becomes unstable in a three-dimensional ferromagnet upon taking into account non-one-dimensional excitations [3].

4. There are also other models of magnets where the Lagrangian involves terms linear in $\partial\theta/\partial t$ and $\partial\varphi/\partial t$. By way of example, we can indicate the sigma model for antiferromagnets in an external magnetic field or in the presence of the Dzyaloshinskiĭ interaction $D_{ik}l_i m_k$ with $D_{ik} \neq \epsilon_{ikj}d_j$, **m** and **l** being, respectively, the magnetization vector and the antiferromagnetism vector (see [2, 6]). In this case, however, the structure of the Lagrangian is such that the flux of the relevant vector **B** through the entire surface of the unit sphere $\mathbf{l}^2 = 1$ is zero for any orientation of an external field and any D_{ik} [6]. Therefore, there are no topological singularities, so that the dispersion relation is not periodic for antiferromagnets. At the same time, the corresponding function $E(p)$ for kinks in ferrimagnets featuring two different spins S_1 and S_2 coupled by an antiferromagnetic interaction is periodic, the corresponding period being given by expression (9) with the substitution of $|S_1 - S_2|$ for S.

5. Thus, we conclude that, by virtue of the topological properties of the Lagrangian for the magnetization field, the dispersion relation for kinks is periodic for a wide class of ferromagnets. This must lead to some special features of the kink motion (for example, to Bloch oscillations [7] in the motion of kinks) induced by the effect of a constant force (in particular, a magnetic field aligned with the easy axis of a given ferromagnet).

This work was supported in part by grants from Volkswagen-Stiftung (Germany) and by grant nos. 2.4/561 (E.G. Galkina) and 2.4/27 (B.A. Ivanov) from the Ukrainian Foundation for Basic Research.

REFERENCES

1. H.-J. Mikeska and M. Steiner, Adv. Phys. **40**, 191 (1991).
2. V. G. Bar'yakhtar and B. A. Ivanov, *Soliton Thermodynamics of Low-Dimensional Magnets*, Ed. by I. M. Khalatnikov, Sov. Sci. Rev., Sect. A **16**, 1 (1993).
3. A. M. Kosevich, B. A. Ivanov, and A. S. Kovalev, Phys. Rep. **194**, 117 (1990).
4. E. Fradkin, *Field Theories of Condensed Matter Systems* (Addison Wesley, New York, 1991), Vol. 82.
5. N. Papanicolaou and T. N. Tomaras, Nucl. Phys. B **360**, 425 (1991).
6. B. A. Ivanov, in *Proceedings of the 6th International Conference on Path-Integrals from peV to TeV*, Ed. by R. Casalbuoni *et al.* (World Sci., Singapore, 1998), p. 410.
7. J. Kyriakidis and D. Loss, Phys. Rev. B **58**, 5568 (1998).

Translated by A. Isaakyan

JETP Letters, Vol. 71, No. 6, 2000, pp. 262–265. Translated from Pis'ma v Zhurnal Éksperimental'noĭ i Teoreticheskoĭ Fiziki, Vol. 71, No. 6, 2000, pp. 377–383.

CONDENSED MATTER

Deformation and Instability of Nematic Drops in an External Electric Field

B. I. Lev, V. G. Nazarenko, A. B. Nych, and P. M. Tomchuk

Institute of Physics, National Academy of Sciences of Ukraine, pr. Nauki 144, Kiev, 258650 Ukraine

e-mail: vnazarenko@iop.kiev.ua

Received February 17, 2000

The behavior of nematic liquid-crystal drops freely suspended in an isotropic liquid polymer exposed to an external electric field was studied. A giant deformation was observed for the drop. As the field intensity increased, its equilibrium shape took the form of a prolate ellipsoid. The dependences of the shape and critical fields on the concentration of ions in the polymer liquid were established. A plausible theoretical explanation is suggested for the observed effect. The experimental dependence of drop size on the electric-field strength is analyzed, and the conditions for the loss of drop stability are determined. © *2000 MAIK "Nauka/Interperiodica".*

PACS numbers: 61.30.Eb; 47.55.Dz

In recent years, both disperse and dispersed liquid crystals have been extensively studied. This was primarily motivated by the necessity of obtaining the desired operating parameters for information display facilities containing the mesophase as a basic element. A broad range of substances were previously recommended for this purpose, among which were polymers dispersed with liquid-crystal inclusions (PDLC) [1–5]. Along with improved characteristics, these substances had certain disadvantages. Among these were the quenched spatial distribution of the liquid-crystal inclusions and, eventually, the impossibility of structural rearrangements in a system of such macroinclusions. One failed to attain collective behavior for the macroinclusion system in a polymeric matrix, so that the operational characteristics largely depended on the experimenter's skill in achieving the smallest scatter in both the macroinclusion sizes and their spatial distribution. Therefore, the necessity arises of obtaining media dispersed with uniform-sized liquid-crystal inclusions suspended in an isotropic matrix having lower viscosity and imposing the mildest constraints on the motion of such macroinclusions. This is all the more necessary because the system of liquid-crystal inclusions in an elastic liquid can generate structures that are caused by interaction both through the elastic strain field of the medium itself and by virtue of a charge or polarization that can appear at some inclusions [6–9]. This can be attained both by the methods of preparation and by the action of an external field with properties allowing only one of the subsystems to be affected. Such properties can be useful in saser design, i.e., in designing a coherent acoustic generator with liquid crystal as the main operating component. Liquid dielectric with uniformly distributed dispersed particles serves as a saser active medium [10–12]. Liquid-crystal macroinclusions may be such particles. The merits of liquid-crystal macroinclusions are primarily that the mesophase itself is a very soft elastic system, so that even a weak external action can initiate substantial changes both in the structure of the macroinclusion system and in the shape of an individual macroinclusion. The deformation of a liquid-crystal macroinclusion under the external action seems to be among promising methods of acoustic generation in an elastic isotropic matrix.

The purpose of this work was to elucidate the physical reasons for the deformation and to reveal the conditions under which a nematic drop freely suspended in a liquid isotropic dielectric becomes unstable upon changing the external electric field, as well as to establish how the drop size and shape depend on the electric-field strength and the concentration of the ions introduced into the medium.

Many works [13–22], both experimental and theoretical, were devoted to studying the equilibrium shape and the stability of uncharged drops, including liquid-crystal drops [23], in a uniform external electric field. Our experiments were different from the previous measurements in that we could vary the medium conductance over a wide range. The behavior of liquid-crystal inclusions suspended in a liquid isotropic dielectric, notably their deformation, also remained to be studied.

Our experimental setup allowed visual observation and direct measurement of the drop shapes for a liquid-crystal inclusion ZhK-1289. The drops were from 30 to 60 μm in size and freely suspended in a liquid isotropic polymer. The cell consisted of two 0.12-mm thick glass plates 1.2 mm apart with electrodes and a polymeric matrix with suspended liquid-crystal drops placed between. Measurements were made at a constant temperature using a polarizing microscope.

0021-3640/00/7106-0262$20.00

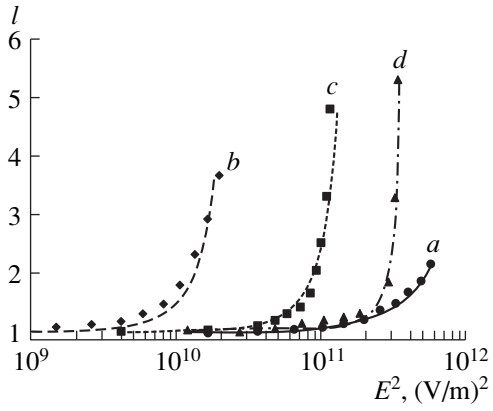

Fig. 1. Plots of the ellipsoid stretching parameter $l \equiv R_\parallel/R_\perp$ against the square of applied field for (curve *a*) the undoped matrix and (curves *b*, *c*, and *d*) various concentrations of the added ions, with increasing concentrations of the latter: $n_\blacklozenge < n_\blacksquare < n_\blacktriangle$; the dots are for the experiment.

The experimental data on the drop deformation, viz., transformation of a spherical drop into an ellipsoid are presented in Fig. 1 as plots of the ellipsoid semiaxes ratio $R_\parallel/R_\perp$ vs. electric-field strength squared. Curve *a* corresponds to the initial low conductance of the system. The instability threshold goes down sharply upon doping the polymeric matrix with ions (Fig. 1, curves *b*–*d*). Moreover, the drop ceased to be ellipsoidal in the doped matrix and became spindle-shaped. Figure 2 presents photographs of the nematic drop shape for different field strengths up to the value of $E_C \sim 3 \times 10^6$ V/m, when the ellipsoidal drop becomes unstable against splitting into two fragments. In this case, a fragment with an uncompensated charge separates from the ellipsoid pole, while the drop shape relaxes to the equilibrium ellipsoidal shape in the time $\tau \approx 0.5$ s. Two nontrivial facts are noteworthy. The first one is that a giant change in the drop shape occurs in rather weak fields and the field dependence of this change is nonlinear. The second fact is that the external-field strength required for the same deformation decreases upon increasing concentration of the ions introduced into the polymeric matrix. It is thus necessary to consistently explain the experimentally observed physical phenomena.

The theoretical description should allow for the polarization of a dispersive medium in an external electric field and for the processes associated with the conductivity of charge carriers. The equilibrium drop shape should be determined by minimizing the free energy of a macroinclusion placed in an external electric field. The free energy of a nematic drop can be written as a sum of three terms,

$$F = F_d + F_S + F_E, \tag{1}$$

where

$$F_d = \frac{1}{2}\int \{K_{11}(\mathrm{div}\mathbf{n})^2 + K_{22}(\mathbf{n}\cdot\mathrm{rot}\mathbf{n})^2 + K_{33}[\mathbf{n}\times\mathrm{rot}\mathbf{n}]^2\}dV \tag{2}$$

is the Frank free energy associated with the director distortions;

$$F_S = \oint \sigma dS - \oint W(\boldsymbol{\gamma}\cdot\mathbf{n})^2 dS \tag{3}$$

is the surface free energy of the drop, with σ being the coefficient of isotropic surface tension and W the director-to-surface anchoring energy; the integration goes over the closed drop-bounding surface;

$$F_E = -\frac{1}{8\pi}\int dV\{\epsilon_\perp \mathbf{E}^2 + \Delta\epsilon(\mathbf{E}\cdot\mathbf{n})^2 - \epsilon_0\mathbf{E}^2\} \tag{4}$$

is the free-energy component caused by the applied electric field, with $\epsilon_\parallel$, $\epsilon_\perp$, and ϵ_0 being the dielectric constants of liquid crystal and polymeric liquid, respec-

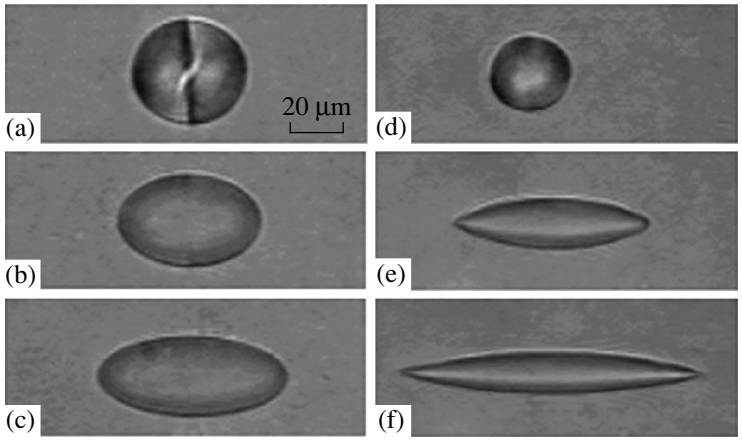

Fig. 2. Photographs of a liquid-crystal drop at different values of applied field for (a–c) undoped and (d–f) ion-doped matrices.

tively. The third term in Eq. (4) is the electric-field energy of a drop filled with polymeric liquid instead of liquid crystal. Now, one should determine the equilibrium shape of a liquid-crystal drop in an isotropic dielectric liquid. The following transformations happen to a nematic drop upon an increase in the electric-field strength. First, the director distribution inside the drop undergoes rearrangement that can be determined from the anisotropic part of the free energy [3, 5]. At $E \geq E_c = K/\Delta\epsilon R^2$, where R is the drop radius, the director is aligned with the field if $\Delta\epsilon > 0$. Further transformations are due to the action of the electric field on the inclusion dielectric medium. The electric field inside the dielectric inclusion differs from the applied external field because of the polarization effects. When subjected to the electric field, the dielectric drop suspended in a foreign dielectric is known to stretch [24] along or perpendicular to the field, depending on the ratio between the dielectric constants of the media, and take the shape of an ellipsoid of revolution. At $R > 2K/\sigma$, the anisotropic energy component is small compared to the surface tension energy, so that the director is almost unchanged upon drop deformation. The drop changes its shape only when the contributions of the field and surface-tension components of free energy are equalized. For this reason, the anisotropic terms associated with the director distribution can be ignored when determining the critical field of drop instability and deformation. As the critical field is approached, the dielectric constant anisotropy and the ratio of the dielectric constants of the drop and medium begin to play the dominant part in the drop orientation and stretching direction. Using the results of [1, 5], one can determine the equilibrium director orientation in the drop and the spatial orientation of the drop itself relative to the applied field and, hence, the drop stretching direction. In our case, the director is aligned with the field and the drop is also stretched along the applied field. It is known [24] that the field inside the drop is determined by expression

$$\mathbf{E} = \mathbf{E}_0/(1 + G(\epsilon)), \tag{5}$$

where E_0 is the strength of the external field and

$$G(\epsilon) = \left(\frac{\epsilon'}{\epsilon_0} - 1\right)\frac{1 - e^2}{e^3}(\mathrm{Arcth}e - e)$$

is the depolarization factor depending on the ratio between the dielectric constants of the liquid crystal and matrix and on the eccentricity of ellipsoid $e^2 = 1 - R_\perp^2/R_\parallel^2$, where $R_\parallel$ and $R_\perp$ are the radii along the major and minor axes, respectively. In the spherical coordinate system, a point on the ellipsoid surface is specified by equation

$$r(\theta) = R_\perp/(1 - e^2\cos^2\theta)^{1/2}. \tag{6}$$

Using explicit form (2)–(4) without the anisotropic energy component and integrating Eq. (1) in spherical coordinates, one obtains the following expression for the free energy:

$$F = 2\pi\sigma R_\perp^2\left(1 + \frac{R_\parallel}{R_\perp}\frac{\arcsin e}{e}\right) - \frac{\epsilon_0 E_0^2 R_\perp^2 R_\parallel^2}{\sigma(1 + G(e))^2}\{\epsilon - 1\}, \tag{7}$$

where $\epsilon = \epsilon_\parallel/\epsilon_0$ and $\epsilon_\perp$ and $\epsilon_\perp$ are, respectively, the longitudinal and transverse dielectric constant components of the liquid crystal. The equilibrium drop shape at a given external field is found through the minimization of free energy (7). The minimization of Eq. (7) yields equation

$$-\frac{2}{3}l^{-5/3} + \frac{1}{3}\frac{C}{A}l^{-1/3} + \frac{1}{A^2}l^{1/3} - \frac{C}{A^3}l^{1/3} + [3lA - (2l^2 + 1)B] \times \frac{\gamma A^4}{(\epsilon - 1)[lB + (l^2 - \epsilon)A/(\epsilon - 1)]^3} = 0, \tag{8}$$

where the ratio $l = R_\parallel/R_\perp$ (ellipsoid stretching parameter) is the desired quantity. The following notations are introduced in Eq. (8):

$$A \equiv \sqrt{l^2 - 1}, \quad B \equiv \mathrm{Arcth}\sqrt{\frac{l^2 - 1}{l^2}}, \quad C \equiv \arcsin\sqrt{\frac{l^2 - 1}{l^2}}, \quad \gamma \equiv \frac{\epsilon_0 E_0^2 R}{6\pi\sigma}, \tag{9}$$

where γ is the well-known Taylor parameter defined as the ratio between the electric and surface energies of a spherical drop and R is the initial drop size. The calculated field dependence of the stretching parameter is shown in Fig. 1 together with the experimental data (Fig. 1, curve *a*). For the experimental values $\epsilon_0 = 2.85$, $\sigma = 0.002$ H/m, and $R \cong 50$ μm, not only the qualitative but also a rather good quantitative agreement is observed between both data. This implies that the mechanisms suggested for the electric-field-induced deformation of the inclusion drops, on the whole, are adequate. The regime of electric-field effect changes from dielectric to conducting upon the introduction of ions into the medium. The polarization processes caused by the charge-carrier redistribution inside the inclusions become operative. Mathematically, this is formulated as a continuity of the normal component of a current flowing in the inhomogeneous medium. In this case, the electric-field contribution to the free energy is written as [14, 15]

$$F_E = \frac{\epsilon_0 E_0^2 R^3}{6[1 + G(e, \sigma)]}\left\{\frac{\epsilon - \sigma}{1 + G(e, \sigma)} - (\sigma - 1)\right\}, \tag{10}$$

where $\epsilon = \epsilon_\parallel/\epsilon_0$, $\sigma = \sigma_\parallel/\sigma_0$, and $G(e, \sigma)$ is the depolarization factor defined as the ratio of conductivities

rather than the ratio of the dielectric constants. Then, the relationship between the stretching parameter $l \equiv R_\parallel/R_\perp$ and the electric-field strength is given by equation

$$-\frac{2}{3}l^{-5/3} + \frac{1}{3}\frac{l^{1/3}C}{A} + \frac{l^{1/3}}{A^2} - \frac{l^{-1/3}C}{A^3} = \frac{\gamma}{(1+G(l,\sigma))^3}\frac{\partial G}{\partial l}\{2(\epsilon-\sigma)-(\sigma-1)(1+G(l,\sigma))\}. \quad (11)$$

This expression enables one to reproduce the experimental curves for the stretching parameter as a function of medium conductivity that was varied by changing the ion concentration. A decrease in the field strength required for the same ellipsoid stretching upon changing the matrix conductivity is explained by the fact that the mechanisms of charge-carrier redistribution and medium polarization act in opposition, thus reducing the effective field inside the drop. The curve for the electric-field strength against the ratio σ of conductivities of the liquid crystal and the polymeric matrix goes through a minimum that can be found from Eq. (11) by minimizing γ as a function of this parameter. The fact that the electric field corresponding to the same ellipsoid stretching continues to increase with a further increase in the matrix conductivity is explained by the depolarization effect caused solely by the charge-carrier redistribution. One can see from Fig. 1 that the theoretical curve based on Eq. (11) and on the above-mentioned premises qualitatively describes the experimental dependence rather well. Another important factor is that the stretching of spherical drops has a threshold character because of the action of surface forces. To elicit stretching, the electric field must overcome the resistance of these forces. The critical field can be determined from the dynamics of a drop surface in an electric field. As is known [16–19], the spectrum of capillary waves of a spheroidal drop of dielectric liquid is given by equation

$$\omega^2 = \frac{n(n^2+1)}{(n+1)\rho_0 + n\rho}\frac{\sigma}{R^3}\left\{n+2-\frac{\epsilon_\parallel\epsilon_0 E_0^2 R}{4\pi\sigma(2\epsilon_0+\epsilon_\parallel)}\right\}, \quad (12)$$

where ρ_0 and ρ are the densities of drop and matrix, respectively, and n is the harmonic number. Hence it follows that the critical field for the second harmonic is determined as

$$E_c^2 > 8\pi\sigma(2\epsilon_0+\epsilon_\parallel)/\epsilon_0\epsilon_\parallel R,$$

which corresponds to the situation where the spheroidal surface becomes unstable and the drop assumes ellipsoidal shape. In our case, $R = 50$ μm and $\sigma = 0.002$ N/m, giving $E_c \approx 2.5 \times 10^6$ N/m, in nice agreement with the experimental data. It was also found experimentally that the ellipsoidal drop shape relaxes to the equilibrium shape in time $\tau \approx 0.5$ s.

Thus, the physical picture suggested in this work allows for the redistribution of both polarization and real charges and is capable of adequately describing the deformation and instability of a nematic drop suspended in an isotropic polymeric liquid.

This work was supported by the STCU (grant no. 637) and the INTAS (grant no. 30234).

REFERENCES

1. J. W. Doane, N. A. Vaz, B. G. Wu, and S. Zummer, Appl. Phys. Lett. **48**, 269 (1986).
2. J. W. Doane, *Liquid Crystals: Applications and Uses*, Ed. by B. Bahadur (World Sci., New York, 1990), Vol. 1, Chap. 14, p. 362.
3. V. G. Nazarenko, S. Sarala, and N. V. Madhusudana, Jpn. J. Appl. Phys. **33**, 2641 (1994).
4. G. E. Volovik and O. D. Lavrentovich, Zh. Éksp. Teor. Fiz. **85**, 1997 (1983) [Sov. Phys. JETP **58**, 1159 (1983)].
5. B. G. Wu, J. E. Erdmann, and J. W. Doane, Liq. Cryst. **5**, 1453 (1989).
6. B. I. Lev and P. M. Tomchuk, Phys. Rev. E **59**, 591 (1999).
7. P. Poulin, H. Stark, T. C. Lubensky, and D. A. Weitz, Science (Washington, D.C.) **275**, 1770 (1997).
8. P. Poulin and D. A. Weitz, Phys. Rev. E **57**, 626 (1998).
9. P. Poulin, V. Cabuil, and D. A. Weitz, Phys. Rev. Lett. **79**, 4862 (1997).
10. S. T. Zavtrak and I. V. Volkov, Zh. Tekh. Fiz. **67**, 92 (1997) [Tech. Phys. **42**, 406 (1997)].
11. S. T. Zavtrak, Phys. Rev. E **51**, 2480 (1995).
12. S. T. Zavtrak, Phys. Rev. E **51**, 3767 (1995).
13. S. N. O'Konski and H. C. Thacher, J. Phys. Chem. **57**, 955 (1953).
14. S. N. O'Konski and F. E. Harris, J. Phys. Chem. **61**, 1172 (1957).
15. S. I. Shchukin and A. I. Grigor'ev, Zh. Tekh. Fiz. **69**, 23 (1999) [Tech. Phys. **44**, 758 (1999)].
16. S. I. Shchukin and A. I. Grigor'ev, Zh. Tekh. Fiz. **69**, 49 (1999) [Tech. Phys. **44**, 913 (1999)].
17. C. G. Garton and Z. Krasucki, Proc. R. Soc. London, Ser. A **280**, 211 (1964).
18. G. I. Taylor, Proc. R. Soc. London, Ser. A **280**, 283 (1964).
19. R. S. Allan and S. G. Masson, Proc. R. Soc. London, Ser. A **267**, 62 (1962).
20. G. I. Taylor, Proc. R. Soc. London, Ser. A **291**, 159 (1966).
21. A. I. Grigor'ev, Zh. Tekh. Fiz. **55**, 1272 (1985) [Sov. Phys. Tech. Phys. **20**, 736 (1985)].
22. S. O. Shiryaeva and A. I. Grigor'ev, Zh. Tekh. Fiz. **66**, 12 (1996) [Tech. Phys. **41**, 865 (1996)].
23. Ch. S. Park, N. A. Clark, and R. D. Noble, Phys. Rev. Lett. **72**, 1838 (1994).
24. L. D. Landau and E. M. Lifshitz, *Course of Theoretical Physics. Vol. 8. Electrodynamics of Continuous Media* (Nauka, Moscow, 1982; Pergamon, New York, 1984).

Translated by V. Sakun

JETP Letters, Vol. 71, No. 6, 2000, pp. 266–270. Translated from Pis'ma v Zhurnal Éksperimental'noĭ i Teoreticheskoĭ Fiziki, Vol. 71, No. 6, 2000, pp. 384–390.

CONDENSED MATTER

Trapped Bose Condensate in a Gravitational Field

D. B. Baranov and V. S. Yarunin

Joint Institute for Nuclear Research, Dubna, Moscow region, 141980 Russia

e-mail: yarunin@thsunl.jinr.dubna.ru

Received June 15, 1999; in final form, February 21, 2000

The Bose condensation of atoms in finite 1D and 2D parabolic traps placed in a gravitational field is considered. The distortion of the trap potential in this field is modeled by a combination of two rectangular 1D and 2D traps. The change in the critical temperature T_c is found with regard to the cutoff and renormalization of the spectrum of these model potentials. The shift of the critical temperature T_c in the gravitational field is calculated. The shift sign and magnitude depend on the way of introducing the gravitational field. For a certain choice, three critical temperatures can be sequentially observed. These temperatures can be attributed to three Bose condensations that occur in the cyclic motion of the trap along the Earth (I)–space (II)–Earth (III) route. © *2000 MAIK "Nauka/Interperiodica".*

PACS numbers: 67.40.Kh; 03.75.Fi

In the last decade, new effects have been discovered in the behavior of the critical temperature T_c of Bose–Einstein condensation (BEC). It is known that the critical temperature of superfluid ^{4}He (the oldest, although indirect, example of BEC) remains the same for any vessel with liquid helium. A decrease in T_c of liquid helium in porous glasses was observed experimentally [1] and explained theoretically [2, 3]. This shift depends on the parameters of porous glasses [4]. At the same time, the calculations of BEC T_c for bosons weakly interacting in an infinite volume suggested that T_c increases [5, 6].

It was shown in [7] that T_c for an ideal gas placed in an external field confining the atoms depends on the shape of this field. The experimental discovery of BEC for alkali-metal atoms in magnetic traps [8, 9] offered a good opportunity for discussing the same properties for systems in finite volumes. The volume finiteness implies the existence of mesoscopic boundary conditions that lead to a new formulation of thermodynamic limit in the theory [10]. A decrease in BEC T_c in an ideal gas was calculated in [11] as a finite-size correction $N \sim \infty \longrightarrow N < \infty$ using the "trap version" of the thermodynamic limit $\hbar\omega/T \longrightarrow 0$, $N \longrightarrow \infty$.

In this paper, we calculate the change in the critical temperature T_c of BEC under the effect of a gravitational field on a trapped gas. The problem of studying the gravity effect on the ^{4}He critical temperature arose in connection with investigations of ^{4}He in space and the same investigations planned for the near future for BEC in trapped gases [12]. It is of interest to theoretically predict the contribution of a gravitational field to the BEC critical temperature in traps. In this work, the theory of spinless noninteracting atoms in a finite volume is considered for 1D and 2D systems. The basic parameters are taken from the experiments on BEC in alkali-metal atoms [8, 9]. We start with an isotropic parabolic trap with potential barrier U_0, frequency ω, and height h and describe the effect of a gravitational field by introducing two rectangular traps.

The trap potentials are different in the cases of zero and nonzero gravitational fields in the z-axis direction. The field potential inside the trap (Fig. 1) can be written as

$$U(z) = U_g + (m\omega^2/2)(z + \Delta)^2, \quad -h/2 < z < h/2, \quad \Delta = g/\omega^2, \tag{1}$$

where m is the atomic mass and g is the gravitational constant. The dashed line describes the initial parabolic potential, and the solid line describes the parabolic potential distorted by the gravitational field. The gravitational field shifts the potential minimum of the trap to the left from its center $z = 0$ by Δ and down by $U_g = -mg^2/2\omega^2$. The difference between the new (displaced) potential barriers U_+ (right) and U_- (left),

$$U_\pm = \frac{m\omega^2}{2}\left(\Delta \pm \frac{h}{2}\right)^2 + U_g,$$

$$U_0 - U_- = U_+ - U_0 = \frac{1}{2}mgh$$

is equal to mgh. It follows from these equations that the $2g < \omega^2 h$ condition for the macroscopic stability of the trap in a gravitational field is fulfilled in the experiments [8, 9] and for trap frequencies higher than 100 Hz. In this case, the quantum dynamics of atoms undergoes nonperturbative gravitational disturbance,

0021-3640/00/7106-0266$20.00

because the shift of the trap potential $U_g \gg \hbar\omega$ is large compared to its frequency.

One-particle boson eigenfunctions u_n and their energies $\varepsilon_n > 0$ in the 2D systems with $r = \{x, z\}$, $u_n(r) = u_{n_x}(x)u_{n_z}(z)$, $n = \{n_x, n_z\}$,

$$\left\{\nabla^2 + \frac{2m}{\hbar^2}[\varepsilon_n - U(r)]\right\}u_n = 0$$
$$\varepsilon_n = \frac{1}{2m}\int \nabla u_n \nabla u_n dr + \int U(r)u_n u_n dr, \quad (2)$$

are the starting points for the quantum analysis of any finite trap $U(r)$ with the ground-state energy $\varepsilon_0 \neq 0$. We introduce Gibbs statistics within the path-integral approach that was used previously [13, 14] for describing BEC in a system of interacting bosons.

A system of N bosons (2) confined in a volume V can be described by the Hamiltonian H

$$\hat{H} \longrightarrow H = \int dr\left[\frac{\hbar^2}{2m}(\nabla\psi^*(r, t)\nabla\psi(r, t)) + \psi^* U(r)\psi\right].$$

Here, ψ^* and ψ are trajectories with periodic boundary conditions $[0, \beta]$. Following [15, 16], we divide these trajectories for $T < T_c$ into slow b_0^*, b_0 and fast b_n^*, b_n $(n \neq 0)$ ones,

$$\psi^*(r, t) = \frac{1}{\sqrt{V}}\left(\sum_{n\neq 0} b_n^*(t)u_n(r) + b_0^*(t)u_0(r)\right),$$
$$|b_0| = \sqrt{N_0} \gg 1,$$

so that the $N_0(t)$ function is a fraction of the Bogolyubov Bose-condensate particles [15] in terms of functional integral. Gauge invariance breakdown is known to be a property of a Bose gas containing a separate subsystem of condensate particles. However, the quasiclassical integral of motion $\bar{N} = N_0 + \bar{N}_1$ for system (2) can be represented by the equation [13]

$$d\bar{N}/dt \equiv \{\hat{H}, N_0\} + i[\hat{H}, \hat{N}_1] = 0,$$
$$\hat{N}_1 = \sum_{n\neq 0} b_n^+ b_n, \quad (3)$$

where N_1 is the number of noncondensate bosons; $\{,\}$ is the Poisson bracket for the classical amplitudes b_0^* and b_0; and $[,]$ is the quantum commutator of the b_n^+ and $b_{n'}$ operators $n, n' \neq 0$. For the case of N noninteracting bosons in an arbitrary volume V, the action S with the kinetic term K is written as

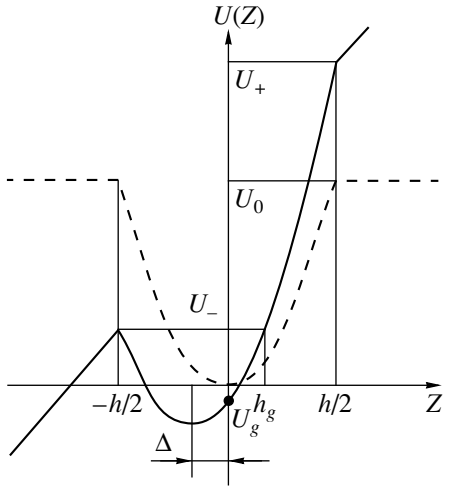

Fig. 1. The dashed and solid lines describe the potentials of parabolic traps in vacuum (U_0) and gravitational field (U_-, U_+).

$$S = \int_0^\beta (K - H)dt$$
$$= -\int_0^\beta \left[b_0^*\frac{db_0}{dt} + \varepsilon_0 b_0^* b_0 + \sum_{n\neq 0}\left(b_n^*\frac{db_n}{dt} + \varepsilon_0 b_n^* b_0\right)\right]dt.$$

The effective action $S_{\text{eff}}(\rho, \mu)$ for the condensate density $\rho = N_0/V$ and chemical potential μ is defined via the expression for a partition function with constraint

$$Q = \int e^{S_{\text{eff}}(\rho,\mu)} d\rho d\mu = \text{Sp}[\exp(-\beta H)\delta_{R, R_1+\rho}],$$
$$R = N/V, \quad R_1 = N_1/V.$$

Eq. (3) serves to determine the chemical potential μ. Using the Fourier transform of $\delta_{R, R_1+\rho}$ at $\mu = iy/\beta$, we express the partition function as the integral over y and the path integral along the slow b_0, b_0^* and fast b_n, $b_{n'}^*$ trajectories with periodic boundary conditions on the $[0, \beta]$ segment. The calculation of the partition function over the fast variables gives the effective action S_{eff} for the Bose condensate:

$$S_{\text{eff}} = \int_0^\beta \left[-b_0^*\frac{db_0}{dt} + \rho(\mu - \varepsilon_0) - \mu R\right]dt$$
$$- \sum_{n\neq 0} \ln(1 - \exp[-\beta(\varepsilon_n - \mu)]).$$

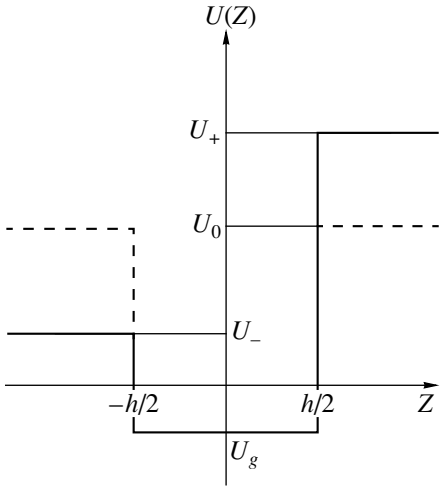

Fig. 2. The dashed and solid lines describe the potentials of rectangular traps modeling the parabolic trap in vacuum (U_0) and gravitational field (U_-, U_+).

The variational equations $\delta S_{\text{eff}}(b_0, b_0^*, \mu) = 0$ are written as

$$\frac{\partial S_{\text{eff}}}{\beta \partial \mu} = \rho + \frac{1}{V}\Sigma - R = 0,$$
$$\Sigma = \sum_{n_x, n_z \neq 0} f(\varepsilon_{n_x, n_z}, \beta, \mu), \tag{4}$$
$$f(\varepsilon_{n_x, n_z}, \beta, \mu) \equiv f = \frac{1}{\exp[\beta(\varepsilon_n - \mu)] - 1},$$
$$n = \{n_x, n_z\},$$

$$\frac{\partial S_{\text{eff}}}{\beta \partial b_0^*} = -\frac{db_0}{dt} - b_0(\varepsilon_0 - \mu) = -Lb_0 = 0,$$
$$\mu = \varepsilon_0 - kT\ln\left(1 + \frac{1}{N_0}\right). \tag{5}$$

Eqs. (4) and (5) determine the BEC solutions of model (2) and (3) for the translationally noninvariant systems below the critical temperature. Thus, the critical temperature T_c for a finite-size trap is determined from the equation $\Sigma(T_c) = N$, $\rho = 0$, whereas the conditions $\rho \sim R$, $R_1 \sim 0$, and $\mu \sim \varepsilon_0$ are fulfilled for temperatures $T \sim 0$. Eqs. (3)–(5) are valid for any trap $U(r)$. We use them in Eqs. (6)–(8) for the parabolic trap.

The best way of detecting the mesoscopic effects in a trap is to observe the shift of the BEC critical temperature T_c. It is evident in Fig. 1 that the finite size h of the parabolic trap manifests itself in the following mesoscopic phenomena:

(i) The number of levels $n_{\max} = U_0/\hbar\omega$ in the initial symmetric parabolic trap is finite.

(ii) The left potential barrier diminishes $U_0 \longrightarrow (U_- - U_g) < U_0$ under the action of the gravitational field.

The renormalization of the one-particle matrix elements ε_n should be taken into account in both cases. This means that one should (i) cut off the upper limit $n < n_{\max}$ for the barrier U_0 and calculate the ε_n^0 energies and (ii) cut off the upper limit in Eq. (2) for the barrier U_- and calculate the $\varepsilon_n^{\pm}$ energies. Thus, further calculations are carried out using the equation

$$N = N_0 + N_1, \quad N_1 = \sum_{n \neq 0}^{n_{\max}} f_n,$$
$$\varepsilon_n = \begin{cases} \varepsilon_n^0, & g = 0, \\ \varepsilon_n^{\pm}, & g \neq 0, \end{cases} \quad n = \{n_x, n_z\} \tag{6}$$

for the total number N of atoms in a trapped ideal Bose gas. The $n_{\max}$ level defines the upper bound for the atomic states in the trap. The approximate numerical parameters of the experiments [8, 9] for the isotropic parabolic trap are (Fig. 1)

$$U_0 \sim 10^{-9}\ \text{eV}, \quad h = 2\ \text{mm},$$
$$U_+ - U_- = mgh, \quad \omega \sim 10^{-13}\ \text{eV}. \tag{7}$$

We assume that the 3D critical density [8, 9] $R \sim 10^{14}\ \text{cm}^{-3}$ is independent of time, because we neglect the loss of atoms upon cooling. The estimate for the number of atoms in a parabolic trap of volume V can be written for the nD case as [10]

$$R|_{n\text{D}} = N/V, \quad V \sim (m\omega^2/T_c)^{-n/2}, \quad n = 1, 2, 3. \tag{8}$$

We simplify the problem by replacing the parabolic trap by a rectangular one (Fig. 2). This means that the distortion of the parabolic potential in the gravitational field is described as a distortion for a symmetric rectangular trap with the potential U_0 to an asymmetric rectangular trap with barriers $U_+ - U_- = mgh$. The shift of the critical temperature in passing from the symmetric rectangular trap to the asymmetric one is to be estimated as a measure of the gravitational field effect on BEC. Note that, in this case, the contribution of tunneling effects is neglected. According to Eq. (8), the R values in the 1D and 2D parabolic traps are equal to $10^5\ \text{cm}^{-1}$ and $10^{10}\ \text{cm}^{-2}$. We retain the same R values for the rectangular traps. Thus, the number of atoms in the 1D and 2D rectangular traps is equal to $N_1|_{1\text{D}} \sim 10^5\ \text{cm}^{-1} \times 0.2\ \text{cm} \sim 2 \times 10^4$ cm and $N_1|_{2\text{D}} \sim 10^{10}\ \text{cm}^{-2} \times (0.2\ \text{cm})^2 \sim 4 \times 10^8$, respectively. The equation for the $\varepsilon_n \longrightarrow E_k$ spectrum

of the symmetric 1D and 2D traps is written for $k = \{k_x, k_z\}$ as [17]

$$\tan(kh) = \frac{2k\hbar}{p_k^0}\left[\frac{k^2\hbar^2}{(p_k^0)^2} - 1\right]^{-1}, \quad E_k = \frac{\hbar^2(k_x^2 + k_z^2)}{2m}$$

$$p_k^0 = \sqrt{2m(U_0 - E_k)},$$

and for the asymmetric (distorted) traps ($k = k_z$) as

$$\tan(kh) = k\hbar\left(\frac{1}{p_k^+} + \frac{1}{p_k^-}\right)\left(\frac{k^2\hbar^2}{p_k^+ p_k^-} - 1\right)^{-1},$$

$$p_k^\pm = \sqrt{2m(U_\pm - E_k)}.$$

The distances between the energy levels E_k of the initial rectangular trap with parameters (7) are equal to $\sim 10^{-19}$ eV in the lower part of the spectrum and $\sim 10^{-13}$ eV near the upper bound U_0. The trap contains $\sim 10^5$ levels ($\sim 10^4$ in the experiments [8, 9]), so that the average distance between the levels $\sim 7 \times 10^{-14}$ eV is equal to the frequency $\hbar\omega \sim 6 \times 10^{-14}$ eV of the parabolic trap.

In order to obtain a more systematic description of the phenomenon, we start with the 1D case and the atomic density $R \sim 10^5$ cm^{-1}. The critical temperature $T_c^0|_{1D} = 2.41 \times 10^{-10}$ K of the initial rectangular trap U_0 is determined from equation (6) with the use of the calculated spectrum E_k,

$$N_0 = 0, \quad N_1^0|_{1D} = N|_{1D}$$

$$= \sum_{k_z \neq 0} f(T_c^0|_{1D}, E_{k_z}^0) = 2 \times 10^4, \quad k < k_{\max}.$$

A reasonable computational accuracy can be attained for the $k_{\max} \sim 1000$ values in the last sum over k_z. The distorted rectangular trap $U_- \sim 10^{-8}U_0$ is defined by the parameters h and $U_+ - U_- = mgh$ given in Eq. (7). It contains only ~10 levels occupied by

$$N_1^\pm|_{1D} = \sum_{k_z \neq 0}^{10} f(T_c^0|_{1D}, E_{k_z}^0) = 1.8 \times 10^4 < N|_{1D}$$

atoms. These atoms undergo new BEC transition in the system with renormalized energy levels at a temperature equal to the critical temperature in the distorted trap $T_c^\pm|_{1D} = 2.27 \times 10^{-10}$, which can be found from the equation

$$N_0 = 0, \quad N_1^\pm|_{1D} = \sum_{k_z \neq 0}^{10} f(T_c^\pm|_{1D}, E_{k_z}^\pm) = 1.8 \times 10^4, \quad k < k_{\max}.$$

Thus, the shift of the critical temperature is $\Delta(T_c)|_{1D} = T_c^\pm|_{1D} - T_c^0|_{1D} = -0.14 \times 10^{-10}$. The remaining 0.2×10^4 atoms escape the trap (continuous spectrum).

As for the 2D case, the sum over k_x and k_z is calculated with regard to the constraint[1] $E_k < E(n|_{\max})$, $k = \{k_x, k_z\}$. The temperature $T^0|_{2D} = 5.05 \times 10^{-7}$ K of the initial rectangular trap is determined from equation (6):

$$N_0 = 0, \quad N_1|_{2D} = N|_{2D}$$

$$= \sum_{k_x, k_z \neq 0} f(T_c^0|_{2D}, E_{k_x k_z}^0) = 4 \times 10^8, \quad k < k_{\max}.$$

In this formula, the summation goes over all values of the partition function variables, including those corresponding to the possible level degeneracy. A reasonable accuracy of calculations for k_x and k_z in the last sum is attained at $k_{\max} \sim 400$. The distorted rectangular trap $U_- \sim 10^{-8}U_0$ contains ten levels occupied by

$$N_1^\pm|_{2D} = \sum_{k_x, k_z \neq 0}^{10} f(T_c^0|_{2D}, E_{k_x k_z}^0) = 0.96 \times 10^8 < N|_{2D}$$

atoms. As in the 1D case, we calculate the transition temperature for the distorted trap from the equation

$$N_0 = 0, \quad N_1^\pm|_{2D} = \sum_{k_x, k_z \neq 0}^{10} f(T_c^\pm|_{2D}, E_{k_x k_z}^0).$$

As a result, we find that $T_c^\pm|_{2D} = 5.03 \times 10^{-7}$ K; i.e., the shift of the critical temperature is

$$\Delta(T_c)|_{2D} = T_c^\pm|_{2D} - T_c^0|_{2D} = -0.02 \times 10^{-7} \text{ K}. \quad (9)$$

Now, let us find the T_c shift for a system with the same number of particles, e.g., 4×10^8 (in the 2D case). It is found above that the critical temperature for the symmetric trap is $T_c^0|_{2D} = 5.05 \times 10^{-7}$ K. The critical temperature for the asymmetric trap $(T_c^\pm|_{2D})^* = 2.02 \times 10^{-6}$ K is determined from the equation

$$N_0 = 0, \quad N_1|_{2D} = N|_{2D}$$

$$= \sum_{k_x, k_z \neq 0}^{10} f[(T_c^\pm|_{2D})^*, E_{k_x k_z}^\pm] = 4 \times 10^8, \quad (10)$$

$$\Delta(T_c) = (T_c^\pm|_{2D})^* - T_c^0|_{2D} = 1.52 \times 10^{-6} \text{ K}.$$

[1] This condition is immaterial for the initial trap but important for the distorted trap.

Note that the value of $(T_c^{\pm}|_{2D})^*$ in Eq. (10) does not coincide with the initial $T_c^{\pm}|_{2D}$ value in Eq. (9), because Eqs. (9) and (10) describe different processes. This important fact is discussed at the end of the article.

The above calculations are carried out for the rectangular trap. The initial parabolic trap has the same potential barriers $U_{\pm}$ and the same shift $U_+ - U_- = mgh$ but differs in spectrum. One can assume that the gravity-induced shift of the BEC critical temperature in the parabolic trap has the same order of magnitude, so that the critical temperatures $T_c^0 \longrightarrow T|_{g=0}$ and $T_c^{\pm} \longrightarrow T|_{q\neq 0}$ in the rectangular and parabolic traps are in qualitative agreement with each other. However, the contribution of tunneling effects is not reproduced in the rectangular trap. It is evident from Eq. (1) that the macroscopic stability of the parabolic trap in a gravitational field is defined by the inequality $\omega^2 > 2g/h$. Clearly, this condition loses its meaning in the absence of gravitation, as well as for a trap extended ever the entire $-\infty < z < \infty$ axis. The finite-size effect accompanied by the most pronounced gravitational shift of T_c in the distorted rectangular trap with $n_{\max} \sim 10$ can be observed for the parabolic trap if

$$(\omega^2 h - 2g) \longrightarrow +0.$$

This condition implies that the largest shift of T_c can be observed immediately before the trap collapses.

The correspondence between Eqs. (9), (10) and the possible motion of a trap between the Earth and space should be determined. First, the critical temperature $(T_c^{\pm}|_{2D})^* = 2.02 \times 10^{-6}$ K is measured for $N|_{2D}$ atoms in a distorted trap on the Earth. Next, the trap is sent into space. The phase transition in space occurs in the undistorted trap with the same number of atoms $N|_{2D}$ at temperature $T_c^0|_{2D} = 5.05 \times 10^{-7}$ K with shift (10). If the trap comes back to the Earth, it becomes distorted and cannot hold some atoms. The remaining portion of atoms $T_1^{\pm}|_{2D}$ undergoes phase transition at temperature $T_c^{\pm}|_{2D} = 5.03 \times 10^{-7}$ K, so that the shift (9) will occur.

Thus, we obtain three transition temperatures (in the same trap) in three different situations I, II, and III:

$$(T_c^{\pm}|_{2D})^* = 2.02 \times 10^{-6} \text{ K}$$
$$\longrightarrow T_c^0|_{2D} = 5.05 \times 10^{-7} \text{ K}$$
$$\longrightarrow T_c^{\pm}|_{2D} = 5.03 \times 10^{-7} \text{ K},$$

start on the Earth (I) $\longrightarrow$ in space (II) $\longrightarrow$ finish on the Earth (III).

This pattern occurs for an ideal Bose gas. The sign of the T_c shift in a nonideal gas was found in [14] without taking into account the renormalization of energy levels in the transition I $\longrightarrow$ II. Apparently, calculations for the 3D case will yield higher critical temperatures.

The mesoscopic nature of this problem consists in the strong dependence of the T_c shift on the initial parameters and the way of establishing their correspondence to the experimental data.

This work was supported by the Russian Foundation for Basic Research, project no. 00-02-16672.

REFERENCES

1. G. K. S. Wong, P. A. Crowell, H. A. Cho, and J. D. Reppy, Phys. Rev. Lett. **65**, 2410 (1990).
2. K. Huang and H.-F. Meng, Phys. Rev. Lett. **69**, 644 (1992).
3. V. Sa-Yakanit, V. Yarunin, and P. Nisameneephong, Phys. Lett. A **237**, 152 (1998).
4. *Proceedings of the International Symposium on Low Temperature Physics, St. Petersburg, 1999.*
5. K. Huang, cond-mat/9904027 (1999).
6. G. Baym, J.-P. Blaziot, and J. Zinn-Justin, cond-mat/9907241 (1999).
7. V. Bagnato, D. Pritchard, and D. Kleppner, Phys. Rev. A **35**, 4354 (1987).
8. K. B. Davis, M. O. Mewes, M. R. Andrews, *et al.*, Phys. Rev. Lett. **75**, 3969 (1995).
9. M. O. Mewes, M. R. Andrews, N. J. van Druten, *et al.*, Phys. Rev. Lett. **77**, 416 (1996).
10. K. Damle, T. Senthil, S. Majumdar, and S. Sachdev, Europhys. Lett. **36**, 7 (1996).
11. L. Pitaevskiĭ, Usp. Fiz. Nauk **168**, 641 (1998) [Phys. Usp. **41**, 569 (1998)]; cond.-mat/9806038 (1998).
12. Roadmap on *Fundamental Physics in Space*, Preprint JPL **400**–**808**, 4/99, NASA (1999).
13. V. Yarunin, Teor. Mat. Fiz. **96**, 37 (1993); **109**, 295 (1996); V. Yarunin and L. Siurakshina, Physica A (Amsterdam) **215**, 261 (1995); V. Yarunin, Teor. Mat. Fiz. **119**, 308 (1999); Fiz. Nizk. Temp. **24**, 176 (1998) [Low Temp. Phys. **24**, 130 (1998)].
14. V. Yarunin and D. Baranov. Preprint JINR E17-99-172; J. Low Temp. Phys. (2000) (in press).
15. N. N. Bogolyubov, Izv. Akad. Nauk SSSR, Ser. Fiz. **11**, 77 (1947).
16. V. N. Popov and L. D. Faddeev, Zh. Éksp. Teor. Fiz. **47**, 1315 (1964) [Sov. Phys. JETP **20**, 890 (1964)].
17. S. Flugge, *Practical Quantum Mechanics* (Springer-Verlag, New York, 1971), Vol. 1.

Translated by A. Bagatur'yants

JETP Letters, Vol. 71, No. 6, 2000, pp. 271–272. Translated from Pis'ma v Zhurnal Éksperimental'noĭ i Teoreticheskoĭ Fiziki, Vol. 71, No. 6, 2000, pp. 391–393.

CONDENSED MATTER

Conductivity of a "Colored" Plane

V. G. Marikhin

Landau Institute of Theoretical Physics, Russian Academy of Sciences, Chernogolovka, Moscow region, 142432 Russia

e-mail: mvg@itp.ac.ru

Received February 24, 2000

The conductivity of a "colored" plane, i.e., a plane divided into domains differing in conductivity, is calculated. The exact relation between the effective conductivities of the cited and dual (with inverse conductivities) systems is derived for the isotropic case (i.e., the effective conductivity tensor is proportional to the unit matrix). The conductivity of two-colored systems such as a "chessboard" or triangular lattice is exactly calculated to give $\sigma = (\sigma_1\sigma_2)^{1/2}$. The particular case of a "hexagon," as well as the duality relations for anisotropic systems and for a system in a magnetic field are discussed. © *2000 MAIK "Nauka/Interperiodica".*

PACS numbers: 73.50.Bk; 75.70.Ak

In 1970, Dykhne [1] used duality relations to calculate the conductivity of a thin film with two randomly distributed phases of the same concentration. It was also claimed in [1] that the "chessboard" conductivity can be calculated by the same method to give $\sigma = (\sigma_1\sigma_2)^{1/2}$, where σ_1 and σ_2 are the conductivities of the "black" and "white" chessboard squares, respectively. This statement was not proved, because, apart from the dual transformation of equations, one should have inspected the transformation of boundary conditions.

It is the purpose of this work to derive the exact dual relations for a multiphase system with allowance made for the boundary conditions.

Therefore, let us consider a certain plane divided into periodic domains (plaquettes), with an elementary cell containing N distinct plaquettes with conductivities σ_i, $i = 1, 2, \ldots, N$. It is required to calculate the conductivity of this system. The simplest solution is obtained for the system with the conductivity tensor proportional to a unit matrix: $\sigma_{\alpha\beta} = \sigma\delta_{\alpha\beta}$, i.e., for the effectively isotropic system.

The equation on the plaquette and the corresponding boundary conditions can be conveniently formulated for field strength because it is a physical observable and, hence, a periodic function on the lattice, as differentiated from the potentials, which are quasi-periodic functions. The corresponding equations have the form

$$\mathrm{div}\mathbf{j} = 0, \quad \mathrm{rot}\mathbf{E} = 0, \tag{1}$$

over the whole plane, with the following equations on each of the plaquettes:

$$\mathrm{div}\mathbf{E}^i = 0, \quad \mathrm{rot}\mathbf{j}^i = 0, \quad \mathbf{j}^i = \sigma_i\mathbf{E}^i. \tag{2}$$

The boundary conditions for the plaquettes are

$$E^i_{\mathbf{t}} = E^j_{\mathbf{t}}, \quad \sigma_i E^i_{\mathbf{n}} = \sigma_j E^j_{\mathbf{n}}. \tag{3}$$

Then, applying the dual transformation

$$E'^i_\alpha = \sigma_i e_{\alpha\beta} E^i_\beta, \quad \sigma'_i = 1/\sigma_i,$$
$$e_{11} = e_{22} = 0, \quad e_{12} = -e_{21} = 1, \tag{4}$$

we obtain a new system satisfying Eqs. (1) and (2) and boundary conditions (3) for $\mathbf{E}'^i$ and σ'_i.

Note that the potentials of both original and transformed systems are calculated by formula

$$\phi = \phi_0 \int_{\mathbf{r}_0}^{\mathbf{r}} (\mathbf{E}d\mathbf{s}). \tag{5}$$

Due to Eqs. (1) and boundary conditions (3), the integral in Eq. (5) is independent of the integration contour, and the potential is a single-valued and continuous function of the coordinates (for both original and transformed systems).

Let now turn to the calculation of conductivities. The integrated field strength for the ith plaquette is

$$\mathbf{e}^i = \int_{'i'square} dxdy\mathbf{E}^i. \tag{6}$$

In the isotropic case, the effective conductivity is a scalar and has the form

$$\sigma_{\mathrm{eff}} = \sum \sigma_i e^i_x / \sum e^i_x = \sum \sigma_i e^i_y / \sum e^i_y. \tag{7}$$

It follows from Eq. (4) that

$$e'^i_x = \sigma_i e^i_y, \quad e'^i_y = -\sigma_i e^i_x. \tag{8}$$

Inserting Eq. (8) into Eq. (7), one obtains

$$\sigma'_{\mathrm{eff}} = 1/\sigma_{\mathrm{eff}}, \quad \sigma'_i = 1/\sigma_i. \tag{9}$$

0021-3640/00/7106-0271$20.00

Finally, the duality relation for the conductivities is written as

$$\sigma_{\text{eff}}(\sigma_1, \sigma_2, \ldots, \sigma_N)\sigma_{\text{eff}}\left(\frac{\sigma_0^2}{\sigma_1}, \frac{\sigma_0^2}{\sigma_1}, \ldots, \frac{\sigma_0^2}{\sigma_N}\right) = \sigma_0^2, \quad (10)$$

with σ_0 being the arbitrary dimensional parameter.

In the case of a chessboard (or a two-colored triangular plane), the substitution of $\sigma_0^2 = \sigma_1\sigma_2$ in Eq. (10) yields

$$\sigma_{\text{eff}} = \sqrt{\sigma_1\sigma_2}. \quad (11)$$

Equation (11) was obtained for the chessboard in [2] by the exact solution of Eqs. (5) in terms of elliptic functions and in [3] using a high-order perturbation theory. In [4], Eq. (11) does not hold for a triangular lattice.

Note that we used the periodicity conditions only to make the summation in the numerator and denominator in Eq. (7) finite. Generalizing Eq. (7) to the infinite case, one can reproduce all the results for mixtures.

Of course, duality relations (10) are insufficient to derive the formula for conductivity in the case of $N > 2$, but this can be done in some particular cases. For example, let us consider a "hexagon," i.e., a hexagonal cover with $N = 3$. If $\sigma_3 = (\sigma_1\sigma_2)^{1/2}$, then $\sigma_{\text{eff}} = (\sigma_1\sigma_2)^{1/2}$.

Consider a system placed in a constant magnetic field. Let the conductivity tensor of each of the plaquettes be of the form

$$\sigma_{\alpha\beta} = \sigma\delta_{\alpha\beta} + \sigma^H e_{\alpha\beta}, \quad \sigma^H \sim H. \quad (12)$$

Duality relation (10) can be generalized to the magnetic field case, because conductivity tensor (12) commutes with the duality transformation tensor $e_{\alpha\beta}$. In this case, the duality transformation is written as

$$E'^i_\alpha = \sigma_{\alpha\beta,i}e_{\beta\gamma}E^i_\gamma, \quad \sigma'^i_{\alpha\beta} = (\sigma^i_{\alpha\beta})^{-1}. \quad (13)$$

Since $\text{div}\mathbf{E} = 0$ and $\text{rot}\mathbf{E} = 0$, these relations and the pertinent boundary conditions are fulfilled for the transformed system as well. One has

$$(E^i_\alpha - E^j_\alpha, e_{\alpha\beta}n_\beta) = 0, \ (n_\alpha, \sigma^i_{\alpha\beta}E^i_\beta - \sigma^j_{\alpha\beta}E^j_\beta) = 0, \quad (14)$$

where $\mathbf{n}$ is the normal vector to the interface between plaquettes i and j. One can then easily see that the boundary conditions for the system obtained through duality transformations (13) have the form (14).

It is convenient to introduce the notations

$$\Sigma = \sigma + i\sigma^H, \quad \sigma^a_{\alpha\beta}\sigma^b_{\beta\gamma} = \sigma^c_{\beta\gamma} \Leftrightarrow \Sigma^a\Sigma^b = \Sigma^c. \quad (15)$$

Then the duality formula for the conductivities becomes

$$\Sigma_{\text{eff}}(\Sigma^1\Sigma^2\ldots\Sigma^N)\Sigma_{\text{eff}}\left(\frac{\sigma_0^2}{\Sigma^1}\frac{\sigma_0^2}{\Sigma^2}\ldots\frac{\sigma_0^2}{\Sigma^N}\right) = \sigma_0^2, \ \sigma_0 \in \Re. \quad (16)$$

For the binary systems, $\Sigma_{\text{eff}} = (\Sigma^1\Sigma^2)^{\frac{1}{2}}$ if $\Sigma^1\Sigma^2 \in \Re$.

It turns out that the answer can also be obtained for the anisotropic case if Eq. (7) are used in the vectorial form. Let $\hat{\sigma} = \text{diag}(\sigma_{xx}, \sigma_{yy})$. Then, omitting the scale factor σ_0, we find that the duality transformation

$$E'^i_\alpha = e_{\alpha\beta}\sigma_{i,\beta\beta}E^i_\beta, \quad \sigma'_{i,xx} = \frac{1}{\sigma_{i,yy}}, \quad \sigma'_{i,yy} = \frac{1}{\sigma_{i,xx}} \quad (17)$$

yields the duality relation

$$\sigma_{xx}\sigma'_{yy} = \sigma'_{xx}\sigma_{yy} = 1. \quad (18)$$

I am grateful to A.M. Dyugaev and Yu.N. Ovchinnikov for presenting the results of their work before publication and to A.Yu. Kamenshchik for helpful discussions.

REFERENCES

1. A. M. Dykhne, Zh. Éksp. Teor. Fiz. **59**, 110 (1970) [Sov. Phys. JETP **32**, 63 (1971)].
2. A. M. Dyugaev and Yu. N. Ovchinnikov, Zh. Éksp. Teor. Fiz. **117** (2000) (in press).
3. A. Yu. Kamenshchik and I. M. Khalatnikov, private communication.
4. Yu. N. Ovchinnikov, submitted for publication in Zh. Éksp. Teor. Fiz.

Translated by V. Sakun